CAPRAM reduction towards an operational multiphase halogen and DMS chemistry treatment in the chemistry transport model COSMO-MUSCAT(5.04e)

Erik H. Hoffmann[1], Roland Schrödner[2], Andreas Tilgner[1], Ralf Wolke[2], Hartmut Herrmann[1]

[1] Atmospheric Chemistry Department (ACD), Leibniz Institute for Tropospheric Research (TROPOS), Permoserstr. 15, 04318 Leipzig, Germany
[2] Modeling of Atmospheric Processes Department (MAPD), Leibniz Institute for Tropospheric Research (TROPOS), Permoserstr. 15, 04318 Leipzig, 04318, Germany

Correspondence to: Hartmut Herrmann (herrmann@tropos.de)

Abstract. A condensed multiphase halogen and dimethyl sulfide (DMS) chemistry mechanism for application in chemistry transport models is developed by reducing the CAPRAM DMS module 1.0 (CAPRAM-DM1.0) and the CAPRAM halogen module 3.0 (CAPRAM-HM3.0). The reduction is achieved by determining the main oxidation pathways from analysing the mass fluxes of complex multiphase chemistry simulations with the air parcel model SPACCIM. These simulations are designed to cover both pristine and polluted marine boundary layer conditions. Overall, the reduced CAPRAM-DM1.0 contains 32 gas-phase reactions, 5 phase transfers, and 12 aqueous-phase reactions, of which two processes are described as equilibrium reactions. The reduced CAPRAM-HM3.0 contains 199 gas-phase reactions, 23 phase transfers, and 87 aqueous-phase reactions. For the aqueous-phase chemistry, 39 processes are described as chemical equilibrium reactions. A comparison of simulations using the complete CAPRAM-DM1.0 and CAPRAM-HM3.0 mechanisms against the reduced ones indicates that the relative deviations are below 5 % for important inorganic and organic air pollutants and key reactive species under pristine ocean and polluted conditions. The reduced mechanism has been implemented into the chemical transport model COSMO-MUSCAT and tested by performing 2D-simulations under prescribed meteorological conditions that investigate the effect of stable (stratiform cloud) and more unstable meteorological conditions (convective clouds) on marine multiphase chemistry. The simulated maximum concentrations of HCl are in the range of 10^9 molecules cm^{-3} and those of BrO are at around 1×10^7 molecules cm^{-3} reproducing the range of ambient measurements. Afterwards, the oxidation pathways of DMS in a cloudy marine atmosphere have been investigated in detail. The simulations demonstrate that clouds have both a direct and an indirect photochemical effect on the multiphase processing of DMS and its oxidation products. The direct photochemical effect is related to in-cloud chemistry that leads to high DMSO oxidation rates and a subsequently enhanced formation of methane sulfonic acid compared to aerosol chemistry. The indirect photochemical effect is characterised by cloud shading, which occurs particularly in the case of stratiform clouds. The lower photolysis rate affects the activation of Br atoms and consequently lowers the formation of BrO radicals. The corresponding DMS oxidation flux is lowered by up to 30 % under thick optical clouds. Moreover, high updraft velocities lead to a strong vertical mixing of DMS into the free troposphere predominately

Gelöscht: chemical

Gelöscht: percentage

Gelöscht: weather

Gelöscht: ·

Gelöscht: pathway

Gelöscht: has

under cloudy conditions. The photolysis of hypohalous acids (HOX, X = Br, Cl, or I) is reduced as well, resulting in higher HOX-driven sulfite to sulfate oxidation in aerosol particles below stratiform clouds. Altogether, the present model simulations have demonstrated the ability of the reduced mechanism to be applied in studying marine aerosol-cloud processing effects in regional models such as COSMO-MUSCAT. The reduced mechanism can be used also by other regional models for more adequate interpretations of complex marine field measurement data.

Gelöscht: Furthermore, HOX

Gelöscht:

Gelöscht: and

Gelöscht: applied

Gelöscht: , also by other regional models

1 Introduction

In the marine and coastal atmosphere the chemical composition of the gas-phase, particles, and clouds as well as the size-distribution of particles are significantly influenced by emissions of sea spray aerosols (SSA) and volatile organic compounds from the sea surface (Simpson et al., 2015; Farmer et al., 2015; Quinn et al., 2015). Sea salt is an important compound of SSA (Quinn et al., 2015) and represents a primary source for reactive chlorine and bromine compounds in the troposphere (Saiz-Lopez and von Glasow, 2012; Simpson et al., 2015). For reactive iodine compounds however, emissions of gaseous iodine compounds from the ocean surface dominate (Carpenter et al., 2012; Carpenter et al., 2013; Carpenter and Nightingale, 2015; Saiz-Lopez et al., 2012). Additionally, the ocean is the main source for dimethyl sulfide (DMS), which is the biggest natural source for atmospheric sulfur (Andreae, 1990; Lana et al., 2011). The oxidation of DMS is the key to understanding the natural radiative forcing as it affects both aerosol and cloud condensation nuclei (CCN) concentrations (Charlson et al., 1987). The chemical systems of halogens and DMS interact with each other strongly and are highly influenced by multiphase chemistry (Barnes et al., 2006; Hoffmann et al., 2016; von Glasow and Crutzen, 2004). As oceans cover around 70 % of the Earth's surface (Joshi et al., 2017; Law et al., 2013) and are in strong interaction with densely populated coastal areas (Kummu et al., 2016; von Glasow et al., 2013), this ocean-related atmospheric chemical subsystem is important for both Earth's climate and air quality.

Gelöscht: source

The chemistry of reactive halogen compounds as well as of DMS is very sensitive to anthropogenic pollution. The advection of NO_x and ozone has strong effects on the activation of reactive halogen compounds (Hoffmann et al., 2019b; Shechner and Tas, 2017; Mahajan et al., 2009b; Mahajan et al., 2009a; McFiggans et al., 2002) and on DMS oxidation (Breider et al., 2010; Barnes et al., 2006; Chen et al., 2018). Moreover, reactive halogen compounds can significantly influence the depletion of NO_x, ozone, SO_2, volatile organic compounds (VOCs), and oxidised volatile organic compounds (OVOCs) (von Glasow et al., 2002b, a; Sherwen et al., 2017; Schmidt et al., 2016; Sherwen et al., 2016). As the NO_3 radical concentration in anthropogenically influenced atmospheric environments is enhanced (Brown and Stutz, 2012), the NO_3 radical-related DMS oxidation is reinforced (Breider et al., 2010; Chen et al., 2018), which influences the formation of sulfate aerosol particles and correspondingly leads to an increase of aerosol acidity (Muniz-Unamunzaga et al., 2018). The changed aerosol acidity further affects the formation of secondary organic aerosol (SOA) (Surratt et al., 2010; Surratt et al., 2007; Gaston et al., 2014) as well as the activation of reactive halogen compounds (Keene et al., 1998). Apart from that, the ongoing reduction of fossil fuel combustion emissions in some parts of the world will promote the oxidation of DMS as an important contributor to the

Gelöscht: Furthermore, in anthropogenically influenced atmospheric environments, the NO_3 radical concentration is enhanced (Brown and Stutz, 2012). Thus,

Gelöscht: aerosol sulfate

Gelöscht: formation

Gelöscht: Moreover

formation of sulfate aerosol particles even in the Northern Hemisphere (Perraud et al., 2015). Therefore, it is important that chemical transport models (CTMs) treat the crucial multiphase chemistry pathways of both reactive halogen compounds and DMS.

Currently, only a couple of multiphase chemistry mechanisms of halogens and DMS have been developed and applied within CTMs, e.g. EMAC, CAM–MECCA, and GEOS-Chem (Chen et al., 2017; Chen et al., 2018; Jöckel et al., 2016; Long et al., 2014). Nevertheless, the applied model core of these CTMs does not treat aqueous-phase chemistry of halogens and DMS by default. In CTMs that deal with the chemistry in the marine boundary layer (MBL) and the free troposphere, the activation of reactive halogen compounds and its dependence on aerosol acidity is often described by heterogeneous reactions. The parameters of these reactions have been determined in laboratory studies for aerosol solutions that are more ideal than they naturally occur, e.g. pure sulfate or sodium chloride/bromide aerosol. Hence, the accuracy of the description of these processes is restricted and it cannot easily be assumed that they are representative under heterogeneous atmospheric conditions (Ammann et al., 2013). The treatment of multiphase chemistry in models allows for more detailed investigations concerning complex sea spray aerosol matrices. However, the level of detail for the implementation of aqueous-phase chemistry into CTMs is limited because of numerical restrictions, since the implementation of aqueous-phase chemistry usually consumes huge amounts of CPU time. Consequently, mostly only specific small sub-systems are investigated, including a low number of halogen or DMS multiphase chemistry reactions (Chen et al., 2018; Chen et al., 2017). Both discussed aspects, consumption of CPU time and investigating only small sub-systems, highlight that an overall picture of multiphase marine chemistry cannot be drawn by chemical transport modelling yet and might lead to an over- or underestimation of important chemical pathways.

To achieve the goal of adequately treating the multiphase chemistry of DMS and reactive halogen compounds within CTMs, not only a solution for the high CPU consumption is necessary, but also the development of a condensed multiphase chemistry mechanism dealing with the complexity of these chemical systems. Currently, an adequate mechanism does not exist and can be derived by reducing detailed multiphase chemistry mechanisms, because important chemical pathways could otherwise be missed resulting in a misinterpretation of field data.

In the present study, a reduced multiphase chemistry mechanism describing halogen and DMS chemistry is developed through a manual reduction using box model studies with the CAPRAM halogen module 3.0 (CAPRAM-HM3.0, Hoffmann et al., 2019a) and the CAPRAM DMS module 1.0 (CAPRAM-DM1.0, Hoffmann et al., 2016). Both modules currently contain the most detailed mechanisms dealing with the multiphase chemistry of these chemical systems. During the reduction procedure, two mechanisms are derived, which are afterwards combined into a single one. The combined reduced mechanism is implemented into the CTM MUSCAT (MUltiScale Chemistry Aerosol Transport; Wolke et al., 2004; Wolke et al., 2012), which now treats detailed marine multiphase chemistry. Finally, the combined reduced mechanism is applied in idealised 2D-simulations with a focus on multiphase DMS oxidation in the MBL and the various effects of clouds on halogens and DMS.

Gelöscht: formation

Gelöscht: However

Gelöscht: the solvation of

Gelöscht: an adequate

Gelöscht: An

Gelöscht: currently

Gelöscht: only

Gelöscht: The

Gelöscht: .

Gelöscht: -

Gelöscht: essentially

2 Reduction of the CAPRAM-DM1.0 and the CAPRAM-HM3.0

2.1 Model setup

The reduction of the marine multiphase chemistry modules CAPRAM-DM1.0 and CAPRAM-HM3.0 is achieved through modelling studies with the air parcel model SPACCIM (SPectral Aerosol Cloud Chemistry Interaction Model, Sehili et al., 2005; Wolke et al., 2005). SPACCIM is a model framework designed to solve complex multiphase chemistry systems and has already been used for the development of reduced aqueous-phase chemistry mechanisms (Deguillaume et al., 2010). The description of the simultaneously occurring chemical and physical processes in tropospheric cloud droplets and aqueous aerosol particles in SPACCIM is realised by combining a complex size-resolved cloud microphysical model and a detailed multiphase chemistry model. The standard atmospheric multiphase chemistry is represented by the near-explicit gas-phase mechanism MCMv3.2 (Jenkin et al., 2003; Saunders et al., 2003) and the near-explicit aqueous-phase mechanism CAPRAM4.0 (Bräuer et al., 2019).

The goal of reducing the CAPRAM-DM1.0 and CAPRAM-HM3.0 is that both modules can be applied in different marine atmospheric environments in CTMs. To this end, simulations are carried out under two environmental conditions: (i) pristine ocean and (ii) polluted coastal area. The simulations run for 48 hours and are equivalent to former simulations of atmospheric marine environments studied with CAPRAM (Bräuer et al., 2013; Hoffmann et al., 2016; Hoffmann et al., 2019b).

In the simulations with pristine ocean conditions, an air parcel is moved along a predefined trajectory at a 900 hPa pressure level. The simulations are carried out at different latitudes (15°, 30°, 45°, 60° and 75°) and in different seasons of the year (summer and winter). The air temperature in the simulations is adjusted accordingly. Furthermore, the simulations are performed at different relative humidity levels (50 %, 70 %, and 90 %). In the simulations with relative humidity levels of 70 % and 90 %, cloud passages of the air parcel are considered. The cloud occurrence is modelled by uplifting the air parcel to an 800 hPa pressure level either at noon and midnight or in the early morning and evening of the first model day. Due to adiabatic cooling, the relative humidity increases, reaching the critical supersaturation so that a cloud is formed. After the cloud passage, the air parcel descends again to 900 hPa. The updraft and downdraft of the air parcel requires half an hour of modelling time in each case. The in-cloud residential time of the air parcel is two hours in the simulations with cloud occurrences at noon and midnight and three hours in those with cloud occurrences in the early morning and evening of the first model day. The simulations with 50 % relative humidity have no cloud passages of the air parcel included. For a detailed description of the emission and initialisation of chemical species within the pristine ocean scenario, the reader is referred to Bräuer et al. (2013) and Hoffmann et al. (2016). The modelled concentration time profiles of specific important trace gases and aerosol compounds within the pristine boundary layer are given in Fig. S1 to S10 in the supplement.

The scenario at the polluted coastal area is divided into two sub-simulations at 45° latitude and 70 % relative humidity. The lower diversity of the simulations compared to the pristine ocean scenario is chosen because previous model studies had revealed that high NO_x concentrations suppress gas-phase halogen radical cross reactions and lead to a domination of halogen nitrate and nitryl chloride photolysis in halogen atom activation (Hoffmann et al., 2019a; Hoffmann et al., 2019b; Faxon and

Gelöscht: dealing the

Gelöscht: .

Gelöscht: The uplifting and down lifting

Gelöscht: .

Gelöscht: .

Allen, 2013; Saiz-Lopez and von Glasow, 2012; von Glasow et al., 2013). The effect of photolysis and temperature change does not affect these four important halogen activation precursors ($ClNO_2$, $ClNO_3$, $BrNO_3$, and INO_3). In the first simulation, the air parcel represents the composition of a pristine marine environment, which is advected over a polluted coastal urban area. The second simulation describes an air-sea breeze circulation system. Details on the model configurations of the first simulation are explicitly given in Hoffmann et al. (2019b) and those of the second simulation in Hoffmann et al. (2019a). The main model results of both simulations do not differ from the present work.

The reduction of both modules is performed by analysing the modelled ten-minute time-resolved source and sink fluxes of key chemical compounds of marine multiphase chemistry. These cover all DMS oxidation intermediates and, for halogen chemistry, all X_y species (X, X_2O_2, XNO_2, XNO_3, XO, XOO, OXO, XY, HOX, and HX, with X/Y = Cl, Br, or I). At first, the CAPRAM-DM1.0 is reduced and afterwards the CAPRAM-HM3.0. In the following Sect 2.2 and Sect 2.3, the development of the reduced CAPRAM-DM1.0 and CAPRAM-HM3.0 is described.

The final reduced marine multiphase chemistry mechanism is evaluated through control simulations, which are carried out by using not only the full but also the reduced marine multiphase chemistry mechanism.

The goal of the mechanism reduction firstly is that the modelled concentration of chemical species that are classically treated as important in CTMs, e.g. ozone, SO_2, NO_x, sulfate or nitrate, only deviate from the modelled concentration obtained from the complete scheme by less than 5 % on average over the full modelling time. Secondly, concentrations of oxidants and important chemical compounds of marine multiphase chemistry should only differ by less than 10 % on average. Important chemical compounds of DMS multiphase oxidation are DMS, dimethyl sulfoxide (DMSO), and methane sulfonic acid (MSA), which represent the key stable compounds from DMS oxidation. Dimethyl sulfone ($DMSO_2$) is not considered, because, according to current scientific knowledge, the oxidation of $DMSO_2$ is negligible under atmospheric conditions of the pristine ocean. Additionally, the deviation of the concentration of methane sulfinic acid (MSIA) is not a reduction criterion. MSIA is very reactive, so that even slight changes will immediately result in differences of the MSA and sulfate concentrations. In the case of halogen multiphase chemistry, important species for the mechanism reduction are the Cl, Br, and I atoms as well as the ClO, BrO, and IO radical and stable halogen compounds, which can act as important reservoir or activation species for halogen radicals, i.e. hypohalous acids, nitryl chloride, and dihalogen molecules. These halogen reservoir/activation species are of high importance as strong changes in their budget will obviously affect the overall oxidation processes in the MBL. For other halogen radicals, it has been shown by previous studies (e.g. see Saiz-Lopez et al. 2012 and Simpson et al., 2015) that these are rapidly converted into the above-mentioned compounds and thus strong concentration changes will show up in the concentration of X atoms or XO radicals. Lastly, the pattern of the concentration time profile for all species has to match between the reduced and the full mechanism ($R^2 \geq 0.75$).

Gelöscht:) species.

Gelöscht: The goal of the reduction is that the concentration of chemical species important for chemical transport modelling, e.g. ozone, sulfate or nitrate, only deviate by less than 5 % on average over the full modelling time. A subordinate goal is that oxidants and important chemical compounds of marine multiphase chemistry only diverge by less than 10 % on average. The important chemical compounds of DMS multiphase oxidation are DMS, dimethyl sulfoxide (DMSO), and methane sulfonic acid (MSA). In the case of halogen multiphase chemistry, they are the Cl, Br, and I atoms as well as ClO, BrO, and IO and stable halogen compounds, which act as important reservoir or activation species for halogen radicals, i.e. hypohalogeneous acids, nitryl chloride, and dihalogen molecules. Lastly, the evolution of the concentration time profile for all species has to match ($R^2 \geq 0.75$).

2.2 Development of the reduced multiphase DMS chemistry module

The oxidation of DMS in the tropospheric multiphase system leads to gaseous SO_2, sulfuric acid, $DMSO_2$, MSA, dissolved sulfate, or methane sulfonate through a sequence of steps (Hoffmann et al., 2016; Barnes et al., 2006). To cover the important intermediate oxidation steps, the reduction consists of six individual ones:

i) Consideration of main multiphase DMS oxidation pathways only;
ii) Lumping of simple reactions;
iii) Application of the pseudo-steady-state approximation;
iv) Neglect of production/oxidation of $DMSO_2$ in the aqueous phase;
v) Lumping of the aqueous-phase oxidation of MSIA;
vi) Reduction of oxidation/production pathways of specific chemical compounds unimportant in the gas or aqueous phase.

In the following, these mechanism reduction steps are outlined in more detail.

2.2.1 Main pathways of multiphase DMS oxidation

In the first reduction step, the main pathways of the multiphase oxidation of DMS and its oxidation products are investigated by analysing the time-resolved source and sink fluxes of all simulations. Main pathways are defined here as chemical production or loss processes that contribute more than 5 % to the overall average mass flux of the investigated compound. This analytical approach has proven its applicability in manual mechanism reduction (Deguillaume et al., 2010; Ervens et al., 2003). To provide a reduced mechanism applicable for a wide range of conditions, a chemical reaction is included in the reduced scheme in any case if the reaction is important under a single simulation condition. The present analyses provide the important DMS multiphase reaction pathways within the troposphere, similar to a former CAPRAM study dealing with multiphase DMS chemistry (Hoffmann et al., 2016). This approach determines the subsequent reduction steps.

2.2.2 Lumping of simple reactions

According to the current knowledge, in the gas phase, the oxidation of DMS or its oxidation products through H-abstraction lead to a corresponding peroxyl radical, which can be further oxidised into an alkoxy radical. Recently, it was suggested that the methylthiomethylperoxyl radical ($CH_3SCH_2O_2$) undergoes a rapid unimolecular H-shift (Wu et al., 2015; Berndt et al., 2019). The final stable product will be an oxidised organic sulfur compound that is characterised by an aldehyde and an organic hydrogen peroxide functionality. This compound can be oxidised in both gas and aqueous phase. Currently, the chemistry of this compound is not further investigated and therefore not treated in the CAPRAM-DM1.0. However, when more laboratory data are available, further mechanisms have to consider this chemistry to improve the modelling of DMS chemistry and its effects.

Gelöscht: dimethyl sulfone (
Gelöscht:)
Gelöscht: methane sulfinic acid (
Gelöscht:);
Gelöscht: leads
Gelöscht: then

Then, the DMS oxidation derived alkoxy radical can undergo thermal decomposition, a reaction with oxygen, or isomerization (Lightfoot et al., 1992). Nevertheless, the current gas-phase chemistry of the CAPRAM-DM1.0 is based on the MCMv3.2, which only treats thermal decomposition for the CH_3SCH_2O, i.e. C-C bond scission leading to the release of formaldehyde (HCHO). Since the analyses of the mass fluxes reveal that decomposition appears immediately after formation, further decomposition products are directly incorporated in every reaction in which an alkoxy radical is formed and the corresponding decomposition reaction is deleted (see Eq. R1-3).

$$CH_3SCH_2O_2 + NO \rightarrow CH_3SCH_2O + NO_2 \quad (R1)$$

$$CH_3SCH_2O \rightarrow CH_3S + HCHO \quad (R2)$$

$$\Sigma: CH_3SCH_2O_2 + NO \rightarrow CH_3S + HCHO + NO_2 \quad (R3)$$

Further simple integrated reactions correspond to reactions of DMS oxidation products in the aqueous-phase, i.e. reactions with water. The reduction of the CAPRAM3.0 has already revealed that peroxyl radical formations in the aqueous phase are not reaction-rate determining steps (Deguillaume et al., 2010). The same is true if reactions of oxidation intermediates occur with water only. Therefore, such aqueous-phase reactions are deleted and the products are directly implemented on the right-hand side of the affected reaction equations.

2.2.3 Application of the pseudo-steady-state-approximation

The oxidation of DMS by the OH radical and the Cl atom occurs not only through H-abstraction but also through the addition of these radicals onto the sulfur atom. The formed DMS adduct is unstable and decompose back into DMS and the corresponding radical if it is not stabilised through a reaction with oxygen, which adds to the sulfur atom (Barnes et al., 2006). It is possible that the DMS adduct reacts with NO_x or decomposes into methane sulfenic acid (CH_3SOH) and a methyl (CH_3) radical (Barnes et al., 2006; Yin et al., 1990). The first reduction step has already revealed that even at polluted coastlines, with NO_x concentrations above 10 ppb, NO_x related decompositions are not of atmospheric importance though. Overall, the analysis shows that oxygen is too reactive against DMS adducts.

The pseudo-steady-state-approximation (PSSA) is a fundamental way to deal with such reactive intermediates to derive the overall rate of a chemical reaction (Seinfeld and Pandis, 2006). The same method is applicable on the oxidation of DMSO, whose oxidation by the Cl atom also leads to a DMSO adduct.

$$\frac{d[DMS]}{dt} = -k_1[DMS][X] + k_2[DMS\text{-}X]; (X = OH \text{ or } Cl) \quad (1)$$

$$\frac{d[DMS\text{-}X]}{dt} = k_1[DMS][X] - k_2[DMS\text{-}X] - k_3[DMS\text{-}X][O_2] \quad (2)$$

$$\downarrow \frac{d[DMS]}{dt} = -\frac{k_1 k_3[O_2]}{k_2 + k_3[O_2]}[DMS][X] \quad (3)$$

As outlined, apart from the DMSO formation, a considerable amount of CH_3SOH is also formed through DMS adduct decomposition. Hence, a PSSA is also effective for this reaction sequence. The implemented rate constant of the DMS adduct decomposition within the CAPRAM-DM1.0 is given temperature independent. The same is true for the oxygen addition

Gelöscht: Classically
Gelöscht: then
Gelöscht: However
Gelöscht: The
Gelöscht: . Therefore
Gelöscht: with
Gelöscht: reactions
Gelöscht: decomposes
Gelöscht: (Barnes et al., 2006). It is recommended that the DMS adduct can also react with NO_x or decompose
Gelöscht: However, the
Gelöscht: . The

reaction. Therefore, under tropospheric conditions both reactions can be aggregated into first order reaction rate constants and merged. This merging gives a ratio between decomposition and oxygen addition that is implemented into the overall reaction (see Eq. R4-7).

$$CH_3SCH_3 + OH \rightleftarrows CH_3S(\text{-}OH)CH_3 \quad (R4)$$

$$CH_3S(\text{-}OH)CH_3 + O_2 \rightarrow CH_3S(O)CH_3 + HO_2 \quad (R5)$$

$$CH_3S(\text{-}OH)CH_3 \xrightarrow{O_2} CH_3SOH + CH_3O_2 \quad (R6)$$

$$\textbf{Σ:}\ CH_3SCH_3 + OH \xrightarrow{O_2} 0.9\ CH_3S(O)CH_3 + 0.9\ HO_2 + 0.1\ CH_3SOH + 0.1\ CH_3O_2 \quad (R7)$$

The PSSA is also applicable on the oxidation of DMSO by the Cl atom and for the methylthiyl radical (CH_3S) reaction with oxygen leading to the methylthio peroxyl radical (CH_3SOO), which has multiple reaction pathways. On the one hand, it can react with NO_x, decompose back into CH_3S, or SO_2 and CH_3, or rearrange itself into the sulfonyl radical (CH_3SO_2) on the other hand. The first reduction step reveals that the reaction with NO_x is negligible, since only a decomposition into SO_2 as well as the formation of the sulfonyl radical occur. For that reason, the PSSA is also applied to these two reaction pathways as well.

$$\frac{d[CH_3S]}{dt} = -k_1[CH_3S][O_2] + k_2[CH_3SOO] \quad (4)$$

$$\frac{d[CH_3SOO]}{dt} = k_1[CH_3S][O_2] - k_2[CH_3SOO] - k_3[CH_3SOO] \quad (5)$$

$$\downarrow \frac{d[CH_3S]}{dt} = -\frac{k_1k_3}{k_2+k_3}[CH_3S][O_2] \quad (6)$$

2.2.4 Neglect of production/oxidation of $DMSO_2$

Though the analysis of the sink and source fluxes has revealed that aqueous-phase chemistry contributes a little more than 5 % to $DMSO_2$ formation and oxidation, yet the modelled overall $DMSO_2$ formation and oxidation flux is negligible compared to that of MSIA. Furthermore, $DMSO_2$ has low reactivity towards OH oxidation in the gas ($k_{OH} < 3.0\times10^{-13}$ cm^3 $molecules^{-1}$ s^{-1}; Falbe-Hansen et al., 2000) and aqueous phase ($k_{OH} = 1.77\times10^7$ $l\ mol^{-1}$ s^{-1}; Zhu et al., 2003). Because of the low measured background gas-phase concentrations of $DMSO_2$ in the single-digit ppt range (Davis et al., 1998; Berresheim et al., 1998), the gas-phase oxidation of $DMSO_2$ by the OH radical is likely to be suppressed through methane oxidation ($k = 3.5\times10^{-15}$ to 6.4×10^{-15} cm^3 $molecules^{-1}$ s^{-1} in the temperature range of 270 to 298 K) plus dry and wet deposition can be assumed as the major atmospheric removal processes for $DMSO_2$. In order to shrink the mechanism, $DMSO_2$ production in the aqueous phase as well as the oxidation of $DMSO_2$ in both the gas- and aqueous phase are neglected as a consequence.

2.2.5 Lumping of the aqueous-phase oxidation of MSIA

In the fifth reduction step, the oxidation of MSIA in the aqueous phase has been simplified. Having a pK_a value of 2.28 (Wudl et al., 1967) MSIA occurs in both its non-dissociated and its dissociated form under atmospheric aerosol as well as cloud conditions. At this point, the only important oxidant for the non-dissociated form is ozone. The deprotonated MSIA reacts with

Gelöscht: a
Gelöscht: valid
Gelöscht: , which leads
Gelöscht:). The CH_3SOO
Gelöscht: It
Gelöscht:).
Gelöscht: . Only
Gelöscht: Therefore
Gelöscht: An
Gelöscht: . However,
Gelöscht: .
Gelöscht:). Therefore,
Gelöscht: Consequently, in
Gelöscht: is neglected and also
Gelöscht: MSIA has a pK_a value of 2.28 (Wudl et al., 1967). Therefore, it
Gelöscht: The

both the OH and the Cl_2^- radical via an electron transfer reaction into aqueous CH_3SO_2. The formed CH_3SO_2 further reacts with O_2 into the methylsulfonylperoxyl radical ($CH_3SO_2O_2$) or decomposes into the CH_3 radical and dissolved SO_2 that is immediately dissociated into HSO_3^-/SO_3^{2-}. Because of its high atmospheric abundance, in our study the O_2 concentration is modelled to be almost constant within the tropospheric aqueous phase. Furthermore, both reaction rate constants are implemented as temperature-independent, which is why a ratio between these reactions can be calculated. The reaction of the $CH_3SO_2O_2$ with MSIA yields MSA and the methylsulfonylalkoxyl radical (CH_3SO_3). The latter decomposes into the CH_3 radical and sulfate. Both reactions occur immediately. As a whole, all reactions of the deprotonated MSIA oxidation can be summarized into one reaction for each oxidant, covering the overall MSIA loss (see below Eq. R8-13 for MSIA oxidation by the OH radical).

Gelöscht: . Therefore,

Gelöscht: later

Gelöscht: Consequently

$$CH_3SO_2^- + OH \xrightarrow{O_{2,aq},\, H_2O} 0.9\ CH_3SO_{2,aq} + 0.9\ OH^- + 0.1\ CH_3O_{2,aq} + 0.1\ HSO_3^- - 0.1\ H_2O \quad \text{(R8)}$$

$$CH_3SO_{2,aq} \xrightarrow{O_{2,aq}} SO_{2,aq} + CH_3O_{2,aq} \quad \text{(R9)}$$

$$CH_3SO_{2,aq} + O_{2,aq} \rightarrow CH_3SO_2O_{2,aq} \quad \text{(R10)}$$

$$CH_3SO_2^- + CH_3SO_2O_{2,aq} \rightarrow CH_3SO_3^- + CH_3SO_{3,aq} \quad \text{(R11)}$$

$$CH_3SO_{3,aq} \xrightarrow{O_{2,aq}} SO_{3,aq} + CH_3O_{2,aq} \quad \text{(R12)}$$

$$\textbf{Σ:}\ CH_3SO_2^- + OH \xrightarrow{O_{2aq},\, H_2O}$$
$$CH_3O_{2,aq} + 0.235\ HSO_3^- + 0.765\ CH_3SO_3^- + 0.765\ SO_{3,aq} + 0.9\ OH^- - 0.765\ CH_3SO_2^- - 0.235\ H_2O \quad \text{(R13)}$$

2.2.6 Reduction of oxidation/production pathways of specific chemical compounds less important in gas or aqueous phase

In the last reduction step, the mechanism is again analysed for residual multiphase chemistry pathways to be combined. These are, for example, reactions of radicals that now treat only one fast reaction sequence and thus are merged into the previous reaction.

2.3 Development of the reduced multiphase halogen chemistry module

The goal of reducing the CAPRAM-HM3.0 is to enable the description of key halogen chemistry affecting ozone, NO_x, SO_2, VOCs, and OVOCs by a reduced mechanism that almost conserves the concentration time profile of the reactive halogen compounds listed earlier. The following three reduction steps are applied to achieve this:

i) Consideration of chemical production or loss processes that contribute more than 5 % to the overall mass flux of halogen compounds only;

ii) Lumping of simple reaction sequences;

iii) Neglect of oxidation/production of specific chemical species modelled to be unimportant in tropospheric gas or aqueous-phase chemistry.

In the following, these mechanism reduction steps are outlined in more detail.

2.3.1 Main pathways of multiphase halogen chemistry

An analysis of the main pathways is performed in a similar manner as for the multiphase DMS chemistry. However, the development of a DMS-like stepwise oxidation scheme is impossible, due to important side pathways and interconnections with other chemical subsystems, e.g. NO_x or HO_x chemistry and various halogen cross interactions (Saiz-Lopez and von Glasow, 2012). Furthermore, halogen multiphase chemistry is characterised by large differences in aqueous-phase oxidation within aerosol particles and cloud droplets (Bräuer et al., 2013; Hoffmann et al., 2019b; von Glasow et al., 2002a). Therefore, an appropriate reduced representation of multiphase halogen chemistry requires the focus of the reduction on different halogen species. Hence, the determination of the main pathways is done for a huge number of halogen compounds covering key halogen atoms, halogen radicals, halogen nitrates, halogenated organics such as halogenated aldehydes, as well as halogen oxo-carboxylic acids. Again, as for the CAPRAM-DM1.0 reduction, a chemical reaction is included in the reduced scheme in any case if the reaction is important under a single simulation condition.

As already modelled in other studies, the analyses revealed that the Cl atom is an important oxidant for VOCs and OVOCs, e.g. alkanes, non-oxidised aromatic compounds, alcohols, and aldehydes (e.g. Hoffmann et al., 2019a; Sherwen et al., 2016; Xue et al., 2015; Pechtl and von Glasow, 2007). In order to restrict computational costs, chemical mechanisms in state-of-the-art CTM applications do not contain a high number of organic compounds as the near-explicit MCM. In order to still represent the chemistry of important VOCs and OVOCs in CTMs, species of the same compound classes or of equal reactivity are typically merged into 'lumped' species in condensed mechanisms applied in CTMs (Baklanov et al., 2014). Based on these limitations, the reduced CAPRAM-HM3.0 has to be linkable with the chemical mechanisms used in CTMs. A first screening on treated VOCs and OVOCs in the gas-phase chemical mechanisms MOZART4.0 (Schultz et al., 2018), RACM2 (Goliff et al., 2013), MECCA (Jöckel et al., 2016), GEOS-Chem (Wang et al., 2019), and SAPRC11 (Yan et al., 2019) has been performed for the main VOCs and OVOCs for this purpose. It has been shown that most of the mechanisms contain the same set of primary VOC/OVOC compound classes, for example, aldehydes and alcohols are often treated up to a carbon number of two. As outlined in Sect. 3, the gas-phase mechanism MOZART4 is chosen for further modelling with COSMO-MUSCAT. As a result, only the Cl atom oxidation of the lumped VOCs and OVOCs that are treated within MOZART4 are considered further. These sets can be applied to the other mechanisms, but have to be adjusted if species are missing. The chosen reaction rate constant is based on the first lumped product. As the k's are higher with longer carbon chain, this approach is suitable, as it gives a lower limit of the reaction rate constant. Thus, no overestimation will occur. However, when the simulations with the reduced version of the CAPRAM-HM3.0 are compared to the simulations with the non-condensed CAPRAM-HM3.0 this approach results in lower HCl but higher ClO formation.

Gelöscht: to be

Gelöscht: . However, because of limited computational costs, state-of-the-art chemical mechanisms of CTMs do not contain a high variability of organic compounds as the near-explicit MCM. In order to still represent the chemistry of important VOCs and OVOCs in CTMs, species of the same compound classes or of equal reactivity are typically merged into 'lumped' species in condensed mechanisms applied in CTMs

Gelöscht: (Baklanov et al., 2014)

Gelöscht: . Because of these limitations, the reduced CAPRAM-HM3.0 has to be linkable with the chemical mechanisms used in CTMs. Therefore, a first screening on treated VOCs and OVOCs in the mechanisms MOZART4.0 (Schultz et al., 2018), RACM2 (Goliff et al., 2013), MECCA (Jöckel et al., 2016), GEOS-Chem (Wang et al., 2019),and SAPRC11 (Yan et al., 2019) has been performed for the main VOCs and OVOCs. As a result, only the Cl atom oxidation of the lumped VOCs and OVOCs that are treated within all of these mechanisms is considered further. However, this approach results in lower HCl but higher ClO formation when the reduced version of the CAPRAM-HM3.0 is compared to the non-condensed MCMv3.2/CAPRAM4.0/ CAPRAM-DM1.0/CAPRAM-HM3.0.¶

2.3.2 Lumping of simple reaction sequences

In the gas-phase, halogen atoms react rapidly with O_2- and CO-yielding unstable molecules that, as the model simulations show, immediately decompose again. Still, within the CAPRAM-HM3.0, specific oxidation pathways lead to unstable molecules (e.g. the oxidation of halogenated oxidised organics). Consequently, in every reaction in which such an unstable molecule occurs as a product it is replaced by the halogen atom and O_2 or CO.

The further processing of halogenated organic peroxyl radicals in the gas phase result in halogenated organic alkoxy radicals. As for DMS, the halogenated organic alkoxy radical decomposition, which is modelled not to be the overall rate-determining step is integrated into these reactions. Overall, the recombination of the halogenated organic peroxyl radicals with other organic peroxyl radicals (RO_2) leads exclusively to halogenated carbonyls (see Eq. R14-17).

$$XCH_2O_2 + RO_2 \rightarrow 0.2\ XCHO + 0.2\ XCH_2OH + 0.6\ XCH_2O;\ (X{=}Cl \text{ or } Br) \quad (R14)$$

$$XCH_2OH + OH \xrightarrow{O_2} XCHO + HO_2 + H_2O \quad (R15)$$

$$XCH_2O \xrightarrow{O_2} XCHO + HO_2 \quad (R16)$$

$$\Sigma: XCH_2O_2 + RO_2 \xrightarrow{O_2,\ OH} XCHO + 0.8\ HO_2 \quad (R17)$$

If the analysis of the main pathways leads to only one further reaction of a compound being left, this reaction has been screened for two criteria: (i) Does the follow-up reaction occur rapidly and (ii) is the overall concentration of the product so low that it would not be a significant interfering factor for the modelling. If both issues are true, the overall reaction is merged together. For example, the recombination of IO in the aqueous phase leads to iodite (HIO_2) which is an intermediate in the conversion between iodide and iodate (IO_3^-). It is quickly oxidized into iodate by H_2O_2, which is ubiquitous in the marine atmospheric multiphase (Jacob and Klockow, 1992; Benedict et al., 2012; Kim et al., 2007; Yuan and Shiller, 2000), and also has a very low modelled concentration. Overall, the IO recombination together with the oxidation of HIO_2 by H_2O_2 results in iodate (see Eq. R18-20).

$$IO_{aq} + IO_{aq} + H_2O \rightarrow HOI_{aq} + HIO_{2,aq} \quad (R18)$$

$$HIO_{2,aq} + H_2O_2 \rightarrow H^+ + IO_3^- + H_2O \quad (R19)$$

$$\Sigma: IO_{aq} + IO_{aq} \xrightarrow{H_2O_{2,aq}} HOI_{aq} + H^+ + IO_3^- \quad (R20)$$

2.3.3 Neglect of oxidation/production of specific chemical species modelled to be less important in tropospheric gas or aqueous-phase chemistry

For the reduction of the halogen chemistry part, less important chemical halogen species are defined as such with low (< 0.1ppt for non-radical species) modelled concentrations or high chemical stability ($k_{OH} < 6.4 \cdot 10^{-15}$ cm^3 $molecules^{-1}$ s^{-1} that is the k_{298} of methane; Atkinson et al., 2006) in order that their non-consideration does not affect the concentrations of the target species under conditions in the lower troposphere. While typical species with a rather high chemical stability are chlorinated and brominated organics (e.g. CH_3Cl), except bromoform ($CHBr_3$), for which oxidation in the lower troposphere is negligible

Gelöscht: Typical

Gelöscht: . Typical

typical species with low modelled concentrations are oxidised halogenated organics derived from the OH oxidation of methylated halogens (e.g. ICHO or ICIO from CH_3I oxidation). As the reduced mechanism is developed to deal with tropospheric multiphase chemistry, the oxidation of such species is not treated within the reduced CAPRAM-HM3.0.

Gelöscht:), precursors of which are mainly removed through photolysis.

2.4 Evaluation of the reduction steps

By comparing simulations with the reduced and with the original CAPRAM-DM1.0 and CAPRAM-HM3.0 added to the multiphase chemistry mechanism MCMv3.2/CAPRAM4.0 the performed reduction steps are evaluated. Being referred to as 'Pristine', 'Breeze' and 'Outflow' scenario the evaluation simulations are carried out for 45° latitude with a relative humidity of 70 % under pristine ocean (Hoffmann et al., 2016) and polluted coastal conditions (Hoffmann et al., 2019a). While the abbreviations 'Pristine' and 'Breeze' stand for the scenarios of the pristine ocean as well as of an air-sea breeze circulation system, 'Outflow' represents the scenario of the advection of polluted air masses over a marine environment. The simulations run for 96 hours in total including cloud passages between 11 am and 1 pm and between 11 pm and 1 am in both scenarios 'Pristine' and 'Outflow' as well as between 1 pm and 2 pm in the third scenario 'Breeze'. The longer simulation time compared to that of previous simulations was chosen in order to investigate the effect of a longer modelling time on concentration divergence. The evaluation by these three simulation cases is appropriate, because both reduced mechanisms contain reactions that were both important and not important under the different performed simulations. Thus, other possible evaluation simulations would also treat reactions that are not necessary under specific conditions. Regardless of the simulation setup a similar performance is expected as a consequence.

Gelöscht: The evaluation of the performed reduction steps is achieved by

Gelöscht: . The evaluation

Gelöscht:

Gelöscht: is

Gelöscht: abbreviation

Gelöscht: scenario, the term 'Breeze' stands for the scenario

Gelöscht: and the term

Gelöscht: and include

Gelöscht: the

Gelöscht: and

Gelöscht: has been

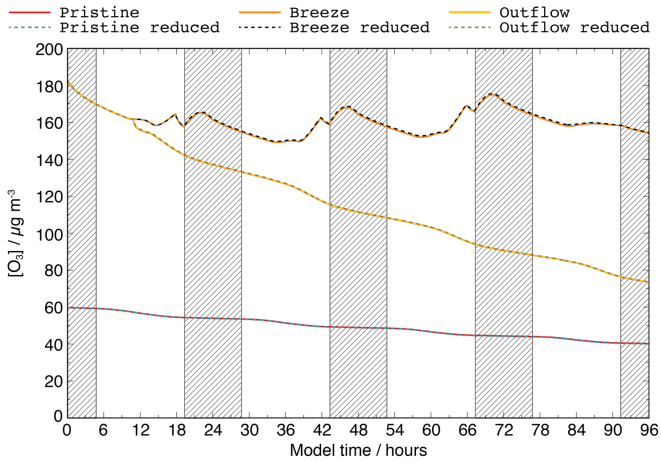

Figure 1 Modelled concentrations of ozone within the scenarios 'Pristine', 'Breeze', and 'Outflow' compared between the simulations with the full (solid lines) and reduced (dotted lines) CAPRAM-DM1.0 and CAPRAM-HM3 mechanism. Grey shaded periods denote the night periods.

The investigation of the modelled evolution of the concentration time profile of ozone is shown in Figure 1, revealing an excellent agreement for all the scenarios ($R^2 = 1$). Moreover, the average ozone concentrations diverge by less than 5 % throughout the entire modelling time, demonstrating that the reduced mechanism is able to reproduce the modelled ozone concentrations of the complex mechanism.

The same analysis is performed for other air pollutants and key aerosol compounds important for air quality modelling, which are NO, NO_2, SO_2, HNO_3, HCl, and DMS in the gas-phase, and also the dry mass as well as the organic mass of the aerosols together with nitrate, sulfate, chloride, and methane sulfonate. Furthermore, the analysis is performed for reactive halogen compounds and the OH, NO_3, and HO_2 radicals. Table 1 shows the average percentage deviation for these chemical species. The main target species, except MSA in the 'Breeze' scenario, do not exceed the 5 % threshold, what is also true for the OH, HO_2, and NO_3 radical in both the gas and aqueous phases. Even for reactive halogen compounds, the deviation rarely exceeds the 5 % mark.

However, especially in the 'Outflow' scenario, reactive bromine compounds exceed the 10 % threshold, being caused by missing brominated organics in the reduced CAPRAM-HM3.0 that trap the bromine from further reaction. For example, 3 ppt of bromine are trapped on average in brominated alcohols formed through Br atom-related oxidation of alkenes and further RO_2 recombination. Regarding the low concentration and the fact that alcohols are further oxidized into carbonyls, only the formation of brominated carbonyls is considered in the reduced CAPRAM-HM3.0 to minimize the mechanism. Consequently, the bromine radical is recycled faster by the following reaction sequence:

Gelöscht: Figure 1

Gelöscht: scenario

Gelöscht: . This demonstrates

Gelöscht: . These

Gelöscht: The

Gelöscht: can be found in Table 1.¶

Gelöscht: . This

Gelöscht: . This is

Gelöscht: is

$$Br_g + C_2H_{4,g} \rightarrow \rightarrow \rightarrow BrCHO_g + 1.8\ HO_2 + HCHO - CH_3O_2 \quad (R21)$$

$$BrCHO_g \rightleftharpoons BrCHO_{aq} \quad (R22)$$

$$BrCHO_{aq} \rightarrow H^+ + Br^- + CO_{aq} \quad (R23)$$

$$Br_g + O_{3,g} \rightarrow BrO_g + O_{2,g} \quad (R24)$$

$$BrO_g + HO_{2,g} \rightarrow HOBr_g + O_{2,g} \quad (R25)$$

$$HOBr_g \rightleftharpoons HOBr_{aq} \quad (R26)$$

$$HOBr_{aq} + Br^- + H^+ \rightleftharpoons Br_{2,aq} + H_2O \quad (R27)$$

$$Br_{2,aq} \rightleftharpoons Br_{2,g} \quad (R28)$$

$$Br_{2,g} + h\nu \rightarrow Br_g + Br_g \quad (R29)$$

Overall, this increases the modelled concentrations of reactive bromine compounds, particularly in the afternoon after cloud occurrence and under high alkene as well as low ozone. However, the evolution of the concentration time profile fits very well (R^2 = 0.98, 0.95, 0.97, and 0.75 for Br, BrO, HOBr, and Br_2, respectively). Apart from bromine, larger differences also occur for HOCl in the 'Breeze' and 'Outflow' scenarios. This is related to the restricted VOC and OVOC oxidations within the reduced CAPRAM-HM3.0 in order to match the condensed gas-phase chemistry mechanisms implemented in the CTMs. Therefore, the HCl concentration is more than 2 % smaller and more Cl atoms react with ozone into ClO that quickly reacts with HO_2 to yield HOCl. As opposed to Br_2 formation by HOBr, the higher HOCl does not necessarily lead to a higher modelled Cl_2 formation, which is related to the significant higher chloride content in sea spray aerosols compared to bromine. It so concludes that the enhanced HOCl seems not to be a driving factor for Cl_2 formation under pristine ocean conditions.

Finally, the methane sulfonate anion (MS^-) is around one quarter lower in the 'Breeze' scenario, which is caused by the Cl_2^- radical oxidation. This reduction revealed that the Cl_2^- radical is an important oxidant for oxalic acid and MS^-. Consequently, other OVOC oxidations are discarded for treatment in the reduced CAPRAM-HM3.0. The modelled Cl_2^- radical concentrations are around one order of magnitude higher in the 'Breeze' scenario compared to the 'Pristine' and 'Outflow' scenarios, resulting in much higher MS^- oxidation rates. Yet, the development of the MS concentration-time profile agrees very well (R^2 = 1). In addition, the MSA concentration deviates by only 6% at the end of the model simulations.

Since, the evaluation reveals that the reduced mechanism system is able to reproduce similar results as the full mechanism system, it is basically appropriate for implementation into CTMs. The reduced mechanisms of the CAPRAM-DM1.0 and CAPRAM-HM3.0 will be called CAPRAM-DM1.0red and CAPRAM-HM3.0red in the following text.

Also, the modelling studies reveal that computational (CPU) time is decreased, especially within the scenario 'Pristine' (see Figure 2). Compared to the base runs, the CPU time is reduced by 16 %, 5 %, and 6 % in the scenarios 'Pristine', 'Breeze', and 'Outflow', respectively. Overall, the CPU time reduction is low, but is accounted to the usage of the MCMv3.2 and CAPRAM4.0 that still treats more than 21000 reactions. Furthermore, the calculation of microphysical processes consumes a huge amount of CPU time, too. Therefore, the still high CPU time is caused by requirements of the standard multiphase chemistry mechanism. These high requirements cover the reduction of CPU time achieved by the reduction efforts. Very low

Gelöscht: conditions compared to an urban environment.

Gelöscht: reacts

Gelöscht: However, as

Gelöscht: too high

Gelöscht: because of

Gelöscht: actually

Gelöscht: However

Gelöscht: evolution

Gelöscht: ·

Gelöscht:

Gelöscht: matches

Gelöscht:) and

Gelöscht: relative difference

Gelöscht: modelling is only a deviation of 6 % from the overall concentration

Gelöscht: Overall

Gelöscht: . Therefore,

Gelöscht: The

Gelöscht: also

Gelöscht: conserved

Gelöscht: Figure 2

Gelöscht: Urban outflow'

Gelöscht: Consequently

Gelöscht: required overlay

Gelöscht: CPU time consumption from

Gelöscht: . The higher time consumption

initialised NO_x concentrations in the pristine scenario induced the stronger decrease of computation time unlike the other scenarios. When it comes to the scenarios 'Breeze' and 'Outflow', the high initialised NO_x concentrations effectively suppress halogen radical cross-interactions in the gas phase. These cross-interactions are very fast and establish reaction cycles that induces high fluxes. Therefore, under high NO_x conditions, much lower CPU time is required to solve these reactions. However, in the scenario 'Pristine', the rapid occurring gas-phase cross-interactions of halogen radicals still exist hindering stronger amplified CPU time reductions.

Gelöscht: 'Pristine' compared

Gelöscht: Urban outflow' is caused by the very low initialised NO_x concentrations. Within the scenarios 'Breeze' and 'Urban outflow'

Gelöscht: equilibria

Gelöscht: thus increase the CPU time.

Gelöscht: halogen multiphase chemistry processes.

Gelöscht: scenario

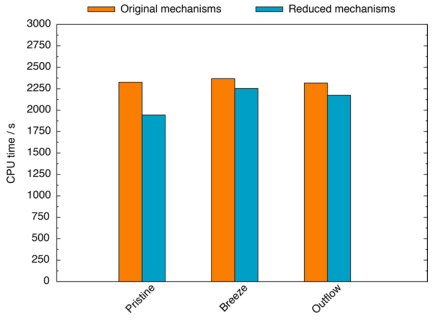

Figure 2 Required CPU time within the scenarios 'Pristine', 'Breeze', and 'Outflow' considering the original multiphase chemistry mechanism system MCMv3.2/CAPRAM4.0/CAPRAM-DM1.0/CAPRAM-HM3.0 and the multiphase chemistry mechanism system with the CAPRAM-DM1.0red and CAPRAM-HM3.0red. The CPU costs include gas and aqueous-phase chemistry, microphysics, model initialization, and output.

2.5 Uncertainties of the new chemistry scheme

The downsizing of the CAPRAM-HM3.0 and CAPRAM-DM1.0 solely considering the most important reactions, has led to two new reduced mechanisms, which consist of reactions that sensitively impact the model outcome. Hence, the uncertainty of these reactions can be crucial for the model results. A discussion of the uncertainties of the mechanism development has already been performed in the previous papers describing the mechanism development of the CAPRAM-HM2.0 (Bräuer et al., 2013), CAPRAM-HM3.0 (Hoffmann et al., 2019a; Hoffmann et al., 2019b) and CAPRAM-DM1.0 (Hoffmann et al., 2016) as well as in the cited laboratory work. That's why only a short discussion is given here.

For the oxidation of DMS in the gas-phase, most of the rate constants are based on recommended values of the IUPAC database (http://iupac.pole-ether.fr/) or JPL panel (Burkholder et al., 2015). Nevertheless, the application of the PSSA has modified the oxidation pathways, in particular the OH-addition reaction for DMS. The incorporation of the oxygen concentration might increase the uncertainty influencing the DMSO formation rate. As oxygen is in excess under tropospheric conditions and the oxygen concentration is treated in the new derived reaction rate constant specifically, minor changes are expectable. By contrast, no recommended values are available for the aqueous-phase reaction rate constants and can hence be stated as more uncertain (Hoffmann et al., 2016). Further laboratory work is required to minimize their uncertainties.

Regarding the CAPRAM-HM3.0red, certain gas-phase reaction rate constants of the halogen chemistry are based on recommended values (Atkinson et al., 2006, 2007; Atkinson et al., 2008; Burkholder et al., 2015). However, for the oxidation of VOCs/OVOCs by the Cl or Br atom often only one reaction rate constant has been measured by laboratory studies. This is also true for many aqueous-phase chemistry reactions. The highest uncertainties are related to iodine chemistry. Here, often reaction rate constants, which might be of high atmospheric significance are based on estimations, only.

3 First applications in chemistry transport modelling with COSMO-MUSCAT

The CTM applied in this study is MUSCAT (Wolke et al., 2004; Wolke et al., 2012). It is either coupled to the weather model COSMO (Consortium for Small Scale Modelling; Steppeler et al., 2003; Baldauf et al., 2011) or ICON (ICOsahedral Non-hydrostatic; Zängl et al., 2015), which provide all required meteorological fields (e.g. wind, temperature, relative humidity, liquid water content, and precipitation) to MUSCAT that are necessary to calculate the advection, diffusion, and physico-chemical interaction of particles and trace gases. While the emission files of gases and aerosols within MUSCAT are generated by pre-processors, the chemical mechanism is imported from ASCII files, which allows for changes without code recompilation. In terms of dust (Heinold et al., 2007) and sea spray aerosols (Barthel et al., 2019), emissions can also be calculated online.

3.1 Implementation of the CAPRAM-DM1.0red and the CAPRAM-HM3.0red into COSMO-MUSCAT

Within the present study, the model framework COSMO-MUSCAT is used, which has recently been extended to be able to treat multiphase chemistry in clouds (Schrödner et al., 2014; Schrödner et al., 2018). The chemistry of DMS and detailed halogen chemistry are still missing. In order to consider them, the mechanisms CAPRAM-DM1.0red and CAPRAM-HM3.0red are implemented into the atmospheric multiphase chemistry core of COSMO-MUSCAT, in which gas-phase chemistry is described by the MOZART4 mechanism (Schultz et al., 2018) and aqueous-phase chemistry by the CAPRAM3.0red mechanism (Deguillaume et al., 2010). MOZART4 treats comprehensive halogen and DMS gas-phase chemistry that is replaced, as well as specific lumped VOCs and OVOCs. As outlined, these lumped species notably cover the VOCs and OVOCs, where the oxidation by the Cl atom is significant. To link the CAPRAM-HM3.0red to the MOZART4, the overall rate constants of the Cl atom are derived for the following lumped VOCs: (i) BIGALK, (ii) ALKOH, (iii) C_2H_5CHO, (iv) BIGALD1, (v) XYL, and (vi) BZALD. The lumped species C_2H_5CHO represents all aldehydes with more than three carbon atoms and is newly implemented into MOZART4, which makes it consistent with CAPRAM3.0red. Accordingly, the oxidation pathways are adjusted and the C_2H_5CHO oxidation by the OH radical and the Br atom has also been implemented.

$$C_2H_5CHO + OH/Cl/Br \rightarrow 1.5\ CH_3C(O)O_2 + H_2O/HCl/HBr \quad \text{(R30)}$$

Table 2 provides the implemented reaction rate constants of lumped VOCs. A full mechanistic description of the adjusted CAPRAM-DM1.0red and CAPRAM-HM3.0red is given in the supplement (Table S2-S10).

Gelöscht: state-of the art
Gelöscht: currently
Gelöscht: at TROPOS
Gelöscht: (ICOsahedral Non-hydrostatic; Zängl et al., 2015), providing all required meteorological data fields (e.g.
Gelöscht: The
Gelöscht: and
Gelöscht: (Heinold et al., 2007)
Gelöscht: (Barthel et al., 2019)
Gelöscht: Therefore
Gelöscht: particularly
Gelöscht: reduced
Gelöscht: 0
Gelöscht: Table 2

The recombination of halogenated peroxyl radicals as described above is adjusted to fit into MOZART4. In the MCM, this recombination is implemented for the sum of all RO_2, whereas in MOZART4 it is often only for CH_3O_2 and $CH_3C(O)O_2$. The ratio of the MCM is applied in the RO_2 recombination reaction, but RO_2 is considered as CH_3O_2. The reaction rate constant is adopted from the corresponding CAPRAM-HM2.0 reaction (Bräuer et al., 2013).

$$XCH_2O_2 + CH_3O_2 \rightarrow XCHO + 1.4\ HO_2 + 0.8\ HCHO + 0.2\ CH_3OH \qquad (R31)$$

Currently, the calculation of aqueous-phase chemical processes in MUSCAT is limited to cloudy conditions, i.e. a liquid water content (LWC) of above 0.01 g m^{-3}. Furthermore, the chemical equilibria are treated dynamically as forward and backward reactions, which represents a critical challenge for the numerical solver. Deviations from the equilibrium state of rapid phase transfers and dissociations may lead to large chemical fluxes and hence small timesteps, i.e. high computational costs. The robustness of the numerical integration is particularly affected at phase boundaries between cloud and non-cloud grid cells. Pre-balancing the aqueous-phase equilibria of CO_2, NH_3, HNO_3, HCl, SO_2, H_2SO_4, and organic acids in cloud-free grid cells at a predefined threshold LWC under cloud conditions (0.01 g m^{-3}, abbreviated with 'sub#1') results in a robust numerical integration. This approach is similar to the pH calculation parameterisation described by Alexander et al. (2012) but is designed to describe cloud chemistry and its effect on cloud droplet acidity in detail. In order to describe the activation of reactive halogen compounds by the chemistry in deliquesced aerosols, an additional sub-mechanism is introduced, assuming an LWC of 10 µg m^{-3} in cloud-free grid cells (abbreviated with 'sub#2'). A schematic on how both sub-mechanisms enable the multiphase chemistry treatment in COSMO-MUSCAT can be seen in Figure 3.

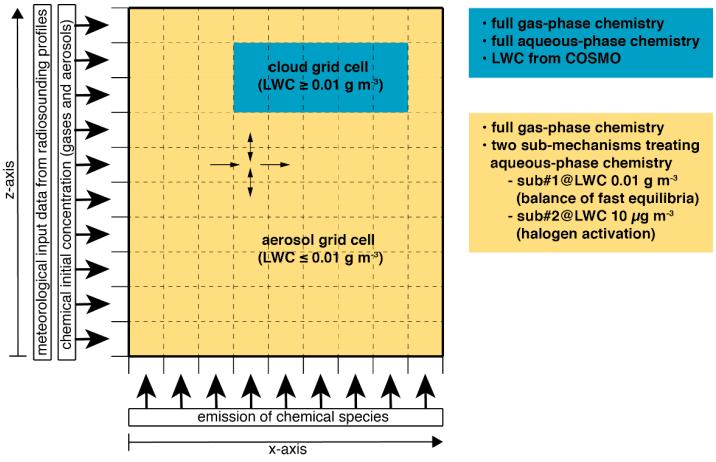

Figure 3 Schematic representation of the multiphase chemistry treatment in COSMO-MUSCAT in an idealised 2D-simulation.

The main halogen chemistry reactions treated in the 'sub#2' sub-mechanism are:

Gelöscht: Therefore, the

Gelöscht: HM2 reaction (Bräuer et al., 2013)

Gelöscht: A robust numerical integration can be achieved by pre

Gelöscht:).

Gelöscht: Figure 3

Gelöscht: that are

$XY_g \rightleftharpoons XY_{aq}$ (with X = Cl, Br or I, and Y = Cl, Br or I) (R32)

$HOX_g \rightleftharpoons HOX_{aq}$ (R33)

$XNO_{3,g} \rightleftharpoons XNO_{3,aq}$ (R34)

$HOX_{aq} + Y^- + H^+ \rightleftharpoons XY_{aq} + H_2O$ (R35)

$XY_{aq} + Z^- \rightleftharpoons XZ_{aq} + Y^-$ (with Z = Cl, Br or I) (R36)

$HX_{aq} \rightleftharpoons H^+ + X^-$ (R37)

$HNO_{3,g} \rightleftharpoons HNO_{3,aq}$ (R38)

$N_2O_{5,g} \rightleftharpoons N_2O_{5,aq}$ (R39)

$N_2O_{5,aq} \rightarrow NO_2^+ + NO_3^-$ (R40)

$NO_2^+ + H_2O \rightarrow NO_3^- + 2\,H^+$ (R41)

$NO_2^+ + Cl^- \rightleftharpoons ClNO_{2,aq}$ (R42)

$XNO_{3,aq} + H_2O \rightarrow HOX_{aq} + HNO_{3,aq}$ (R43)

$HSO_3^- + HOX_{aq} \rightarrow HSO_4^- + X^- + H^+$ (R44)

$H_2O_{2,g} \rightleftharpoons H_2O_{2,aq}$ (R45)

$HSO_3^- + H_2O_2 + H^+ \rightarrow SO_4^{2-} + 2\,H^+ + H_2O$ (R46)

The activation of halogens is in accordance with the heterogeneous reactions used in other CTMs (Badia et al., 2019; Hossaini et al., 2016; Jöckel et al., 2016; Long et al., 2014; Muniz-Unamunzaga et al., 2018; Saiz-Lopez et al., 2014; Wang et al., 2019). However, the 'sub#2' sub-mechanism is able to treat pH-dependent processes, including (i) the activation of reactive halogen compounds and (ii) sulfite formation induced by HOX and H_2O_2 in the MBL online. Tables S8-S10 in the supplement provide here a complete overview of the treated aqueous-phase reactions and phase transfers in both the 'sub#1' and the 'sub#2' sub-mechanism in the CAPRAM-DM1.0red and CAPRAM-HM3.0red. Overall, COSMO-MUSCAT now represents the CTM with the most detailed description of marine multiphase chemistry (see Figure 4).

Gelöscht: A

Gelöscht: is provided in the supplement in Tables S8-S10

Gelöscht: Figure 4

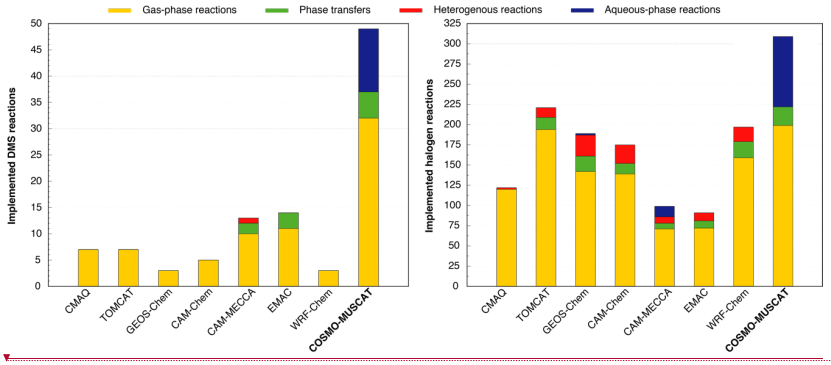

Figure 4. Comparison of applied tropospheric DMS and halogen chemistry mechanisms within the chemical transport models: CMAQ (Muniz-Unamunzaga et al., 2018), TOMCAT (Hossaini et al., 2016), Geos-Chem (Wang et al., 2019), CAM-Chem (Saiz-Lopez et al., 2014), CAM-MECCA (Long et al., 2014), EMAC (Jöckel et al., 2016), and WRF-Chem (Badia et al., 2019). EMAC is a chemistry climate model that can be run as a CTM.

3.2 Evaluation of the 2D-implementation

The evaluation of the implementation is carried out by two 2D-simulations (x-z-cross section) dealing with a 'pristine ocean' scenario under two meteorological conditions, namely a convective and stable atmospheric layer, which will result in modelled convective and stratiform clouds, respectively. Both scenarios are further applied to investigate DMS oxidation in more detail. The evaluation of the implementation is performed by investigating the activation of halogen compounds in the MBL and comparing it with available ambient measurements and other model data. 2D-simulations are preferred over 3D ones because they are based on the same meteorological dynamics but have one lower degree of freedom. As a result, the system under investigation is less computationally expensive. Additionally, 2D-simulations enable a comprehensive understanding of multiphase chemistry in the atmospheric column, including vertical mixing processes.

3.2.1 2D model setup

The chemical model setup, i.e. the initialisation, deposition, and emission of trace gases and VOCs as well as the aerosol composition to describe the atmospheric composition of the pristine ocean, is the same as the one used during the mechanism reduction. Because of the lumped species within MOZART4, specific VOC emissions are merged. Table S1 in the supplement provides the emission rates. Initialised concentrations of gas-phase and aerosol compounds represent ground values and are distributed vertically as constant mass mixing ratios within the model domain of MUSCAT. These values are used as constant boundary conditions on the left-hand side of the model domain (see Figure 3).

Two different meteorological cases are simulated: One with a high diversity of clouds and a strong vertical wind velocity (further called 'unstable meteorological condition') and another with a stable cloud cover at the top of the marine boundary

Gelöscht:

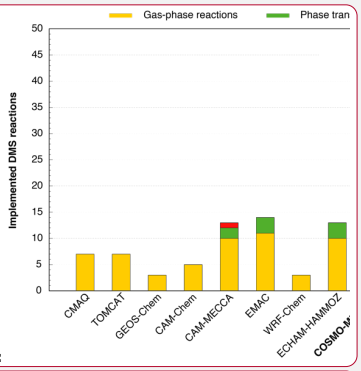

Gelöscht: 4

Gelöscht: , TOMCAT (Hossaini et al., 2016), Geos-Chem (Wang et al., 2019), CAM-Chem (Saiz-Lopez et al., 2014), CAM-MECCA (Long et al., 2014), EMAC (Jöckel et al., 2016), WRF-Chem (Badia et al., 2019), and ECHAM-HAMMOZ (Schultz et al., 2018).¶
3.2 Verification

Gelöscht: verification

Gelöscht: . These conditions

Gelöscht: Moreover, this scenario is

Gelöscht: in order

Gelöscht: verification

Gelöscht: for

Gelöscht: together. The emission rates are provided

Gelöscht: (Table S1).

Gelöscht: Figure 3

layer and a weak vertical wind velocity (further called 'stable meteorological condition'). These two different meteorological 'pristine ocean' simulations are chosen to evaluate the numerical robustness of the model. The meteorological scenarios are initialised using radiosonde profiles ('unstable meteorological condition' station: Camborne Observations, station identifier: 3808 on 12Z 21.06.2016 and 'stable meteorological condition' station: GVAC Sal Observations, station identifier: 8594 on 12Z 12.06.2017), which can be read and processed by COSMO by default and are considered constant meteorological boundary conditions on the left-hand side of the model domain (see Figure 3).

The model domain spans 400 horizontal grid cells with a resolution of 1.11 km per grid cell and 100 vertical levels with a resolution of 100 m. Whereas COSMO is run on the full domain, only the inner 200 horizontal grid cells (overall 222 km) and lowermost 15 vertical levels (overall 1500 m) are used for the multiphase chemistry simulations with MUSCAT. MUSCAT uses a smaller domain as the interaction is sufficient to describe the multiphase chemistry in the marine boundary layer (MBL). Furthermore, the height of the MBL is often lower than 1000 m (Norris, 1998; Carrillo et al., 2016), which enables an investigation of the interactions between the MBL and the free troposphere and significantly saves computation time compared to the full domain. So, this chosen model setup can capture almost all essential chemical processes as well as the distribution of important species in the marine troposphere. Overall, the modelling domain for multiphase chemistry encompasses 3000 grid cells.

3.2.2 Comparison with measurements

HCl gas-phase concentration

Firstly, the modelled concentration range of gaseous HCl is compared to actual measurements. Figure 5 shows that very high HCl concentrations are modelled, especially in the 'stable meteorological condition' simulation above the MBL. These are results of the constant vertical distributed mass mixing ratios of the initial values. Since the evaluation focuses on the activation of HCl within the MBL, these values can be neglected. The modelled values below 1000 m outside of clouds are in the order of 10^9 molecules cm^{-3} after 12 hours of modelling time and thus in the range of both other modelled (Hossaini et al., 2016; Wang et al., 2019) and measured values within the marine pristine boundary layer (e.g., Keene and Savoie, 1999; Sander et al., 2013; Pszenny et al., 2004). The higher LWC of clouds results in strongly reduced HCl gas-phase concentrations due to the phase partitioning shift from the gas to the aqueous phase. Further chemical cloud processing increases aerosol acidity, yielding higher HCl gas-phase concentrations behind the cloud in wind direction (see Figure 5).

Gelöscht: Figure 3
Gelöscht: columns
Gelöscht: The
Gelöscht: distribution for MUSCAT is used because
Gelöscht: Therefore
Gelöscht: resolution
Gelöscht: are
Gelöscht: In
Gelöscht: Figure 5
Gelöscht: , it can be seen
Gelöscht: a result
Gelöscht: Figure 5

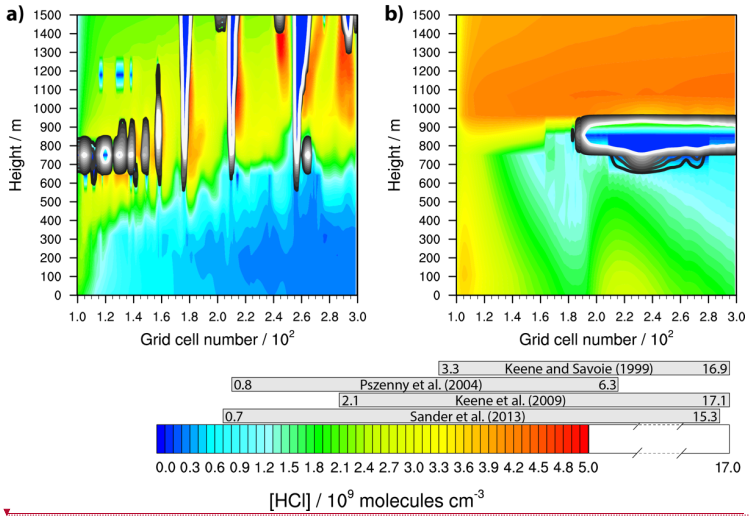

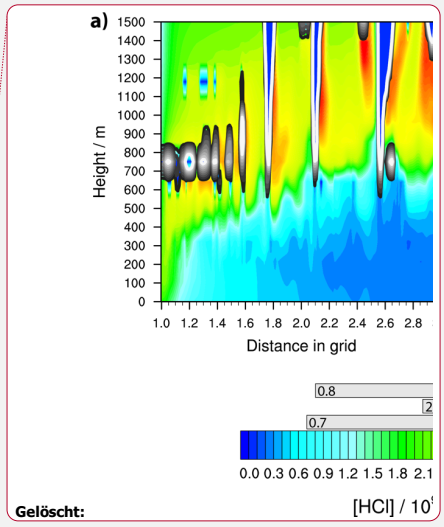

Figure 5 Simulated concentrations of HCl in the gas phase by COSMO-MUSCAT (a) in the 'unstable meteorological condition' simulation with convective clouds and (b) in the 'stable meteorological condition' simulation with stratiform clouds after 12 hours of modelling time. The x-axis represents the innermost horizontal grid cells divided by 100. The grey bars represent measured values in most likely pristine marine environments (see Table S11 for further details). The black contour lines represent the simulated clouds. The black line corresponds to a liquid water content of 0.01 g m^{-3} and the white line to 0.1 g m^{-3}. The area framed by the white line includes LWC above 0.1 g m^{-3}.

BrO gas-phase concentration

Contrary to HCl, the measured concentrations of HBr over the pristine ocean are missing. However, a high number of measured gas-phase BrO concentrations in the MBL are available (Saiz-Lopez and von Glasow, 2012; Simpson et al., 2015). Therefore, as a second step, the modelled gas-phase BrO concentration range is compared to measurements. Figure 6 shows that the modelled values outside of the cloud grid cells ranging between 10^6 to 10^7 molecules cm^{-3} after 12 hours of modelling time. Thus, they are in the range of other modelled (Zhu et al., 2019) as well as measured values within the pristine MBL (e.g., Leser et al., 2003; Read et al., 2008; Chen et al., 2016). Apart from that, the vertical distribution significantly differs between both simulations resulting into distinct spatial pattern. At the left-hand side of the model domain, the BrO concentration is similar, which is related to the activation of reactive bromine species from the initialised marine aerosols. However, when clouds are formed the profiles change. This is related to the high differences in the vertical wind field (see Fig. 7a and b). Because of the stronger updrafts in the 'unstable meteorological condition' simulation, the reactive halogen compounds are advected towards higher altitudes compared to the slow vertical winds in the 'stable meteorological condition' simulation. A second remarkable

Gelöscht: The denser the crowding, the higher the simulated
Gelöscht: the clouds (with a max of
Gelöscht: 9
Gelöscht: 3
Gelöscht: in the 'unstable meteorological condition' and 'stable meteorological condition' simulations, respectively).
Gelöscht: In
Gelöscht: Figure 6
Gelöscht: , it can be seen
Gelöscht: are in the range
Gelöscht: .

difference is the much lower BrO concentration at the right-hand side of the model domain in the 'stable meteorological condition' simulation. This effect is more explicitly discussed in Sect. 3.3.3.

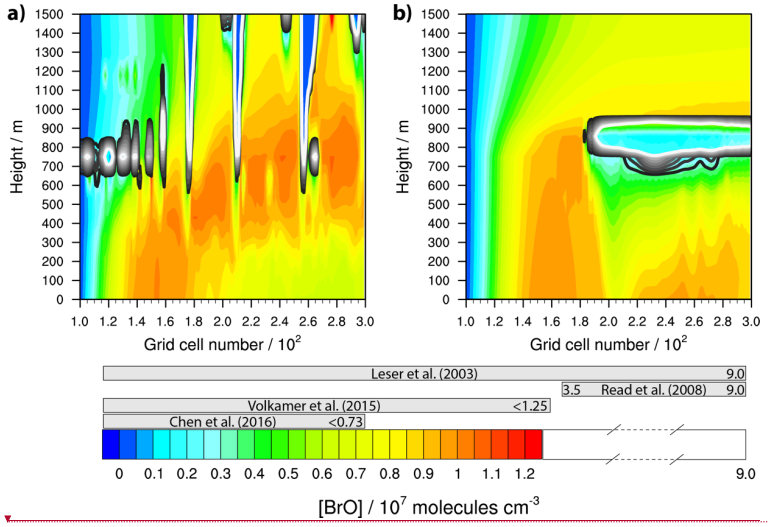

Figure 6 Simulated concentrations of bromine monoxide in the gas phase by COSMO-MUSCAT (a) in the 'unstable meteorological condition' simulation with convective clouds and (b) in the 'stable meteorological condition' simulation with stratiform clouds after 12 hours of modelling time. The x-axis represents the innermost horizontal grid cells divided by 100. The grey bars represent measured values in most likely pristine marine environments (see Table S11 for further details). The black contour lines represent the simulated clouds. The black line corresponds to a liquid water content of 0.01 g m^{-3} and the white line to 0.1 g m^{-3}. The area framed by the white line includes LWC above 0.1 g m^{-3}.

Apart from that, many field studies had the problem that the BrO concentration in the MBL was always below the detection limit (Sander et al., 2003). In a recent measurement study, the measured BrO in the MBL was also always below the detection limit of 0.5 pptv, i.e. around $1.2 \cdot 10^7$ molecules cm^{-3} (Volkamer et al., 2015). Hence, the BrO concentrations are modelled adequately. Since the activation of reactive bromine is highly related to that of chlorine, the mechanism is able to represent the activation of reactive halogen compounds within the MBL. A comparison of reactive iodine compounds with measurements is not performed, because the concentration range is highly sensitive to the chosen emission values of molecular iodine and iodinated organics from the sea surface and is thus uncertain.

Overall, the new marine multiphase chemistry model can represent marine aerosol chemistry and linked halogen activation under consideration of meteorological dynamics and shows a good agreement to other field as well as model data. Thus, it is applicable for further detailed 3D studies.

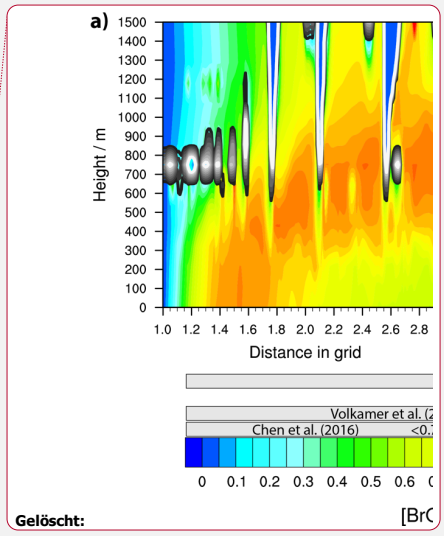

Gelöscht: The denser the crowding, the higher the simulated

Gelöscht: the clouds

Gelöscht: suffered

Gelöscht: (Sander et al., 2003)

Gelöscht: The measured BrO in the MBL in

Gelöscht:

Gelöscht: modelled

Gelöscht: should be adequate.

Gelöscht: initialised

Gelöscht: can

Gelöscht: be stated as

3.3 Results of pristine ocean scenarios

3.3.1 Vertical wind and DMS distribution

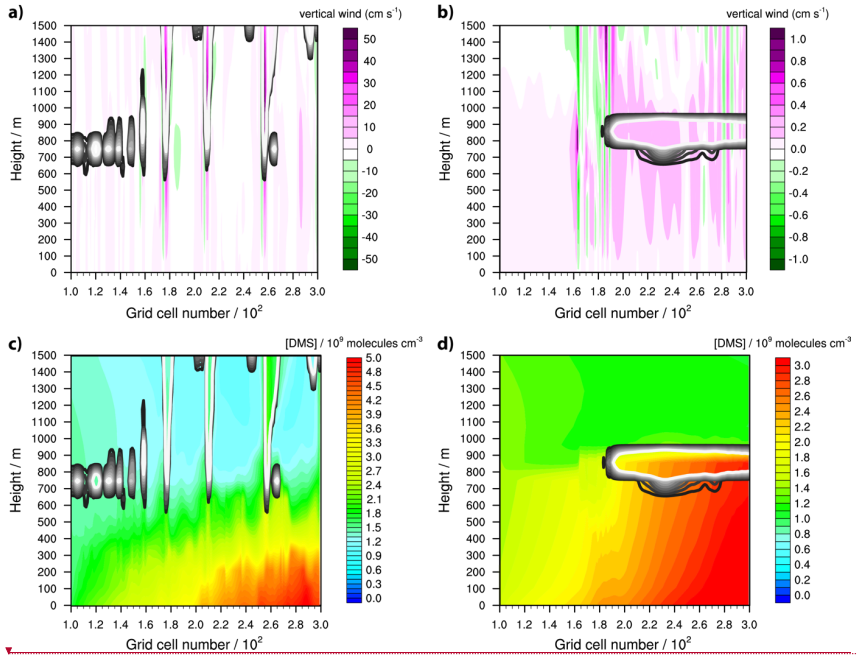

Figure 7 Modelled vertical winds (cm s^{-1}) (a) in the 'unstable meteorological condition' simulation with convective clouds and (b) in the 'stable meteorological condition' simulation with stratiform clouds after 12 hours of modelling time. The x-axis represents the innermost horizontal grid cells divided by 100. The black contour lines represent the simulated clouds. The black line corresponds to a liquid water content of 0.01 g m^{-3} and the white line to 0.1 g m^{-3}. The area framed by the white line includes LWC above 0.1 g m^{-3}. Further, the modelled concentrations of DMS in the gas phase (10^9 molecules cm^{-3}) are shown (c) in the 'unstable meteorological condition' simulation with convective clouds and (d) in the 'stable meteorological condition' simulation with stratiform clouds after 12 hours of modelling time.

Both scenarios are further applied to investigate the multiphase oxidation pathways of DMS in a cloudy marine atmosphere in detail. Figure 7 shows the modelled distribution of clouds and the strength of the vertical wind field as well as the modelled DMS concentration distribution for both simulations after 12 hours of modelling time. In the 'unstable meteorological condition' simulation, the clouds extend up to a height of more than 2000 m, whereas in the 'stable meteorological condition' simulation, the top of the cloud is capped below an inversion layer at around 1000 m. Also, the vertical winds are much stronger in the 'unstable meteorological condition' simulation. Because of the strong vertical winds, gas-phase DMS concentrations of

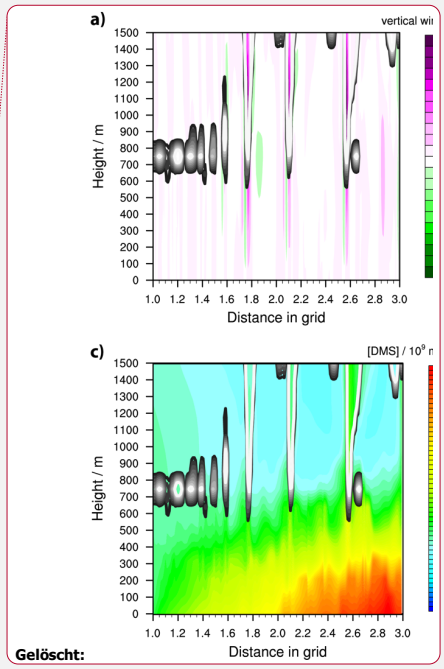

Gelöscht:

Gelöscht: The denser the crowding, the higher the simulated

Gelöscht: the clouds

Gelöscht: In

Gelöscht: Figure 7

Gelöscht: ,

Gelöscht: is shown

Gelöscht: Furthermore

around $2 \cdot 10^9$ molecules cm^{-3} are transported into the lower free troposphere. The strong inversion and low magnitude of the vertical wind speed in the 'stable meteorological condition' simulation hinders effective DMS transportation into the free troposphere resulting in a DMS concentration of around $1 \cdot 10^9$ molecules cm^{-3} above the MBL. This is consistent with the initialised background DMS concentration. Below the inversion, DMS concentrations are more homogeneously distributed, which is different to the 'unstable meteorological condition' simulation, with a stronger variability related to the vertical wind field, i.e. the peaking of DMS concentrations into higher vertical levels because of strong updrafts (cp. Figure 7).

Gelöscht: . Therefore, above the MBL, the

Gelöscht: is at

Gelöscht: , which

Gelöscht: Figure 7

3.3.2 Vertical DMSO distribution

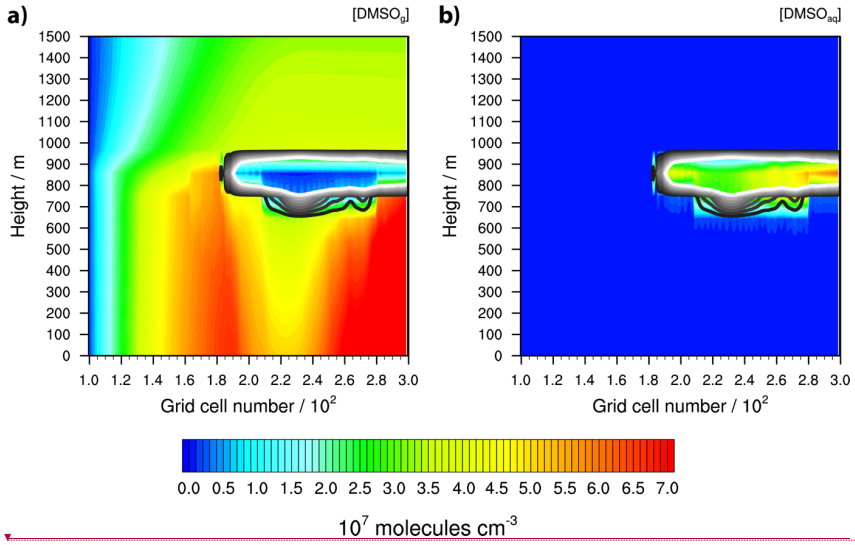

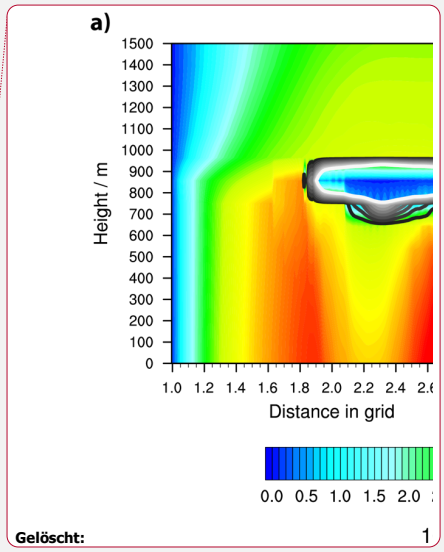

Gelöscht: 1

Figure 8 Simulated concentrations of DMSO (a) in the gas phase and (b) in the aqueous phase under the 'stable meteorological condition' simulation with stratiform clouds after 12 hours of modelling time. The x-axis represents the innermost horizontal grid cells divided by 100. The black contour lines represent the simulated clouds. The black line corresponds to a liquid water content of 0.01 g m^{-3} and the white line to 0.1 g m^{-3}. The area framed by the white line includes LWC above 0.1 g m^{-3}.

Gelöscht: The denser the crowding, the higher the simulated

Gelöscht: the clouds

If such homogeneously distributed DMS concentrations are modelled as in the 'stable meteorological condition' simulation in a clear sky atmosphere, a similar concentration distribution for the first stable DMS oxidation products will be modelled. Hence, the concentration distribution of DMSO is a good indicator to investigate the effect of clouds on DMS oxidation. In Figure 8, the distribution of DMSO in the gas and aqueous phases in the 'stable meteorological condition' simulation after 12 hours of modelling time is shown. Furthermore, the overall modelled DMSO production and loss rates separated into gas and aqueous-phase reactions were added to the supplement (see Fig. S11).

Gelöscht: Figure 8

The stratiform clouds have a very high influence on the DMSO concentration in both the gas and the aqueous phase. The spatial gas-phase DMSO concentration distribution differs from the DMS concentration. Below the optically thickest clouds, the gas-phase DMSO concentration is significantly reduced, whereas above the cloud it slightly increases. In the cloud grid cells, the gas-phase DMSO concentration is reduced significantly because of the uptake into the aqueous phase. The reduced gas-phase concentrations below the cloud cannot be explained by vertical or horizontal transportation because, as can be seen in Figure 7, an updraft would result in observable concentration peaks in the higher vertical levels. Therefore, the gas-phase DMSO formation in the MBL is somehow influenced by the cloud above, what makes it necessary to investigate the cloud-induced effect on such crucial DMS oxidants in the pristine MBL.

Gelöscht: Figure 7

Gelöscht: and

Gelöscht: is

3.3.3 Effects of stratiform clouds on DMS oxidation

Within the pristine MBL, the BrO radical is a primary DMS oxidant that forms DMSO (Barnes et al., 2006; Breider et al., 2010; Hoffmann et al., 2016; von Glasow and Crutzen, 2004; Chen et al., 2018). This radical is formed through reaction of O_3 by the Br atom that is activated by multiphase chemistry. The following reactions are important pathways of activation in a clear sky MBL (von Glasow and Crutzen, 2004; von Glasow et al., 2002b):

Gelöscht: (von Glasow and Crutzen, 2004; von Glasow et al., 2002b)

$$BrCl_g + h\nu \rightarrow Br_g + Cl_g \quad (R47)$$

$$Br_g + O_{3,g} \rightarrow BrO_g + O_{2,g} \quad (R48)$$

$$BrO_g + DMS_g \rightarrow DMSO_g + Br \quad (R49)$$

$$BrO_g + HO_{2,g} \rightarrow HOBr_g + O_{2,g} \quad (R50)$$

$$HOBr_g + h\nu \rightarrow Br_g + OH_g \quad (R51)$$

$$HOBr_g \rightleftharpoons HOBr_{aq} \quad (R52)$$

$$HOBr_{aq} + Br^- + H^+ \rightleftharpoons BrCl_{aq} + H_2O \quad (R53)$$

$$BrCl_{aq} \rightleftharpoons BrCl_g \quad (R54)$$

In the pristine marine boundary layer, two competing pathways determine the main fate of the BrO radical through (i) a reaction with DMS and (ii) a reaction with HO_2. The oxidation of DMS leads to DMSO and the Br atom, so that a cycle is established that continuously depletes O_3 and forms DMSO as long as DMS is emitted or ozone is available. This cycle is disturbed by the reaction of BrO with HO_2, yielding HOBr, which can be photolyzed back into the Br atom again or converted by multiphase chemistry into BrCl or Br_2. Overall, the photolysis of HOBr, Br_2 and BrCl determine the DMS to DMSO conversion. Clouds suppress the photolysis of Br_2, BrCl and HOBr due to the reflection of incoming solar radiation. The thicker the cloud, the lower the radiation flux below. Consequently, Br atom activation below the cloud is hindered, affecting the BrO concentration and thus the reaction rate of BrO with DMS that yields DMSO (see Figure 9). Due to a longer lifetime against further oxidation and corresponding horizontal advection, the DMSO concentration profile is shifted towards the right compared to BrO. The lowest oxidation flux between DMS and BrO is modelled between grid cell 2.0 and 2.15. The effect on DMSO concentration is modelled between grid cell 2.1 to 2.4.

Gelöscht: particularly

Gelöscht: Figure 9

Gelöscht: to

Gelöscht: the

Gelöscht: one

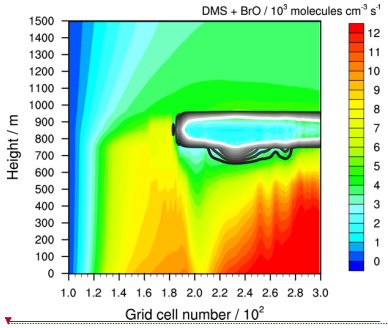

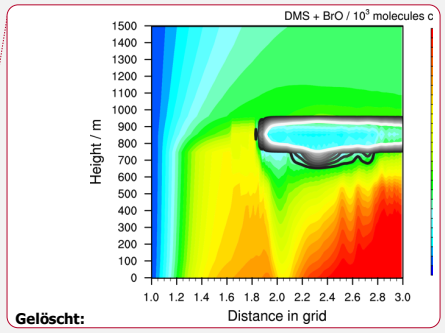

Gelöscht:

Figure 9 Simulated oxidation rate of DMS by BrO in the 'stable meteorological condition' simulation with stratiform clouds after 12 hours of modelling time. The x-axis represents the innermost horizontal grid cells divided by 100. The black contour lines represent the simulated clouds. The black line corresponds to a liquid water content of 0.01 g m^{-3} and the white line to 0.1 g m^{-3}. The area framed by the white line includes LWC above 0.1 g m^{-3}.

Gelöscht: The denser the crowding, the higher the simulated

Gelöscht: the clouds

The photolysis of BrCl and Br_2 is highly sensitive to cloud shading and thus has a high impact on the formation of reactive bromine and the linked DMS oxidation. Moreover, model studies suggest that BrCl photolysis is an important contributor to Cl atom activation in the MBL (Wang et al., 2019; von Glasow et al., 2002b). Hence, the outlined model results reveal that the shading effect of clouds is also very important for the atmospheric Cl atom concentration budget, affecting the atmospheric oxidation capacity within the MBL.

Gelöscht: compounds

Gelöscht: Furthermore

3.3.4 The formation of MSA and aqueous sulfate

DMSO is rapidly oxidised into MSIA and thus a similar MSIA profile is modelled. As MSIA is highly reactive in the gas and aqueous phases as well as highly soluble, it is rapidly oxidised into methane sulfonate (MS^-) in both the aerosol and the cloud phases. There, O_3 is the preferred oxidant in the aerosol phase, whereas in cloud droplets it is the OH radical (Hoffmann et al., 2016). The MS^- formed in-cloud can be transported towards the ground by downdrafts. However, comparing the DMS concentrations in Figure 7 with the DMSO concentrations in Figure 8, the up- and downdrafts in the 'stable meteorological condition' simulations have little effect on the concentration distribution in height. The strongest effect relates to the advection from the left-hand to the right-hand side of the model domain and continuous emission from the surface. In the grid cells left of the cloud, the DMSO concentration is high and consequently the aerosol particle chemistry of DMSO and of the subsequent oxidation product MSIA leads to a sharp increase of MS^- formation at the grid cells below the left cloud edge (see Figure 10a). Due to the advection of the stable MS^- to the right-hand side of the model domain, the spatial profiles of DMSO (Figure 8) and MS^- differ. The high modelled chemical fluxes in cloud droplets indicate the highest MS^- concentrations to be within and below the cloud grid cells.

Gelöscht: However, because of its high reactivity

Gelöscht: its high solubility, MSIA

Gelöscht: OH is

Gelöscht: . In

Gelöscht: next time step, the

Gelöscht: as can be seen from

Gelöscht: Figure 7

Gelöscht: Figure 8

Gelöscht: before

Gelöscht: occurrence

Gelöscht: is as well.

Gelöscht: DMSO profile is not modelled

Gelöscht: (see Figure 10).

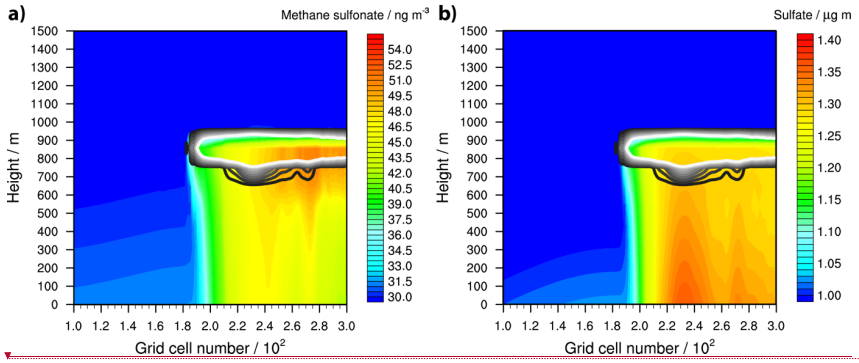

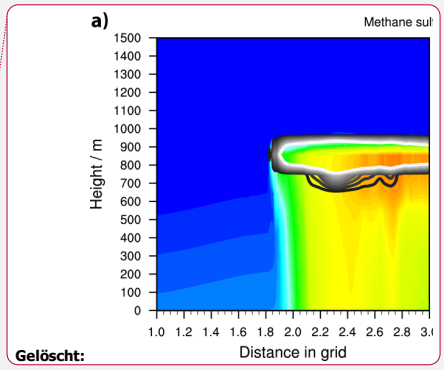

Gelöscht:

Figure 10 Simulated aqueous-phase concentrations of (a) methane sulfonate and (b) sulfate in the 'stable meteorological condition' simulation with stratiform clouds after 12 hours of modelling time. The x-axis represents the innermost horizontal grid cells divided by 100. The black contour lines represent the simulated clouds. The black line corresponds to a liquid water content of 0.01 g m^{-3} and the white line to 0.1 g m^{-3}. The area framed by the white line includes LWC above 0.1 g m^{-3}. The initial background concentration of methane sulfonate is at about 30 ng m^{-3} and that of sulfate at 1 µg m^{-3}.

Also, the concentration of sulfate (see Figure 10b) is enhanced in the grid cells at the left cloud edge, but because of different reasons. At the left cloud edge, the lower photolysis rates increase the SO_2 oxidation into sulfate by HOX and H_2O_2. Hence, a stronger HOX-related (especially HOI) reactive SO_2 uptake on the aerosols is modelled. The reaction of HOBr results into the formation of bromide. In addition to the uptake of HBr, this increases the bromide concentration in cloud droplets by up to one order of magnitude compared to the ground level concentration before the left cloud edge (see Fig. S12). The uptake is highest under the optically thickest modelled clouds, resulting in the highest modelled sulfate concentrations. Therefore, the modelled spatial concentration is contrary to that of DMSO.

Gelöscht: -
Gelöscht: As for MSA
Gelöscht: formation
Gelöscht: directly or indirectly affected by clouds.
Gelöscht: beginning
Gelöscht: being there

4 Conclusion and Outlook

Reduced multiphase chemistry mechanisms of DMS and reactive halogen compounds are developed through the reduction of the near-explicit multiphase chemistry mechanisms CAPRAM-DM1.0 and CAPRAM-HM3.0. Simulations that compare the reduced with the original mechanisms revealed that the reduced mechanisms are able to reproduce the concentrations and time evolutions of main air pollutants as well as key reactive halogen compounds. Additionally, CPU time in the box model simulations is reduced by 16 %, 5 %, and 6 %, depending on the model scenario. Afterwards, the reduced mechanisms are implemented into the chemistry transport model COSMO-MUSCAT. This process is evaluated by idealised 2D-simulations of an atmospheric pristine ocean environment. It was proven that the reduced marine multiphase chemistry mechanism can represent marine aerosol chemistry and linked halogen activation as it matches measured field concentrations, e.g. HCl and BrO.

Gelöscht: A reduced
Gelöscht: mechanism
Gelöscht: is
Gelöscht: The implementation
Gelöscht: The verification has

Following that implementation, 2D-simulations of a pristine ocean scenario are carried out, investigating the effect of stable (stratiform cloud) and more unstable meteorological conditions (convective clouds) on multiphase DMS oxidation. The simulations reveal that clouds have both strong direct and indirect photochemical effects on the oxidation and vertical distribution of DMS in the marine atmosphere. Firstly, locally high updraft velocities in the unstable scenario result in fast transport of DMS from the marine boundary layer into the free troposphere. Hence, transport and further oxidation of DMS can be an important source of SO_2 within the free troposphere, particularly in the Southern Ocean region that is less affected by anthropogenic pollution. Secondly, clouds enhance the formation of MSA via the DMS addition channel. The formed DMSO is effectively consumed by cloud droplets where it is rapidly oxidised into MSA. Thirdly, the shading of clouds has a high impact on the photolysis of dihalogens that are the main contributor to Cl and Br atom activation. Thus, a much lower oxidation of DMS into DMSO occurs below stratiform clouds. In contrast, the lower HOX photolysis induces stronger sulfate formation. The results indicate that clouds strongly affect the oxidation of DMS directly because of enhanced aqueous-phase oxidation into MSA and indirectly by suppressing the DMSO formation due to lower halogen atom activation. In total, a strong possible effect on the atmospheric oxidation capacity within the MBL of the pristine ocean is assumed. The important effect of wet scavenging by clouds was not investigated as the current COSMO-MUSCAT(5.04e) did not implemented it in detail, but represented it using a first-order scavenging rate. Future studies aim to implement a more precise scheme. Since the clouds modelled in this study are not known to precipitate, the propagated error should be small.

Overall, the 2D-simulations demonstrate the capability of COSMO-MUSCAT to now cover the multiphase chemistry in marine influenced atmospheric environments. This allows for deeper investigations of multiphase chemistry in a wide range of temporal and spatial resolutions together with transport and microphysical processes in the future. In a next step, the mechanism will be applied in simulations with COSMO-MUSCAT for modelling measurement campaigns at the Cape Verde Atmospheric Observatory (Carpenter et al., 2010), supporting the interpretation of the measurement data and enabling further model/mechanism evaluation. Finally, the reduced mechanism is designed in such a way that new findings in DMS or halogen chemistry can easily be implemented, e.g. improved understanding of the multiphase chemistry of the unimolecular H-shift of $CH_3SCH_2O_2$.

Code and Data availability

The code for the COSMO model is available according to the Software License Agreement by Deutscher Wetterdienst (German Weather Service, http://cosmo-model.org). The source code of MUSCAT and SPACCIM, external parameters, and applied mechanisms are archived on a local Git server and can be obtained by request through Ralf Wolke (wolke@tropos.de). Access to the model code used in the paper has been granted to the editor.

Gelöscht: Afterwards
Gelöscht: weather
Gelöscht: a
Gelöscht: transportation
Gelöscht: the transportation
Gelöscht: Hence
Gelöscht: formations
Gelöscht: marine boundary layer is assumed
Gelöscht: transportation
Gelöscht: to model
Gelöscht: validations. Furthermore

Author contribution

EHH, AT, and RW did the model development on SPACCIM. EHH, AT, and HH designed the SPACCIM modelling work. EHH performed the SPACCIM simulations. EHH, AT, and HH analysed the SPACCIM model results. EHH, RS, and RW did the model development on COSMO-MUSCAT. EHH, RS, and RW designed the COSMO-MUSCAT modelling work. EHH performed the COSMO-MUSCAT simulations. EHH analysed the COSMO-MUSCAT model results. EHH, RS, AT, and HH wrote the paper.

Competing interests

The authors declare that they have no conflict of interest.

Special issue statement. This article is part of the special issue "Simulation chambers as tools in atmospheric research (AMT/ACP/GMD inter-journal SI)". It is not associated with a conference.

Acknowledgements

E.H.H. thanks the Ph.D. scholarship program of the German Federal Environmental Foundation (Deutsche Bundesstiftung Umwelt, DBU, AZ: 2016/424) for its financial support. This work has received funding from the European Union's Horizon 2020 research and innovation program through the EUROCHAMP-2020 Infrastructure Activity under grant agreement no. 730997. This work was also supported by the EU Marie Skłodowska-Curie Actions, (690958-MARSU-RISE-2015).

Financial support

This research has been supported by the European Commission (grant no. EUROCHAMP-2020 (730997)).
This work was also supported by the EU Marie Skłodowska-Curie Actions, (690958-MARSU-RISE-2015).

References

Alexander, B., Allman, D. J., Amos, H. M., Fairlie, T. D., Dachs, J., Hegg, D. A., and Sletten, R. S.: Isotopic constraints on the formation pathways of sulfate aerosol in the marine boundary layer of the subtropical northeast Atlantic Ocean, J. Geophys. Res.-Atmos., 117, D06304, https://doi.org/10.1029/2011jd016773, 2012.
Ammann, M., Cox, R. A., Crowley, J. N., Jenkin, M. E., Mellouki, A., Rossi, M. J., Troe, J., and Wallington, T. J.: Evaluated kinetic and photochemical data for atmospheric chemistry: Volume VI – heterogeneous reactions with liquid substrates, Atmos. Chem. Phys., 13, 8045-8228, https://doi.org/10.5194/acp-13-8045-2013, 2013.
Andreae, M. O.: Ocean-atmosphere interactions in the global biogeochemical sulfur cycle, Mar. Chem., 30, 1-29, https://doi.org/10.1016/0304-4203(90)90059-L, 1990.

Atkinson, R., Baulch, D. L., Cox, R. A., Crowley, J. N., Hampson, R. F., Hynes, R. G., Jenkin, M. E., Rossi, M. J., and Troe, J.: Evaluated kinetic and photochemical data for atmospheric chemistry: Volume II – gas phase reactions of organic species, Atmos. Chem. Phys., 6, 3625-4055, https://doi.org/10.5194/acp-6-3625-2006, 2006.

Atkinson, R., Baulch, D. L., Cox, R. A., Crowley, J. N., Hampson, R. F., Hynes, R. G., Jenkin, M. E., Rossi, M. J., and Troe, J.: Evaluated kinetic and photochemical data for atmospheric chemistry: Volume III – gas phase reactions of inorganic halogens, Atmos. Chem. Phys., 7, 981-1191, https://doi.org/10.5194/acp-7-981-2007, 2007.

Atkinson, R., Baulch, D. L., Cox, R. A., Crowley, J. N., Hampson, R. F., Hynes, R. G., Jenkin, M. E., Rossi, M. J., Troe, J., and Wallington, T. J.: Evaluated kinetic and photochemical data for atmospheric chemistry: Volume IV – gas phase reactions of organic halogen species, Atmos. Chem. Phys., 8, 4141-4496, https://doi.org/10.5194/acp-8-4141-2008, 2008.

Badia, A., Reeves, C. E., Baker, A. R., Saiz-Lopez, A., Volkamer, R., Koenig, T. K., Apel, E. C., Hornbrook, R. S., Carpenter, L. J., Andrews, S. J., Sherwen, T., and von Glasow, R.: Importance of reactive halogens in the tropical marine atmosphere: a regional modelling study using WRF-Chem, Atmos. Chem. Phys., 19, 3161-3189, https://doi.org/10.5194/acp-19-3161-2019, 2019.

Baklanov, A., Schlünzen, K., Suppan, P., Baldasano, J., Brunner, D., Aksoyoglu, S., Carmichael, G., Douros, J., Flemming, J., Forkel, R., Galmarini, S., Gauss, M., Grell, G., Hirtl, M., Joffre, S., Jorba, O., Kaas, E., Kaasik, M., Kallos, G., Kong, X., Korsholm, U., Kurganskiy, A., Kushta, J., Lohmann, U., Mahura, A., Manders-Groot, A., Maurizi, A., Moussiopoulos, N., Rao, S. T., Savage, N., Seigneur, C., Sokhi, R. S., Solazzo, E., Solomos, S., Sørensen, B., Tsegas, G., Vignati, E., Vogel, B., and Zhang, Y.: Online coupled regional meteorology chemistry models in Europe: current status and prospects, Atmos. Chem. Phys., 14, 317-398, https://doi.org/10.5194/acp-14-317-2014, 2014.

Baldauf, M., Seifert, A., Förstner, J., Majewski, D., Raschendorfer, M., and Reinhardt, T.: Operational Convective-Scale Numerical Weather Prediction with the COSMO Model: Description and Sensitivities, Mon. Weather Rev., 139, 3887-3905, https://doi.org/10.1175/mwr-d-10-05013.1, 2011.

Barnes, I., Hjorth, J., and Mihalopoulos, N.: Dimethyl sulfide and dimethyl sulfoxide and their oxidation in the atmosphere, Chem. Rev., 106, 940-975, https://doi.org/10.1021/Cr020529+, 2006.

Barthel, S., Tegen, I., and Wolke, R.: Do new sea spray aerosol source functions improve the results of a regional aerosol model?, Atmos. Environ., 198, 265-278, https://doi.org/10.1016/j.atmosenv.2018.10.016, 2019.

Benedict, K. B., Lee, T., and Collett, J. L.: Cloud water composition over the southeastern Pacific Ocean during the VOCALS regional experiment, Atmos. Environ., 46, 104-114, https://doi.org/10.1016/j.atmosenv.2011.10.029, 2012.

Berndt, T., Scholz, W., Mentler, B., Fischer, L., Hoffmann, E. H., Tilgner, A., Hyttinen, N., Prisle, N. L., Hansel, A., and Herrmann, H.: Fast Peroxy Radical Isomerization and OH Recycling in the Reaction of OH Radicals with Dimethyl Sulfide, J. Phys. Chem. Lett., https://doi.org/10.1021/acs.jpclett.9b02567, 2019.

Berresheim, H., Huey, J. W., Thorn, R. P., Eisele, F. L., Tanner, D. J., and Jefferson, A.: Measurements of dimethyl sulfide, dimethyl sulfoxide, dimethyl sulfone, and aerosol ions at Palmer Station, Antarctica, J. Geophys. Res.-Atmos., 103, 1629-1637, https://doi.org/10.1029/97JD00695, 1998.

Bräuer, P., Tilgner, A., Wolke, R., and Herrmann, H.: Mechanism development and modelling of tropospheric multiphase halogen chemistry: The CAPRAM Halogen Module 2.0 (HM2), J. Atmos. Chem., 70, 19-52, https://doi.org/10.1007/s10874-013-9249-6, 2013.

Bräuer, P., Mouchel-Vallon, C., Tilgner, A., Mutzel, A., Böge, O., Rodigast, M., Poulain, L., van Pinxteren, D., Wolke, R., Aumont, B., and Herrmann, H.: Development of a protocol for the auto-generation of explicit aqueous-phase oxidation schemes of organic compounds, Atmos. Chem. Phys., 19, 9209-9239, https://doi.org/10.5194/acp-19-9209-2019, 2019.

Breider, T. J., Chipperfield, M. P., Richards, N. A. D., Carslaw, K. S., Mann, G. W., and Spracklen, D. V.: Impact of BrO on dimethylsulfide in the remote marine boundary layer, Geophys. Res. Lett., 37, L02807, https://doi.org/10.1029/2009gl040868, 2010.

Brown, S. S., and Stutz, J.: Nighttime radical observations and chemistry, Chem. Soc. Rev., 41, 6405-6447, https://doi.org/10.1039/c2cs35181a, 2012.

Burkholder, J. B., Sander, S. P., Abbatt, J., Barker, J. R., Huie, R. E., Kolb, C. E., Kurylo, M. J., Orkin, V. L., Wilmouth, D. M., and Wine, P. H.: Chemical Kinetics and Photochemical Data for Use in Atmospheric Studies, Evaluation No. 18, Jet Propulsion Laboratory, Pasadena, 2015.

Carpenter, L. J., Fleming, Z. L., Read, K. A., Lee, J. D., Moller, S. J., Hopkins, J. R., Purvis, R. M., Lewis, A. C., Müller, K., Heinold, B., Herrmann, H., Fomba, K. W., van Pinxteren, D., Müller, C., Tegen, I., Wiedensohler, A., Müller, T., Niedermeier,

N., Achterberg, E. P., Patey, M. D., Kozlova, E. A., Heimann, M., Heard, D. E., Plane, J. M. C., Mahajan, A., Oetjen, H., Ingham, T., Stone, D., Whalley, L. K., Evans, M. J., Pilling, M. J., Leigh, R. J., Monks, P. S., Karunaharan, A., Vaughan, S., Arnold, S. R., Tschritter, J., Pöhler, D., Frieß, U., Holla, R., Mendes, L. M., Lopez, H., Faria, B., Manning, A. J., and Wallace, D. W. R.: Seasonal characteristics of tropical marine boundary layer air measured at the Cape Verde Atmospheric Observatory, J. Atmos. Chem., 67, 87-140, https://doi.org/10.1007/s10874-011-9206-1, 2010.

Carpenter, L. J., Archer, S. D., and Beale, R.: Ocean-atmosphere trace gas exchange, Chem. Soc. Rev., 41, 6473-6506, https://doi.org/10.1039/c2cs35121h, 2012.

Carpenter, L. J., MacDonald, S. M., Shaw, M. D., Kumar, R., Saunders, R. W., Parthipan, R., Wilson, J., and Plane, J. M. C.: Atmospheric iodine levels influenced by sea surface emissions of inorganic iodine, Nature Geosci., 6, 108-111, https://doi.org/10.1038/ngeo1687, 2013.

Carpenter, L. J., and Nightingale, P. D.: Chemistry and release of gases from the surface ocean, Chem. Rev., 115, 4015-4034, https://doi.org/10.1021/cr5007123, 2015.

Carrillo, J., Guerra, J. C., Cuevas, E., and Barrancos, J.: Characterization of the Marine Boundary Layer and the Trade-Wind Inversion over the Sub-tropical North Atlantic, Bound.-Lay. Meteorol., 158, 311-330, https://doi.org/10.1007/s10546-015-0081-1, 2016.

Charlson, R. J., Lovelock, J. E., Andreae, M. O., and Warren, S. G.: Oceanic phytoplankton, atmospheric sulfur, cloud albedo and climate, Nature, 326, 655-661, https://doi.org/10.1038/326655a0, 1987.

Chen, D., Huey, L. G., Tanner, D. J., Salawitch, R. J., Anderson, D. C., Wales, P. A., Pan, L. L., Atlas, E. L., Hornbrook, R. S., Apel, E. C., Blake, N. J., Campos, T. L., Donets, V., Flocke, F. M., Hall, S. R., Hanisco, T. F., Hills, A. J., Honomichl, S. B., Jensen, J. B., Kaser, L., Montzka, D. D., Nicely, J. M., Reeves, J. M., Riemer, D. D., Schauffler, S. M., Ullmann, K., Weinheimer, A. J., and Wolfe, G. M.: Airborne measurements of BrO and the sum of HOBr and Br_2 over the Tropical West Pacific from 1 to 15 km during the CONvective TRansport of Active Species in the Tropics (CONTRAST) experiment, J. Geophys. Res.-Atmos., 121, 12560-12578, https://doi.org/10.1002/2016JD025561, 2016.

Chen, Q., Schmidt, J. A., Shah, V., Jaegle, L., Sherwen, T., and Alexander, B.: Sulfate production by reactive bromine: Implications for the global sulfur and reactive bromine budgets, Geophys. Res. Lett., 44, 7069-7078, https://doi.org/10.1002/2017gl073812, 2017.

Chen, Q., Sherwen, T., Evans, M., and Alexander, B.: DMS oxidation and sulfur aerosol formation in the marine troposphere: a focus on reactive halogen and multiphase chemistry, Atmos. Chem. Phys., 18, 13617-13637, https://doi.org/10.5194/acp-18-13617-2018, 2018.

Davis, D., Chen, G., Kasibhatla, P., Jefferson, A., Tanner, D., Eisele, F., Lenschow, D., Neff, W., and Berresheim, H.: DMS oxidation in the Antarctic marine boundary layer: Comparison of model simulations and held observations of DMS, DMSO, $DMSO_2$, H_2SO_4(g), MSA(g), and MSA(p), J. Geophys. Res.-Atmos., 103, 1657-1678, https://doi.org/10.1029/97JD03452, 1998.

Deguillaume, L., Tilgner, A., Schrödner, R., Wolke, R., Chaumerliac, N., and Herrmann, H.: Towards an operational aqueous phase chemistry mechanism for regional chemistry-transport models: CAPRAM-RED and its application to the COSMO-MUSCAT model, J. Atmos. Chem., 64, 1-35, https://doi.org/10.1007/s10874-010-9168-8, 2010.

Ervens, B., George, C., Williams, J. E., Buxton, G. V., Salmon, G. A., Bydder, M., Wilkinson, F., Dentener, F., Mirabel, P., and Herrmann, H.: CAPRAM 2.4 (MODAC mechanism): An extended and condensed tropospheric aqueous phase mechanism and its application, J. Geophys. Res., 108, 4426, https://doi.org/10.1029/2002jd002202, 2003.

Falbe-Hansen, H., Sørensen, S., Jensen, N. R., Pedersen, T., and Hjorth, J.: Atmospheric gas-phase reactions of dimethylsulphoxide and dimethylsulphone with OH and NO_3 radicals, Cl atoms and ozone, Atmos. Environ., 34, 1543-1551, https://doi.org/10.1016/S1352-2310(99)00407-0, 2000.

Farmer, D. K., Cappa, C. D., and Kreidenweis, S. M.: Atmospheric processes and their controlling influence on cloud condensation nuclei activity, Chem. Rev., 115, 4199-4217, https://doi.org/10.1021/cr5006292, 2015.

Faxon, C. B., and Allen, D. T.: Chlorine chemistry in urban atmospheres: a review, Environ. Chem., 10, 221-233, https://doi.org/10.1071/en13026, 2013.

Gaston, C. J., Riedel, T. P., Zhang, Z., Gold, A., Surratt, J. D., and Thornton, J. A.: Reactive uptake of an isoprene-derived epoxydiol to submicron aerosol particles, Environ. Sci. Technol., 48, 11178-11186, https://doi.org/10.1021/es5034266, 2014.

Goliff, W. S., Stockwell, W. R., and Lawson, C. V.: The regional atmospheric chemistry mechanism, version 2, Atmos. Environ., 68, 174-185, https://doi.org/10.1016/j.atmosenv.2012.11.038, 2013.

Heinold, B., Helmert, J., Hellmuth, O., Wolke, R., Ansmann, A., Marticorena, B., Laurent, B., and Tegen, I.: Regional modeling of Saharan dust events using LM-MUSCAT: Model description and case studies, J. Geophys. Res.-Atmos., 112, D11204, https://doi.org/10.1029/2006JD007443, 2007.

Hoffmann, E. H., Tilgner, A., Schrodner, R., Brauer, P., Wolke, R., and Herrmann, H.: An advanced modeling study on the impacts and atmospheric implications of multiphase dimethyl sulfide chemistry, Proc. Natl. Acad. Sci. USA, 113, 11776-11781, https://doi.org/10.1073/pnas.1606320113, 2016.

Hoffmann, E. H., Tilgner, A., Vogelsberg, U., Wolke, R., and Herrmann, H.: Near-explicit multiphase modeling of halogen chemistry in a mixed urban and maritime coastal area, ACS Earth Space Chem., 3, 2452-2471, https://doi.org/10.1021/acsearthspacechem.9b00184, 2019a.

Hoffmann, E. H., Tilgner, A., Wolke, R., and Herrmann, H.: Enhanced chlorine and bromine atom activation by hydrolysis of halogen nitrates from marine aerosols at polluted coastal areas, Environ. Sci. Technol., 53, 771-778, https://doi.org/10.1021/acs.est.8b05165, 2019b.

Hossaini, R., Chipperfield, M. P., Saiz-Lopez, A., Fernandez, R., Monks, S., Feng, W. H., Brauer, P., and von Glasow, R.: A global model of tropospheric chlorine chemistry: Organic versus inorganic sources and impact on methane oxidation, J. Geophys. Res.-Atmos., 121, 14271-14297, https://doi.org/10.1002/2016jd025756, 2016.

Jacob, P., and Klockow, D.: Hydrogen peroxide measurements in the marine atmosphere, J. Atmos. Chem., 15, 353-360, https://doi.org/10.1007/BF00115404, 1992.

Jenkin, M. E., Saunders, S. M., Wagner, V., and Pilling, M. J.: Protocol for the development of the Master Chemical Mechanism, MCM v3 (Part B): Tropospheric degradation of aromatic volatile organic compounds, Atmos. Chem. Phys., 3, 181-193, https://doi.org/10.5194/acp-3-181-2003, 2003.

Jöckel, P., Tost, H., Pozzer, A., Kunze, M., Kirner, O., Brenninkmeijer, C. A. M., Brinkop, S., Cai, D. S., Dyroff, C., Eckstein, J., Frank, F., Garny, H., Gottschaldt, K.-D., Graf, P., Grewe, V., Kerkweg, A., Kern, B., Matthes, S., Mertens, M., Meul, S., Neumaier, M., Nützel, M., Oberländer-Hayn, S., Ruhnke, R., Runde, T., Sander, R., Scharffe, D., and Zahn, A.: Earth System Chemistry integrated Modelling (ESCiMo) with the Modular Earth Submodel System (MESSy) version 2.51, Geosci. Model Dev., 9, 1153-1200, https://doi.org/10.5194/gmd-9-1153-2016, 2016.

Joshi, M., von Glasow, R., Smith, R. S., Paxton, C. G. M., Maycock, A. C., Lunt, D. J., Loptson, C., and Markwick, P.: Global warming and ocean stratification: A potential result of large extraterrestrial impacts, Geophys. Res. Lett., 44, 3841-3848, https://doi.org/10.1002/2017gl073330, 2017.

Keene, W. C., Sander, R., Pszenny, A. A. P., Vogt, R., Crutzen, P. J., and Galloway, J. N.: Aerosol pH in the marine boundary layer: A review and model evaluation, J. Aerosol Sci., 29, 339-356, https://doi.org/10.1016/S0021-8502(97)10011-8, 1998.

Keene, W. C., and Savoie, D. L.: Correction to "The pH of deliquesced sea-salt aerosol in polluted marine air", Geophys. Res. Lett., 26, 1315-1316, https://doi.org/10.1029/1999gl900221, 1999.

Kim, Y.-M., Lee, M., Chang, W., Lee, G., Kim, K.-R., and Kato, S.: Atmospheric peroxides over the North Pacific during IOC 2002 shipboard experiment, Chemosphere, 69, 1638-1646, https://doi.org/10.1016/j.chemosphere.2007.05.057, 2007.

Kummu, M., de Moel, H., Salvucci, G., Viviroli, D., Ward, P. J., and Varis, O.: Over the hills and further away from coast: global geospatial patterns of human and environment over the 20th–21st centuries, Environ. Res. Lett., 11, https://doi.org/10.1088/1748-9326/11/3/034010, 2016.

Lana, A., Bell, T. G., Simó, R., Vallina, S. M., Ballabrera-Poy, J., Kettle, A. J., Dachs, J., Bopp, L., Saltzman, E. S., Stefels, J., Johnson, J. E., and Liss, P. S.: An updated climatology of surface dimethlysulfide concentrations and emission fluxes in the global ocean, Global Biogeochem. Cy., 25, GB1004, https://doi.org/10.1029/2010gb003850, 2011.

Law, C. S., Brévière, E., de Leeuw, G., Garçon, V., Guieu, C., Kieber, D. J., Kontradowitz, S., Paulmier, A., Quinn, P. K., Saltzman, E. S., Stefels, J., and von Glasow, R.: Evolving research directions in Surface Ocean - Lower Atmosphere (SOLAS) science, Environ. Chem., 10, 1-16, https://doi.org/10.1071/en12159, 2013.

Leser, H., Hönninger, G., and Platt, U.: MAX-DOAS measurements of BrO and NO_2 in the marine boundary layer, Geophys. Res. Lett., 30, 1537, https://doi.org/10.1029/2002gl015811, 2003.

Lightfoot, P. D., Cox, R. A., Crowley, J. N., Destriau, M., Hayman, G. D., Jenkin, M. E., Moortgat, G. K., and Zabel, F.: Organic Peroxy-Radicals - Kinetics, Spectroscopy and Tropospheric Chemistry, Atmos. Environ. A - Gen., 26, 1805-1961, https://doi.org/10.1016/0960-1686(92)90423-I, 1992.

Long, M. S., Keene, W. C., Easter, R. C., Sander, R., Liu, X., Kerkweg, A., and Erickson, D.: Sensitivity of tropospheric chemical composition to halogen-radical chemistry using a fully coupled size-resolved multiphase chemistry–global climate

system: halogen distributions, aerosol composition, and sensitivity of climate-relevant gases, Atmos. Chem. Phys., 14, 3397-3425, https://doi.org/10.5194/acp-14-3397-2014, 2014.
Mahajan, A. S., Oetjen, H., Lee, J. D., Saiz-Lopez, A., McFiggans, G. B., and Plane, J. M. C.: High bromine oxide concentrations in the semi-polluted boundary layer, Atmos. Environ., 43, 3811-3818, https://doi.org/10.1016/j.atmosenv.2009.05.033, 2009a.
Mahajan, A. S., Oetjen, H., Saiz-Lopez, A., Lee, J. D., McFiggans, G. B., and Plane, J. M. C.: Reactive iodine species in a semi-polluted environment, Geophys. Res. Lett., 36, L16803, https://doi.org/10.1029/2009gl038018, 2009b.
McFiggans, G., Cox, R. A., Mössinger, J. C., Allan, B. J., and Plane, J. M. C.: Active chlorine release from marine aerosols: Roles for reactive iodine and nitrogen species, J. Geophys. Res., 107, 4271, https://doi.org/10.1029/2001jd000383, 2002.
Muniz-Unamunzaga, M., Borge, R., Sarwar, G., Gantt, B., de la Paz, D., Cuevas, C. A., and Saiz-Lopez, A.: The influence of ocean halogen and sulfur emissions in the air quality of a coastal megacity: The case of Los Angeles, Sci. Total Environ., 610-611, 1536-1545, https://doi.org/10.1016/j.scitotenv.2017.06.098, 2018.
Norris, J. R.: Low cloud type over the ocean from surface observations. Part I: Relationship to surface meteorology and the vertical distribution of temperature and moisture, J. Climate, 11, 369-382, https://doi.org/10.1175/1520-0442(1998)011<0369:Lctoto>2.0.Co;2, 1998.
Pechtl, S., and von Glasow, R.: Reactive chlorine in the marine boundary layer in the outflow of polluted continental air: A model study, Geophys. Res. Lett., 34, https://doi.org/10.1029/2007gl029761, 2007.
Perraud, V., Horne, J. R., Martinez, A. S., Kalinowski, J., Meinardi, S., Dawson, M. L., Wingen, L. M., Dabdub, D., Blake, D. R., Gerber, R. B., and Finlayson-Pitts, B. J.: The future of airborne sulfur-containing particles in the absence of fossil fuel sulfur dioxide emissions, Proc. Natl. Acad. Sci. USA, 112, 13514-13519, https://doi.org/10.1073/pnas.1510743112, 2015.
Pszenny, A. A. P., Moldanov , J., Keene, W. C., Sander, R., Maben, J. R., Martinez, M., Crutzen, P. J., Perner, D., and Prinn, R. G.: Halogen cycling and aerosol pH in the Hawaiian marine boundary layer, Atmos. Chem. Phys., 4, 147-168, https://doi.org/10.5194/acp-4-147-2004, 2004.
Quinn, P. K., Collins, D. B., Grassian, V. H., Prather, K. A., and Bates, T. S.: Chemistry and related properties of freshly emitted sea spray aerosol, Chem. Rev., 115, 4383-4399, https://doi.org/10.1021/cr500713g, 2015.
Read, K. A., Mahajan, A. S., Carpenter, L. J., Evans, M. J., Faria, B. V., Heard, D. E., Hopkins, J. R., Lee, J. D., Moller, S. J., Lewis, A. C., Mendes, L., McQuaid, J. B., Oetjen, H., Saiz-Lopez, A., Pilling, M. J., and Plane, J. M.: Extensive halogen-mediated ozone destruction over the tropical Atlantic Ocean, Nature, 453, 1232-1235, https://doi.org/10.1038/nature07035, 2008.
Saiz-Lopez, A., Plane, J. M., Baker, A. R., Carpenter, L. J., von Glasow, R., Martin, J. C., McFiggans, G., and Saunders, R. W.: Atmospheric chemistry of iodine, Chem. Rev., 112, 1773-1804, https://doi.org/10.1021/cr200029u, 2012.
Saiz-Lopez, A., and von Glasow, R.: Reactive halogen chemistry in the troposphere, Chem. Soc. Rev., 41, 6448-6472, https://doi.org/10.1039/c2cs35208g, 2012.
Saiz-Lopez, A., Fernandez, R. P., Ordóñez, C., Kinnison, D. E., Gómez Martín, J. C., Lamarque, J. F., and Tilmes, S.: Iodine chemistry in the troposphere and its effect on ozone, Atmos. Chem. Phys., 14, 13119-13143, https://doi.org/10.5194/acp-14-13119-2014, 2014.
Sander, R., Keene, W. C., Pszenny, A. A. P., Arimoto, R., Ayers, G. P., Baboukas, E., Cainey, J. M., Crutzen, P. J., Duce, R. A., Hönninger, G., Huebert, B. J., Maenhaut, W., Mihalopoulos, N., Turekian, V. C., and Van Dingenen, R.: Inorganic bromine in the marine boundary layer: a critical review, Atmos. Chem. Phys., 3, 1301-1336, https://doi.org/10.5194/acp-3-1301-2003, 2003.
Sander, R., Pszenny, A. A. P., Keene, W. C., Crete, E., Deegan, B., Long, M. S., Maben, J. R., and Young, A. H.: Gas phase acid, ammonia and aerosol ionic and trace element concentrations at Cape Verde during the Reactive Halogens in the Marine Boundary Layer (RHaMBLe) 2007 intensive sampling period, Earth Syst. Sci. Data, 5, 385-392, https://doi.org/10.5194/essd-5-385-2013, 2013.
Saunders, S. M., Jenkin, M. E., Derwent, R. G., and Pilling, M. J.: Protocol for the development of the Master Chemical Mechanism, MCM v3 (Part A): Tropospheric degradation of non-aromatic volatile organic compounds, Atmos. Chem. Phys., 3, 161-180, https://doi.org/10.5194/acp-3-161-2003, 2003.
Schmidt, J. A., Jacob, D. J., Horowitz, H. M., Hu, L., Sherwen, T., Evans, M. J., Liang, Q., Suleiman, R. M., Oram, D. E., Le Breton, M., Percival, C. J., Wang, S., Dix, B., and Volkamer, R.: Modeling the observed tropospheric BrO background:

Importance of multiphase chemistry and implications for ozone, OH, and mercury, J. Geophys. Res.-Atmos, 121, 11,819-811,835, https://doi.org/10.1002/2015jd024229, 2016.
Schrödner, R., Tilgner, A., Wolke, R., and Herrmann, H.: Modeling the multiphase processing of an urban and a rural air mass with COSMO–MUSCAT, Urban Clim., 10, 720-731, https://doi.org/10.1016/j.uclim.2014.02.001, 2014.
Schrödner, R., Wolke, R., Tilgner, A., van Pinxteren, D., and Herrmann, H.: Modelling Multiphase Aerosol-Cloud Processing with the 3-D CTM COSMO-MUSCAT: Application for Cloud Events During HCCT-2010, Air Pollution Modeling and its Application XXV, Cham, 2018, 587-592,
Schultz, M. G., Stadtler, S., Schröder, S., Taraborrelli, D., Franco, B., Krefting, J., Henrot, A., Ferrachat, S., Lohmann, U., Neubauer, D., Siegenthaler-Le Drian, C., Wahl, S., Kokkola, H., Kühn, T., Rast, S., Schmidt, H., Stier, P., Kinnison, D., Tyndall, G. S., Orlando, J. J., and Wespes, C.: The chemistry–climate model ECHAM6.3-HAM2.3-MOZ1.0, Geosci. Model Dev., 11, 1695-1723, https://doi.org/10.5194/gmd-11-1695-2018, 2018.
Sehili, A. M., Wolke, R., Knoth, O., Simmel, M., Tilgner, A., and Herrmann, H.: Comparison of different model approaches for the simulation of multiphase processes, Atmos. Environ., 39, 4403-4417, https://doi.org/10.1016/j.atmosenv.2005.02.039, 2005.
Seinfeld, J. H., and Pandis, S. N.: Atmospheric Chemistry and Physics, John Wiley & Sons, Inc., Hoboken, New Jersey, USA, 1248 pp., 2006.
Shechner, M., and Tas, E.: Ozone Formation Induced by the Impact of Reactive Bromine and Iodine Species on Photochemistry in a Polluted Marine Environment, Environ. Sci. Technol., 51, 14030-14037, https://doi.org/10.1021/acs.est.7b02860, 2017.
Sherwen, T., Schmidt, J. A., Evans, M. J., Carpenter, L. J., Großmann, K., Eastham, S. D., Jacob, D. J., Dix, B., Koenig, T. K., Sinreich, R., Ortega, I., Volkamer, R., Saiz-Lopez, A., Prados-Roman, C., Mahajan, A. S., and Ordóñez, C.: Global impacts of tropospheric halogens (Cl, Br, I) on oxidants and composition in GEOS-Chem, Atmos. Chem. Phys., 16, 12239-12271, https://doi.org/10.5194/acp-16-12239-2016, 2016.
Sherwen, T., Evans, M. J., Sommariva, R., Hollis, L. D. J., Ball, S. M., Monks, P. S., Reed, C., Carpenter, L. J., Lee, J. D., Forster, G., Bandy, B., Reeves, C. E., and Bloss, W. J.: Effects of halogens on European air-quality, Faraday Discuss., 200, 75-100, https://doi.org/10.1039/c7fd00026j, 2017.
Simpson, W. R., Brown, S. S., Saiz-Lopez, A., Thornton, J. A., and Glasow, R.: Tropospheric halogen chemistry: sources, cycling, and impacts, Chem. Rev., 115, 4035-4062, https://doi.org/10.1021/cr5006638, 2015.
Steppeler, J., Doms, G., Schattler, U., Bitzer, H. W., Gassmann, A., Damrath, U., and Gregoric, G.: Meso-gamma scale forecasts using the nonhydrostatic model LM, Meteorol. Atmos. Phys., 82, 75-96, https://doi.org/10.1007/s00703-001-0592-9, 2003.
Surratt, J. D., Lewandowski, M., Offenberg, J. H., Jaoui, M., Kleindienst, T. E., Edney, E. O., and Seinfeld, J. H.: Effect of Acidity on Secondary Organic Aerosol Formation from Isoprene, Environ. Sci. Technol., 41, 5363-5369, https://doi.org/10.1021/es0704176, 2007.
Surratt, J. D., Chan, A. W., Eddingsaas, N. C., Chan, M., Loza, C. L., Kwan, A. J., Hersey, S. P., Flagan, R. C., Wennberg, P. O., and Seinfeld, J. H.: Reactive intermediates revealed in secondary organic aerosol formation from isoprene, Proc. Natl. Acad. Sci. USA, 107, 6640-6645, https://doi.org/10.1073/pnas.0911114107, 2010.
Volkamer, R., Baidar, S., Campos, T. L., Coburn, S., DiGangi, J. P., Dix, B., Eloranta, E. W., Koenig, T. K., Morley, B., Ortega, I., Pierce, B. R., Reeves, M., Sinreich, R., Wang, S., Zondlo, M. A., and Romashkin, P. A.: Aircraft measurements of BrO, IO, glyoxal, NO_2, H_2O, O_2–O_2 and aerosol extinction profiles in the tropics: comparison with aircraft-/ship-based in situ and lidar measurements, Atmos. Meas. Tech., 8, 2121-2148, https://doi.org/10.5194/amt-8-2121-2015, 2015.
von Glasow, R., Sander, R., Bott, A., and Crutzen, P. J.: Modeling halogen chemistry in the marine boundary layer 2. Interactions with sulfur and the cloud-covered MBL, J. Geophys. Res.-Atmos., 107, 4323, https://doi.org/10.1029/2001jd000943, 2002a.
von Glasow, R., Sander, R., Bott, A., and Crutzen, P. J.: Modeling halogen chemistry in the marine boundary layer 1. Cloud-free MBL, J. Geophys. Res.-Atmos., 107, 4341, https://doi.org/10.1029/2001jd000942, 2002b.
von Glasow, R., and Crutzen, P. J.: Model study of multiphase DMS oxidation with a focus on halogens, Atmos. Chem. Phys., 4, 589-608, https://doi.org/10.5194/acp-4-589-2004, 2004.
von Glasow, R., Jickells, T. D., Baklanov, A., Carmichael, G. R., Church, T. M., Gallardo, L., Hughes, C., Kanakidou, M., Liss, P. S., Mee, L., Raine, R., Ramachandran, P., Ramesh, R., Sundseth, K., Tsunogai, U., Uematsu, M., and Zhu, T.:

Megacities and large urban agglomerations in the coastal zone: interactions between atmosphere, land, and marine ecosystems, Ambio, 42, 13-28, https://doi.org/10.1007/s13280-012-0343-9, 2013.
Wang, X., Jacob, D. J., Eastham, S. D., Sulprizio, M. P., Zhu, L., Chen, Q., Alexander, B., Sherwen, T., Evans, M. J., Lee, B. H., Haskins, J. D., Lopez-Hilfiker, F. D., Thornton, J. A., Huey, G. L., and Liao, H.: The role of chlorine in global tropospheric chemistry, Atmos. Chem. Phys., 19, 3981-4003, https://doi.org/10.5194/acp-19-3981-2019, 2019.
Wolke, R., Knoth, O., Hellmuth, O., Schröder, W., and Renner, E.: The parallel model system LM-MUSCAT for chemistry-transport simulations: Coupling scheme, parallelization and application, in: Parallel Computing: Software Technology, Algorithms, Architectures, and Applications, edited by: G.R. Joubert, W. E. N., F.J. Peters, and W.V. Walter, Elsevier, Amsterdam, Netherlands, 363-370, 2004.
Wolke, R., Sehili, A. M., Simmel, M., Knoth, O., Tilgner, A., and Herrmann, H.: SPACCIM: A parcel model with detailed microphysics and complex multiphase chemistry, Atmos. Environ., 39, 4375-4388, https://doi.org/10.1016/j.atmosenv.2005.02.038, 2005.
Wolke, R., Schröder, W., Schrödner, R., and Renner, E.: Influence of grid resolution and meteorological forcing on simulated European air quality: A sensitivity study with the modeling system COSMO–MUSCAT, Atmos. Environ., 53, 110-130, https://doi.org/10.1016/j.atmosenv.2012.02.085, 2012.
Wu, R., Wang, S., and Wang, L.: New mechanism for the atmospheric oxidation of dimethyl sulfide. The importance of intramolecular hydrogen shift in a CH_3SCH_2OO radical, J. Phys. Chem. A, 119, 112-117, https://doi.org/10.1021/jp511616j, 2015.
Wudl, F., Lightner, D. A., and Cram, D. J.: Methanesulfinic acid and Its properties, J. Am. Chem. Soc., 89, 4099-4101, https://doi.org/10.1021/Ja00992a026, 1967.
Xue, L. K., Saunders, S. M., Wang, T., Gao, R., Wang, X. F., Zhang, Q. Z., and Wang, W. X.: Development of a chlorine chemistry module for the Master Chemical Mechanism, Geosci. Model Dev., 8, 3151-3162, https://doi.org/10.5194/gmd-8-3151-2015, 2015.
Yan, Y., Cabrera-Perez, D., Lin, J., Pozzer, A., Hu, L., Millet, D. B., Porter, W. C., and Lelieveld, J.: Global tropospheric effects of aromatic chemistry with the SAPRC-11 mechanism implemented in GEOS-Chem version 9-02, Geosci. Model Dev., 12, 111-130, https://doi.org/10.5194/gmd-12-111-2019, 2019.
Yin, F. D., Grosjean, D., and Seinfeld, J. H.: Photooxidation of dimethyl sulfide and dimethyl disulfide. 1. Mechanism Development, J. Atmos. Chem., 11, 309-364, https://doi.org/10.1007/Bf00053780, 1990.
Yuan, J., and Shiller, A. M.: The variation of hydrogen peroxide in rainwater over the South and Central Atlantic Ocean, Atmos. Environ., 34, 3973-3980, https://doi.org/10.1016/S1352-2310(00)00167-9, 2000.
Zängl, G., Reinert, D., Rípodas, P., and Baldauf, M.: The ICON (ICOsahedral Non-hydrostatic) modelling framework of DWD and MPI-M: Description of the non-hydrostatic dynamical core, Q. J. Royal Meteorol. Soc., 141, 563-579, https://doi.org/10.1002/qj.2378, 2015.
Zhu, L., Nicovich, J. M., and Wine, P. H.: Temperature-dependent kinetics studies of aqueous phase reactions of hydroxyl radicals with dimethylsulfoxide, dimethylsulfone, and methanesulfonate, Aquat. Sci., 65, 425-435, https://doi.org/10.1007/s00027-003-0673-6, 2003.
Zhu, L., Jacob, D. J., Eastham, S. D., Sulprizio, M. P., Wang, X., Sherwen, T., Evans, M. J., Chen, Q., Alexander, B., Koenig, T. K., Volkamer, R., Huey, L. G., Le Breton, M., Bannan, T. J., and Percival, C. J.: Effect of sea salt aerosol on tropospheric bromine chemistry, Atmos. Chem. Phys., 19, 6497-6507, https://doi.org/10.5194/acp-19-6497-2019, 2019.

Table 1 Average percentage deviations [%] of some inorganic and organic target compounds between the simulations with the full and reduced CAPRAM-DM1.0 and CAPRAM-HM3 mechanisms (deviations calculated throughout the full SPACCIM simulation). Exceedances of the threshold are marked in italic.

Species	**'Pristine'**		**'Breeze'**		**'Outflow'**	
Gas phase	**Average**	**R^2**	**Average**	**R^2**	**Average**	**R^2**
5% treshold						
O_3	-0.2%	1.00	0.3%	1.00	0.1%	1.00
NO	-3.9%	1.00	0.4%	1.00	-0.8%	1.00
NO_2	-2.1%	1.00	0.7%	1.00	-0.1%	1.00
SO_2	1.5%	1.00	1.3%	1.00	0.6%	1.00
HNO_3	1.2%	1.00	-0.5%	1.00	-1.0%	1.00
DMS	-4.2%	1.00	-1.6%	1.00	-3.2%	1.00
HCl	0.6%	1.00	-2.1%	1.00	-0.6%	1.00
10% treshold						
DMSO	6.1%	1.00	-1.5%	1.00	*10.6%*	0.99
OH	0.0%	1.00	0.0%	1.00	0.1%	1.00
HO_2	-0.5%	1.00	0.1%	1.00	-0.1%	1.00
NO_3	-0.5%	1.00	0.6%	1.00	0.0%	1.00
H_2O_2	0.0%	1.00	-3.3%	1.00	-2.4%	1.00
Cl	6.4%	1.00	5.1%	1.00	0.8%	1.00
Br	9.8%	1.00	4.2%	1.00	*29.0%*	0.98
I	-0.6%	1.00	-6.1%	0.99	-1.2%	0.99
ClO	7.4%	1.00	7.9%	1.00	2.0%	1.00
BrO	9.7%	0.99	4.2%	1.00	*24.5%*	0.95
IO	-1.8%	1.00	-3.1%	0.99	-0.9%	1.00
HOCl	5.0%	1.00	*37.5%*	0.96	*17.8%*	1.00
HOBr	8.9%	1.00	*10.2%*	1.00	*27.7%*	0.97
HOI	-2.4%	1.00	3.5%	0.98	-3.4%	0.98
Cl_2	0.4%	1.00	5.6%	0.97	-2.4%	0.97
Br_2	*36.0%*	0.96	-1.1%	0.93	*24.0%*	0.75
$ClNO_2$	-0.9%	1.00	0.0%	1.00	0.3%	1.00
Aqueous phase	**Average**	**R^2**	**Average**	**R^2**	**Average**	**R^2**
5% treshold						
OrgMass	1.1%	1.00	-0.2%	1.00	0.0%	1.00
DryMass	0.2%	1.00	-0.3%	1.00	0.1%	1.00
H^+	0.2%	1.00	-1.2%	1.00	-0.2%	1.00
Sulfate	1.1%	1.00	-0.6%	1.00	-0.1%	1.00
Nitrate	0.0%	1.00	0.8%	1.00	1.7%	1.00
Cl^-	-0.4%	1.00	0.0%	1.00	0.7%	1.00
Methane sulfonate	2.5%	1.00	*-18.7%*	1.00	2.1%	1.00
10% treshold						
OH_{aq}	-1.9%	1.00	2.0%	0.99	2.1%	0.99
$HO_{2,\,aq}$	0.2%	1.00	0.7%	1.00	0.1%	1.00
$O_2^-{}_{aq}$	-0.1%	1.00	2.8%	1.00	3.0%	1.00

Gelöscht: red

Formatiert: Schriftart: 10 Pt., Kursiv, Schriftfarbe: Automatisch

Formatiert: Schriftart: Kursiv

Formatiert: Schriftart: 10 Pt., Kursiv, Schriftfarbe: Automatisch

Formatiert: Schriftart: Kursiv

Formatiert: Schriftart: 10 Pt., Kursiv, Schriftfarbe: Automatisch

Formatiert: Schriftart: Kursiv

Formatiert: Schriftart: 10 Pt., Kursiv, Schriftfarbe: Automatisch

Formatiert: Schriftart: Kursiv

Formatiert: Schriftart: 10 Pt., Kursiv, Schriftfarbe: Automatisch

Formatiert: Schriftart: Kursiv

Formatiert: Schriftart: 10 Pt., Kursiv, Schriftfarbe: Automatisch

Formatiert: Schriftart: Kursiv

Formatiert: Schriftart: 10 Pt., Kursiv, Schriftfarbe: Automatisch

Formatiert: Schriftart: Kursiv

Formatiert: Schriftart: 10 Pt., Kursiv, Schriftfarbe: Automatisch

Formatiert: Schriftart: Kursiv

Formatiert: Schriftart: 10 Pt., Kursiv, Schriftfarbe: Automatisch

Formatiert: Schriftart: Kursiv

Formatiert: Schriftart: 10 Pt., Kursiv, Schriftfarbe: Automatisch

Formatiert: Schriftart: Kursiv

Table 2 Description of the lumped MOZART4 species and the corresponding kinetic reaction rate constants.

Species	Comment	k	Comment on k
BIGALK	Alkanes with C ≥ 4	2.05×10^{-10}	same as for butane
ALKOH	Alcohols with C ≥ 3	$2.7\times10^{-11}e^{525/T}$	same as for propanol
C_2H_5CHO	Aldehydes with C ≥ 3	$4.9\times10^{-12}e^{405/T}$	OH; same as for propionaldehyde
		1.3×10^{-10}	Cl; same as for propionaldehyde
		$5.75\times10^{-11}e^{-610/T}$	Br; same as for propionaldehyde
BIGALD1	Unsaturated dialdehyde	1.35×10^{-10}	same as for 2-butenedial
XYL	Lumped xylenes	1.4×10^{-10}	mean value of o-, p- and m-xylene
BZALD	Lumped aromatic aldehydes	1.0×10^{-10}	same as for benzaldehyde

Formatierte Tabelle

Supporting information for:

CAPRAM reduction towards an operational multiphase halogen and DMS chemistry treatment in the chemistry transport model COSMO-MUSCAT(5.04e)

Erik H. Hoffmann[1], Roland Schrödner[2], Andreas Tilgner[1], Ralf Wolke[2], Hartmut Herrmann[1]

[1] Atmospheric Chemistry Department (ACD), Leibniz Institute for Tropospheric Research (TROPOS), Permoserstr. 15, 04318 5 Leipzig, Germany
[2] Modeling of Atmospheric Processes Department (MAPD), Leibniz Institute for Tropospheric Research (TROPOS), Permoserstr. 15, 04318 Leipzig, 04318, Germany

Correspondence to: Hartmut Herrmann (herrmann@tropos.de)

Number of pages: 44
Figures: 12
Tables: 11

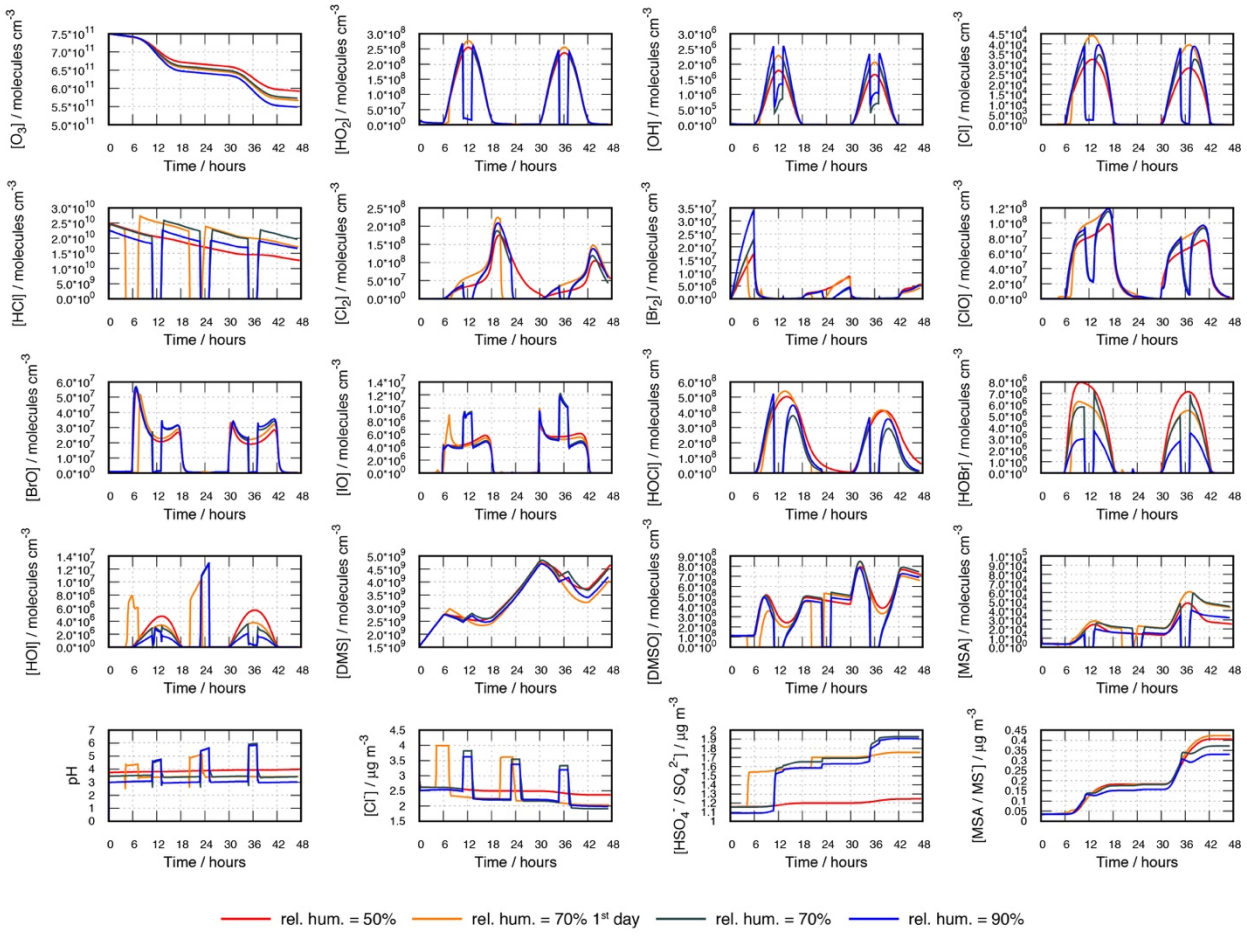

Figure S1 **Modelled concentration time-profile of key compounds within the pristine marine boundary layer for the summer simulations at 15° latitude. Red: simulation at rel. humidity of 50% (red). Orange: simulation at relative humidity of 70% and cloud occurrence at early morning and evening of the first model day. Dark green: simulation at relative humidity of 70% and cloud occurrence at noon and midnight. Blue: simulation at relative humidity of 90% and cloud occurrence at noon and midnight.**

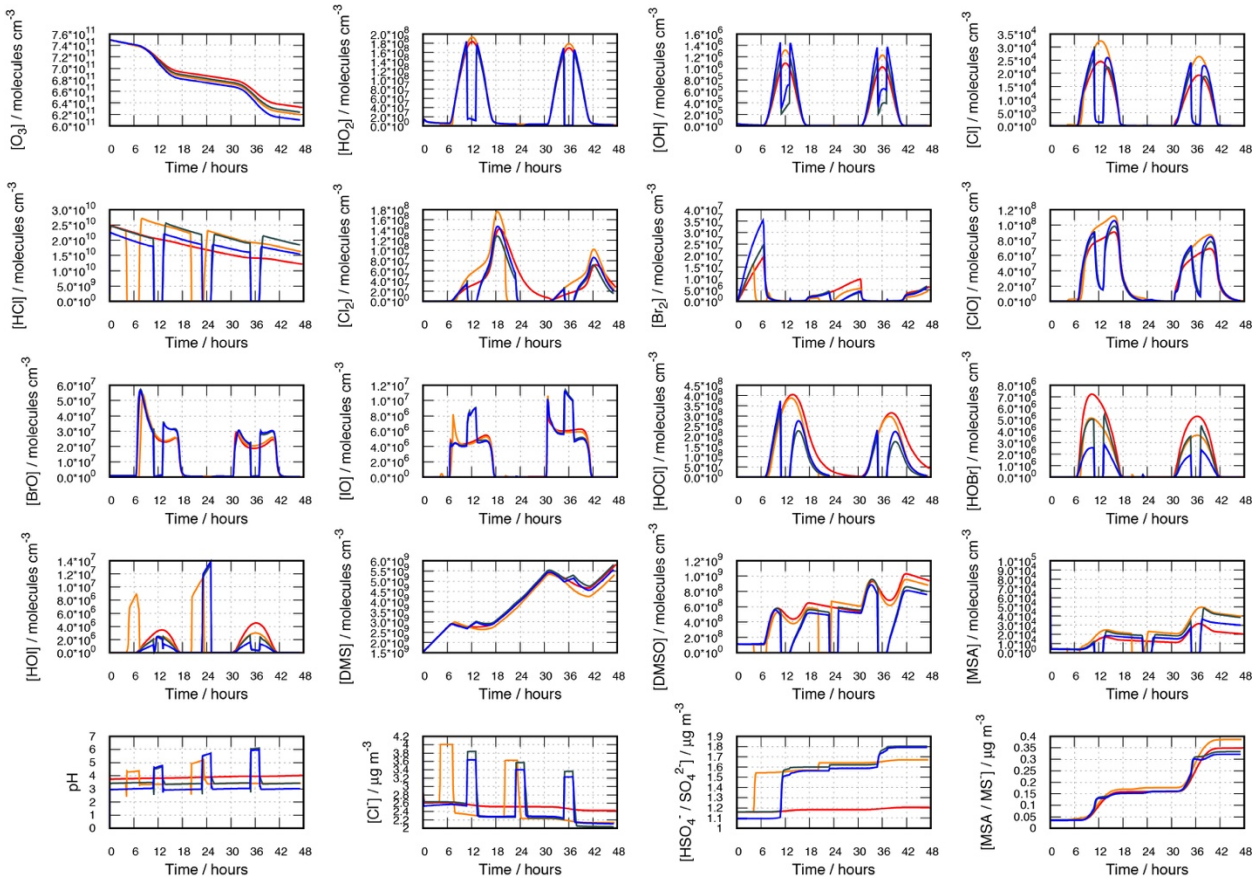

Figure S2 **Modelled concentration time-profile of key compounds within the pristine marine boundary layer for the winter simulations at 15° latitude. Red: simulation at rel. humidity of 50% (red). Orange: simulation at relative humidity of 70% and cloud occurrence at early morning and evening of the first model day. Dark green: simulation at relative humidity of 70% and cloud occurrence at noon and midnight. Blue: simulation at relative humidity of 90% and cloud occurrence at noon and midnight.**

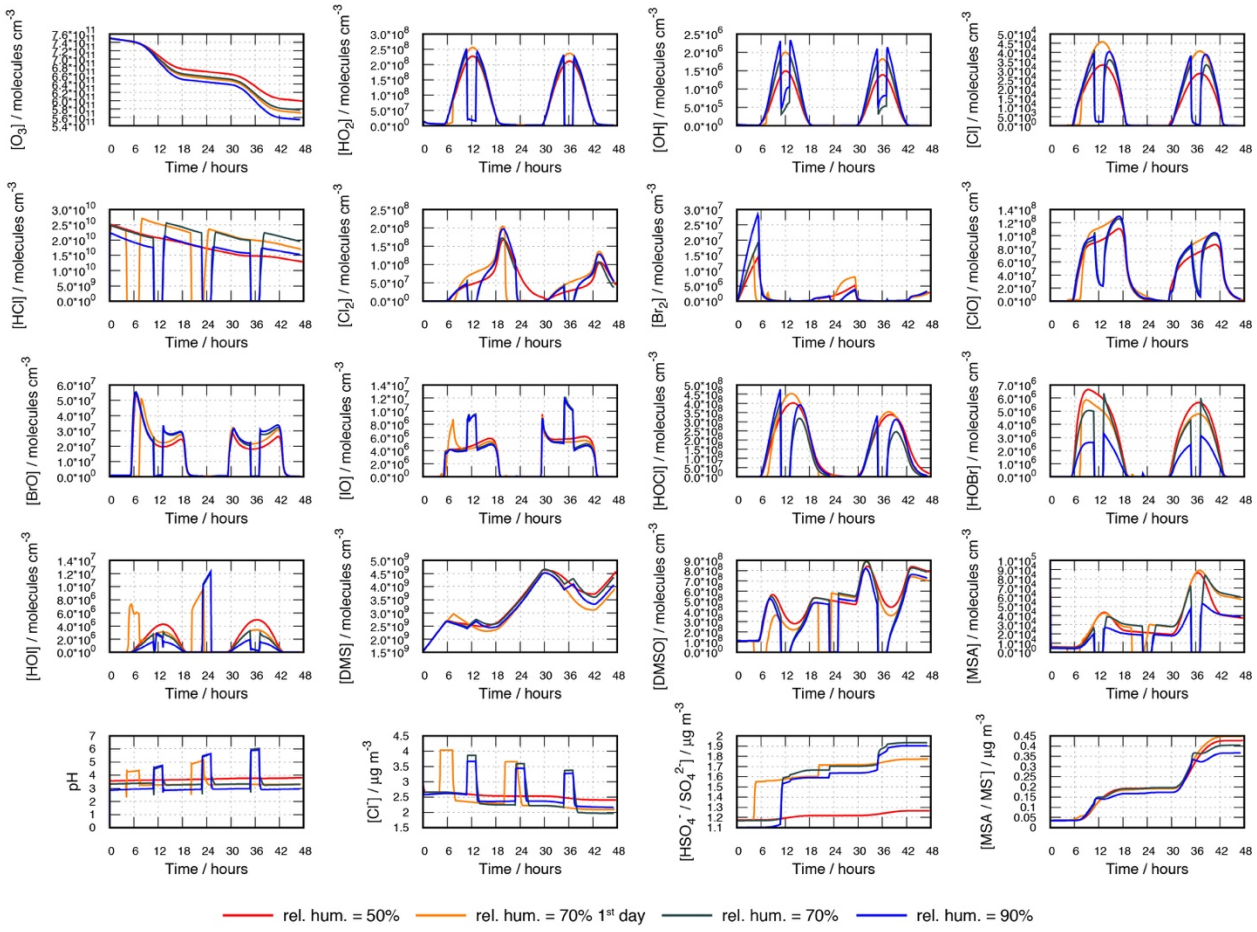

Figure S3 **Modelled concentration time-profile of key compounds within the pristine marine boundary layer for the summer simulations at 30° latitude. Red: simulation at rel. humidity of 50% (red). Orange: simulation at relative humidity of 70% and cloud occurrence at early morning and evening of the first model day. Dark green: simulation at relative humidity of 70% and cloud occurrence at noon and midnight. Blue: simulation at relative humidity of 90% and cloud occurrence at noon and midnight.**

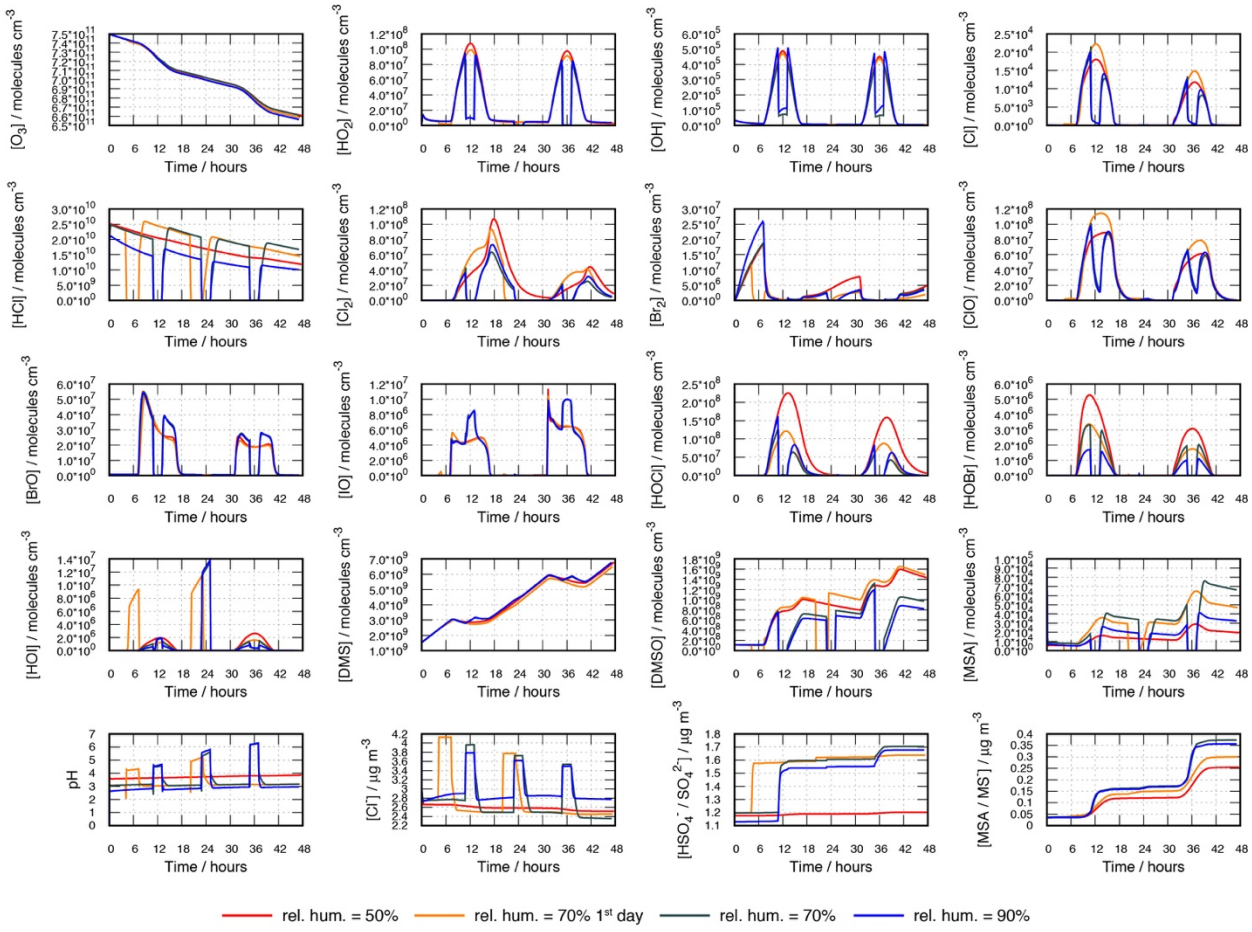

Figure S4 **Modelled concentration time-profile of key compounds within the pristine marine boundary layer for the winter simulations at 30° latitude. Red: simulation at rel. humidity of 50% (red). Orange: simulation at relative humidity of 70% and cloud occurrence at early morning and evening of the first model day. Dark green: simulation at relative humidity of 70% and cloud occurrence at noon and midnight. Blue: simulation at relative humidity of 90% and cloud occurrence at noon and midnight.**

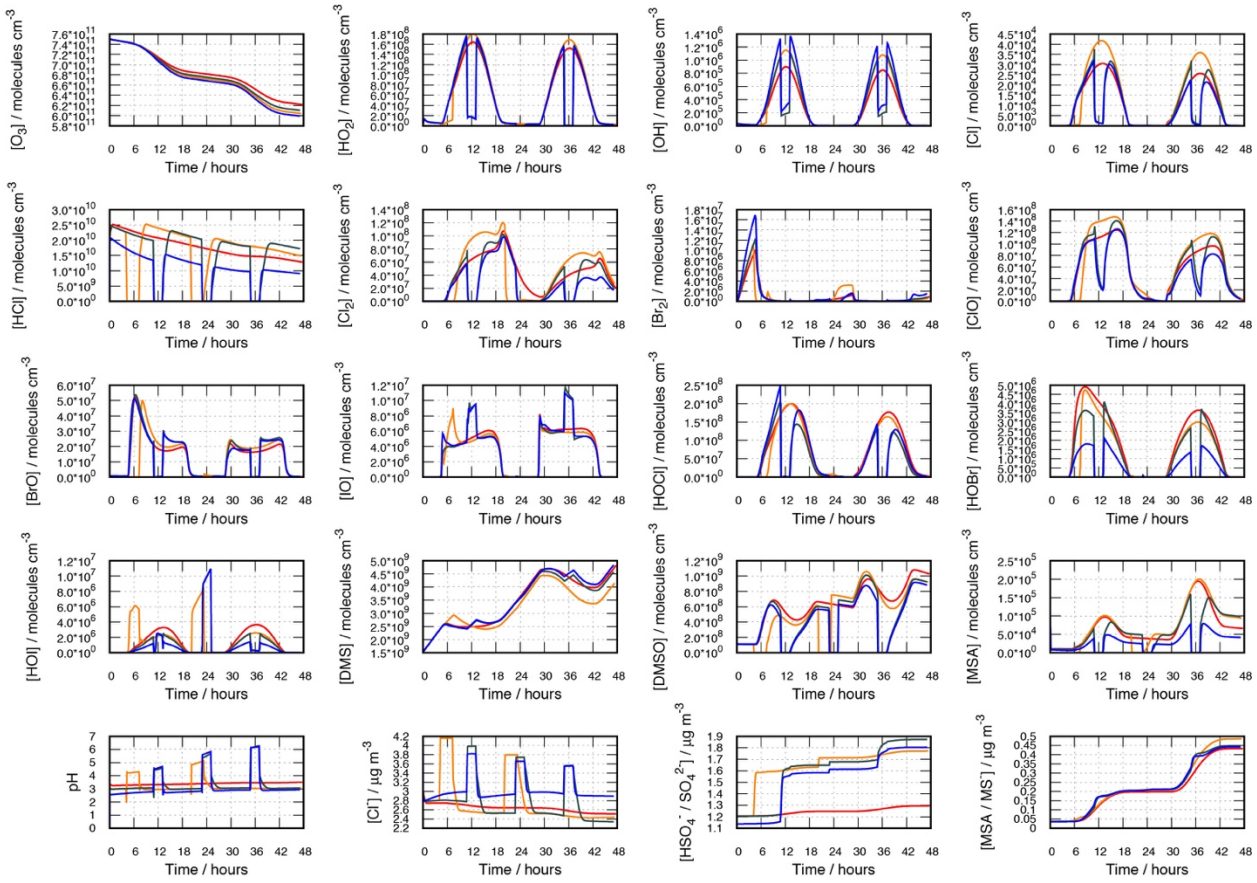

Figure S5 **Modelled concentration time-profile of key compounds within the pristine marine boundary layer for the summer simulations at 45° latitude. Red: simulation at rel. humidity of 50% (red). Orange: simulation at relative humidity of 70% and cloud occurrence at early morning and evening of the first model day. Dark green: simulation at relative humidity of 70% and cloud occurrence at noon and midnight. Blue: simulation at relative humidity of 90% and cloud occurrence at noon and midnight.**

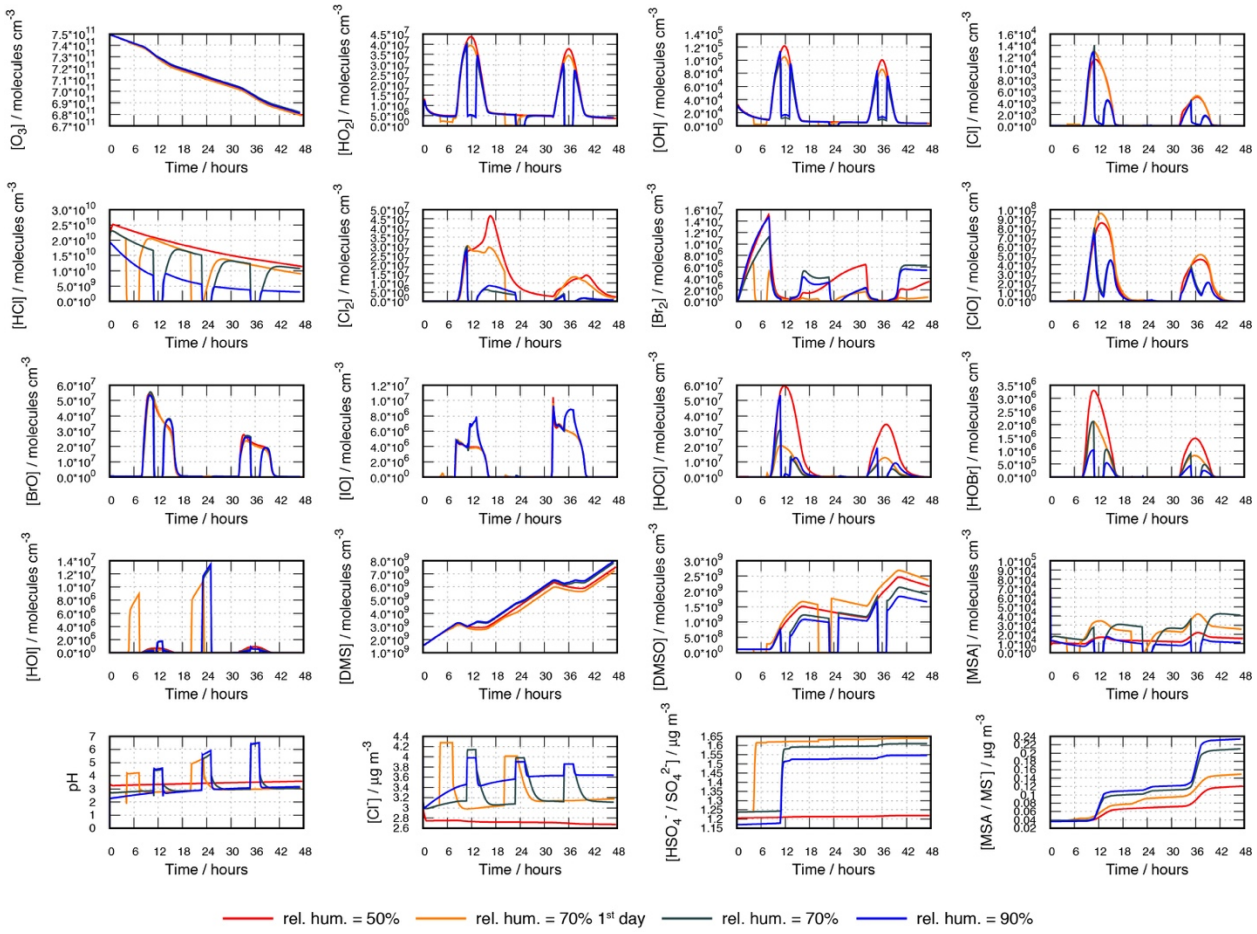

Figure S6 **Modelled concentration time-profile of key compounds within the pristine marine boundary layer for the winter simulations at 45° latitude. Red: simulation at rel. humidity of 50% (red). Orange: simulation at relative humidity of 70% and cloud occurrence at early morning and evening of the first model day. Dark green: simulation at relative humidity of 70% and cloud occurrence at noon and midnight. Blue: simulation at relative humidity of 90% and cloud occurrence at noon and midnight.**

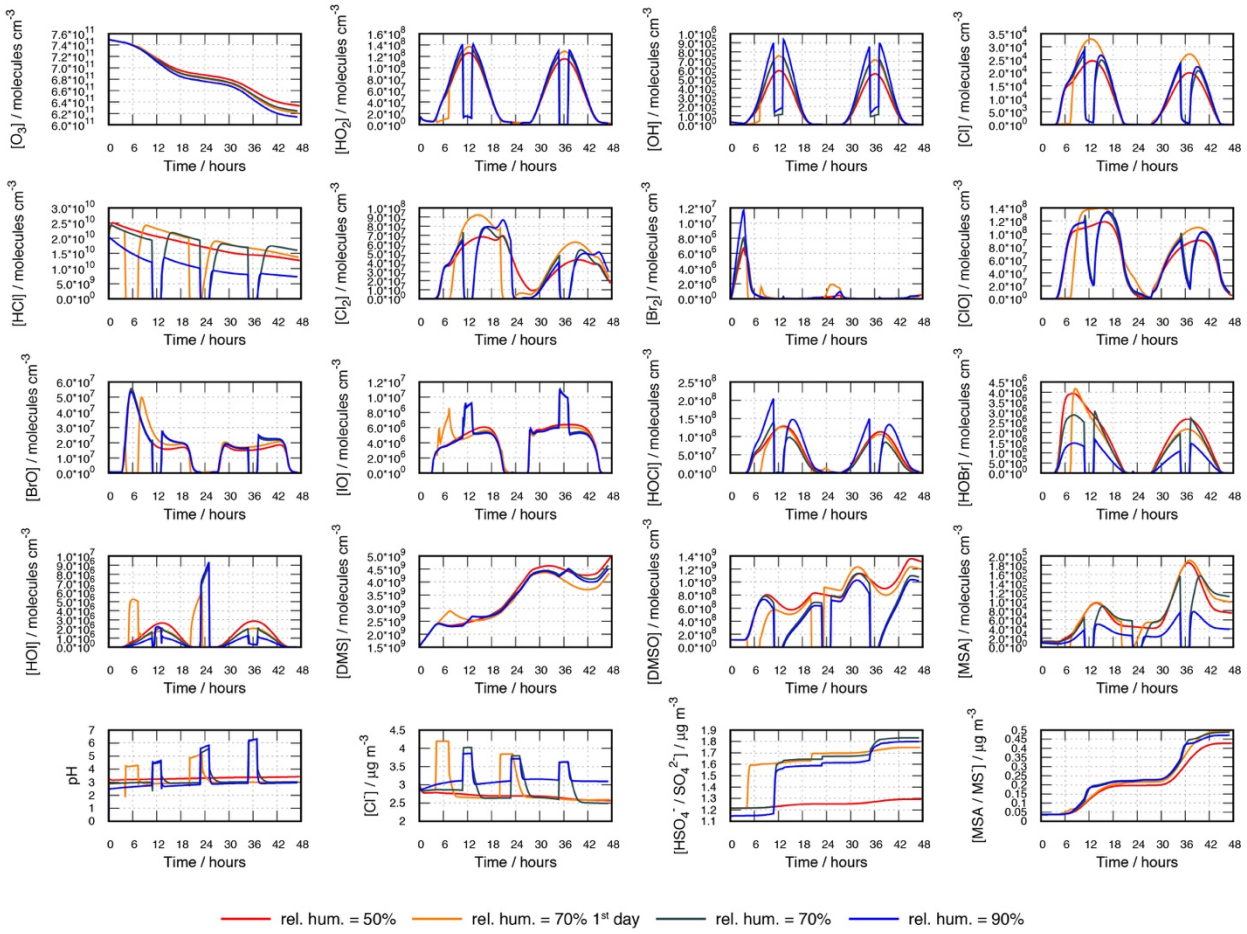

Figure S7 **Modelled concentration time-profile of key compounds within the pristine marine boundary layer for the summer simulations at 60° latitude. Red: simulation at rel. humidity of 50% (red). Orange: simulation at relative humidity of 70% and cloud occurrence at early morning and evening of the first model day. Dark green: simulation at relative humidity of 70% and cloud occurrence at noon and midnight. Blue: simulation at relative humidity of 90% and cloud occurrence at noon and midnight.**

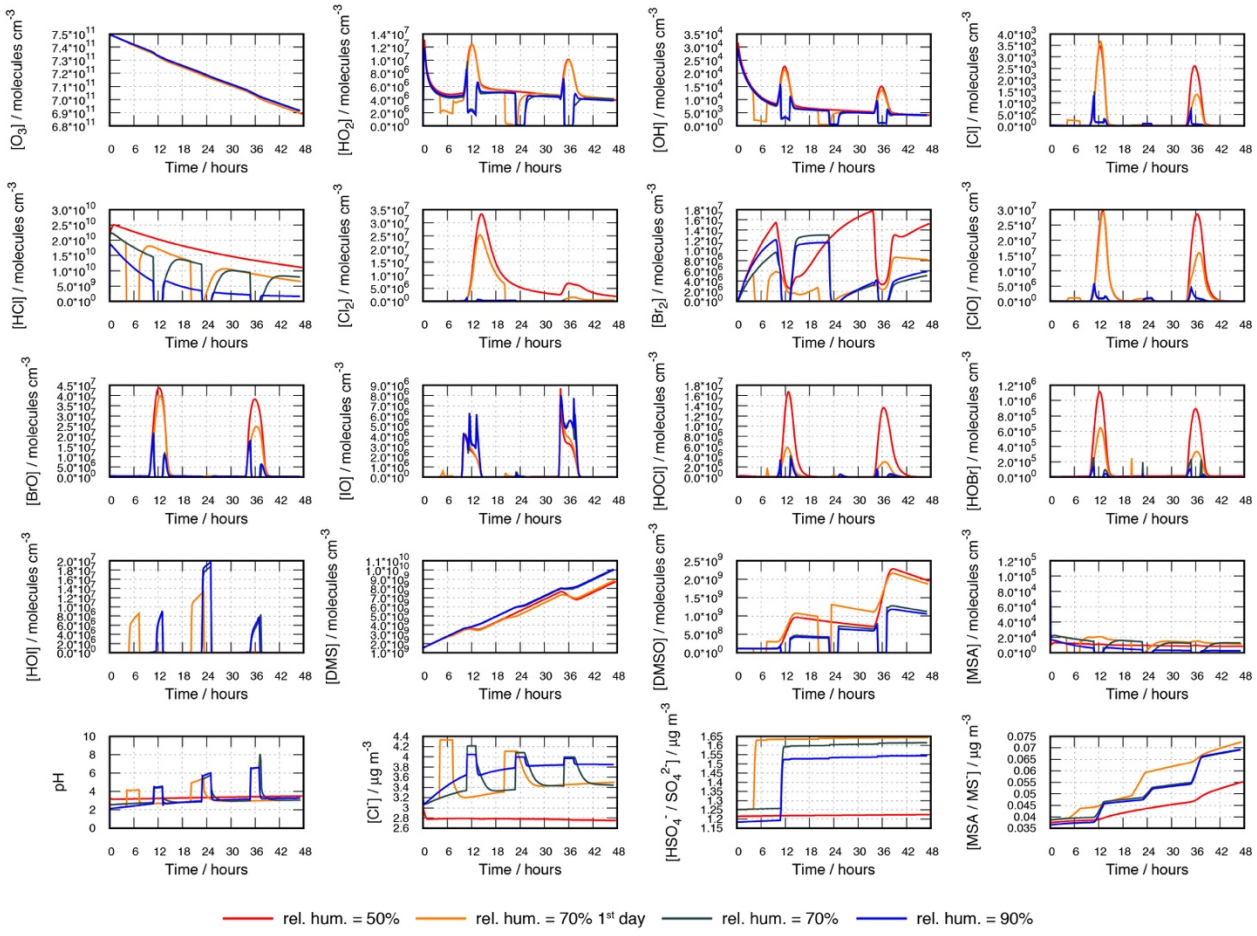

Figure S8 **Modelled concentration time-profile of key compounds within the pristine marine boundary layer for the winter simulations at 60° latitude. Red: simulation at rel. humidity of 50% (red). Orange: simulation at relative humidity of 70% and cloud occurrence at early morning and evening of the first model day. Dark green: simulation at relative humidity of 70% and cloud occurrence at noon and midnight. Blue: simulation at relative humidity of 90% and cloud occurrence at noon and midnight.**

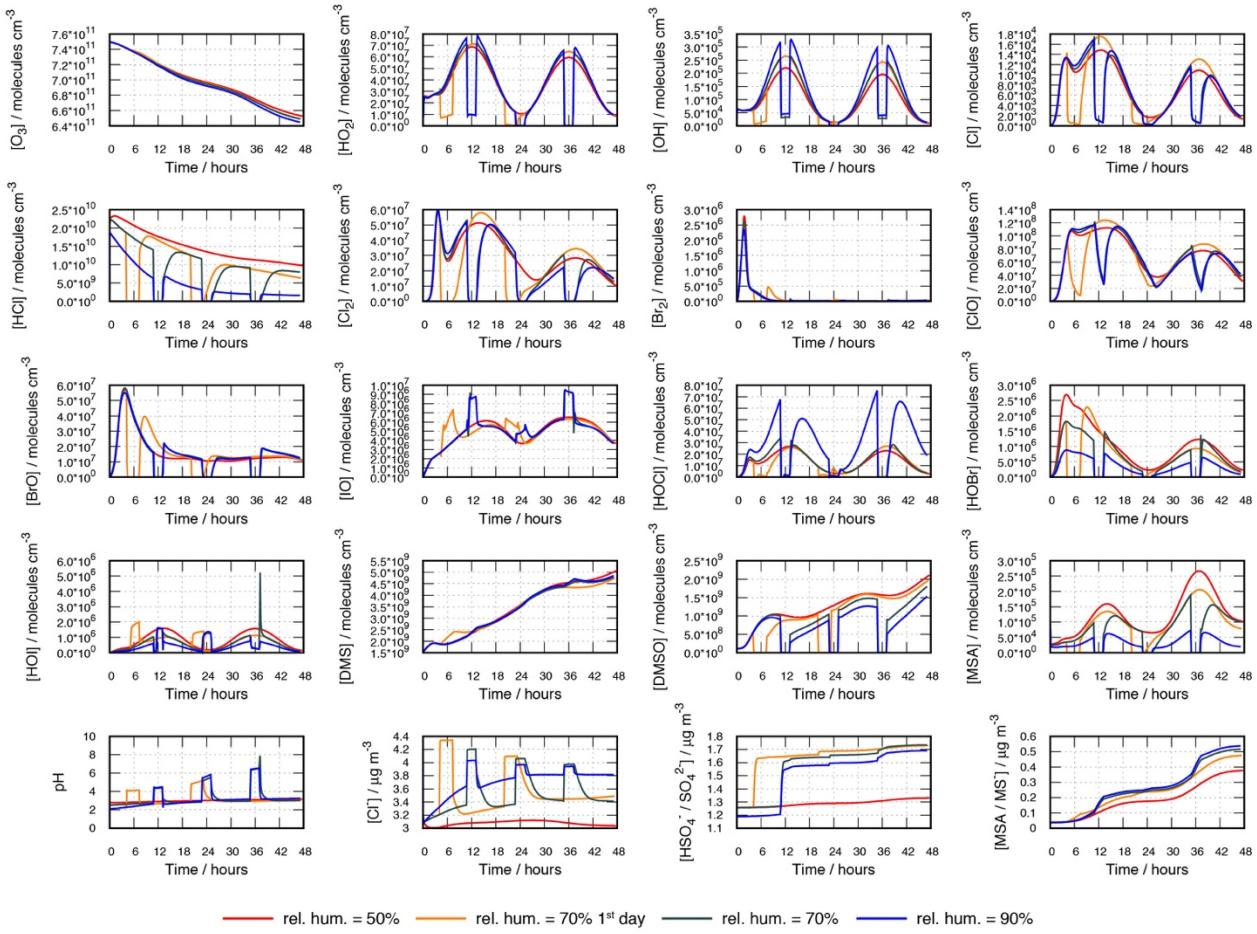

Figure S9 **Modelled concentration time-profile of key compounds within the pristine marine boundary layer for the summer simulations at 75° latitude. Red: simulation at rel. humidity of 50% (red). Orange: simulation at relative humidity of 70% and cloud occurrence at early morning and evening of the first model day. Dark green: simulation at relative humidity of 70% and cloud occurrence at noon and midnight. Blue: simulation at relative humidity of 90% and cloud occurrence at noon and midnight.**

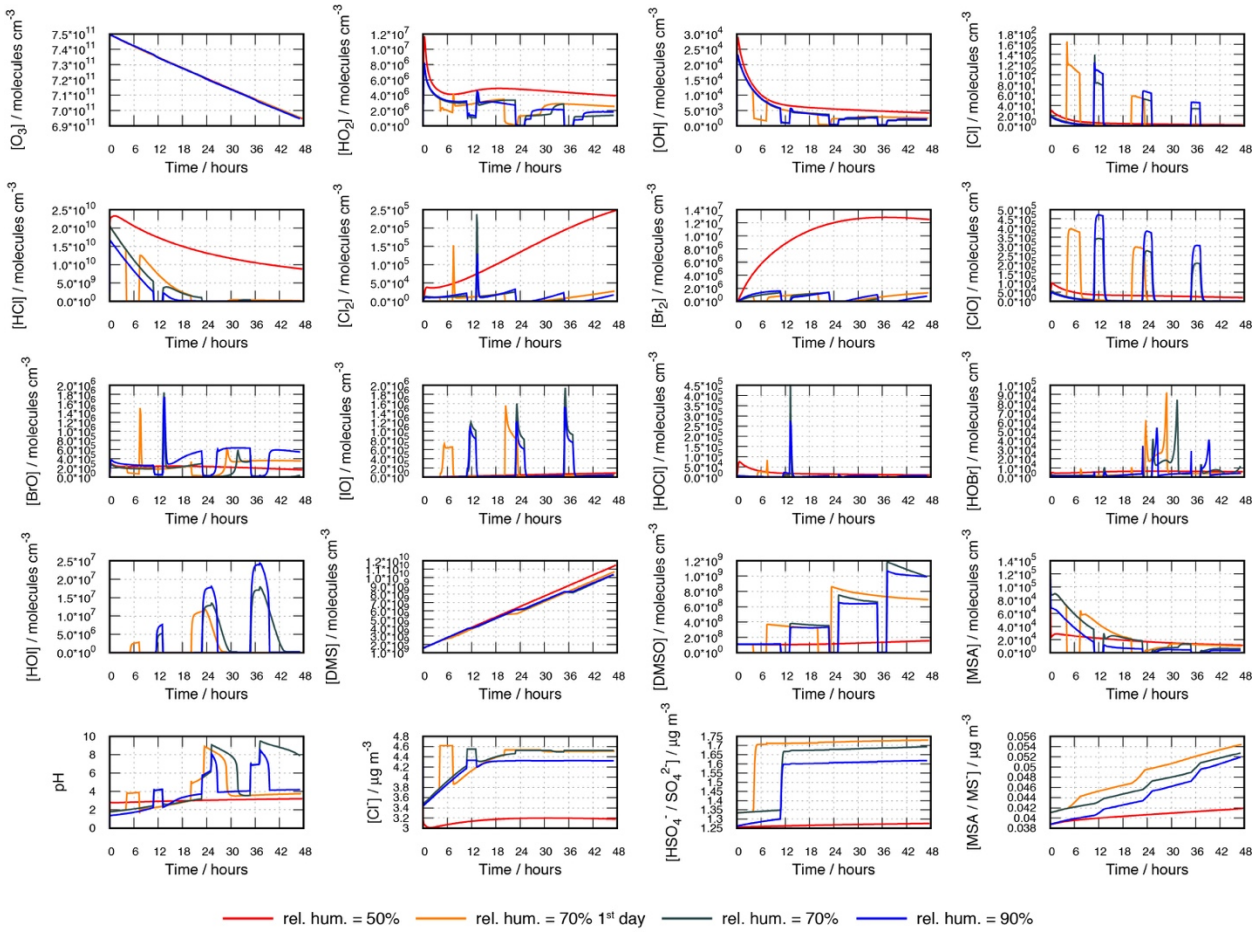

Figure S10 **Modelled concentration time-profile of key compounds within the pristine marine boundary layer for the winter simulations at 75° latitude. Red: simulation at rel. humidity of 50% (red). Orange: simulation at relative humidity of 70% and cloud occurrence at early morning and evening of the first model day. Dark green: simulation at relative humidity of 70% and cloud occurrence at noon and midnight. Blue: simulation at relative humidity of 90% and cloud occurrence at noon and midnight.**

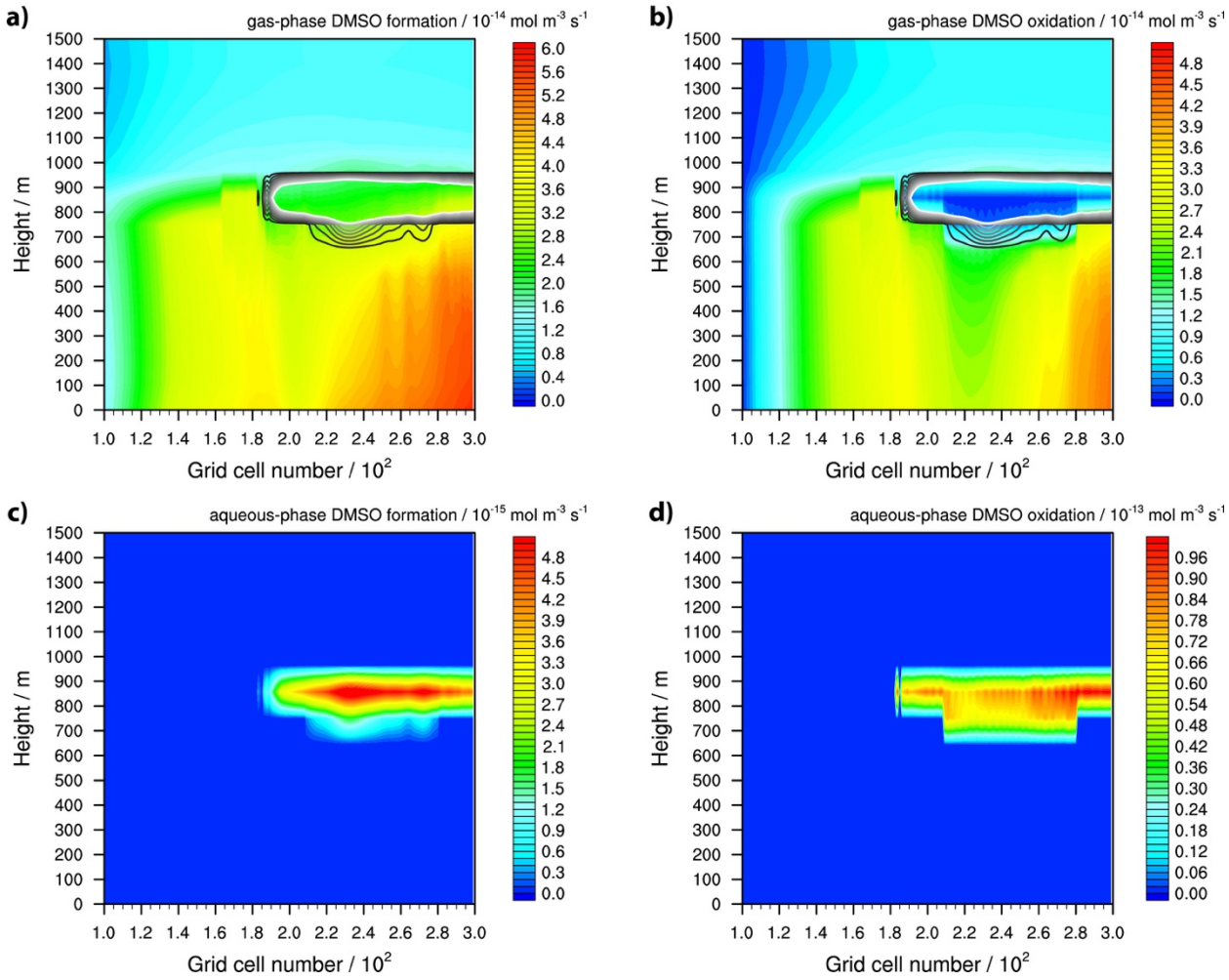

Figure S11 **Modelled formation rate of DMSO in (a) the gas phase and (c) the aqueous phase together with the modelled oxidation rate in (b) the gas phase and (d) the aqueous phase in the 'stable meteorological condition' simulation with stratiform clouds after 12 hours of modelling time. The x-axis represents the innermost horizontal grid cells divided by 100. The black contour lines represent the simulated clouds. The black line corresponds to a liquid water content of 0.01 g m^{-3} and the white line to 0.1 g m^{-3}. The area framed by the white line includes LWC above 0.1 g m^{-3}.**

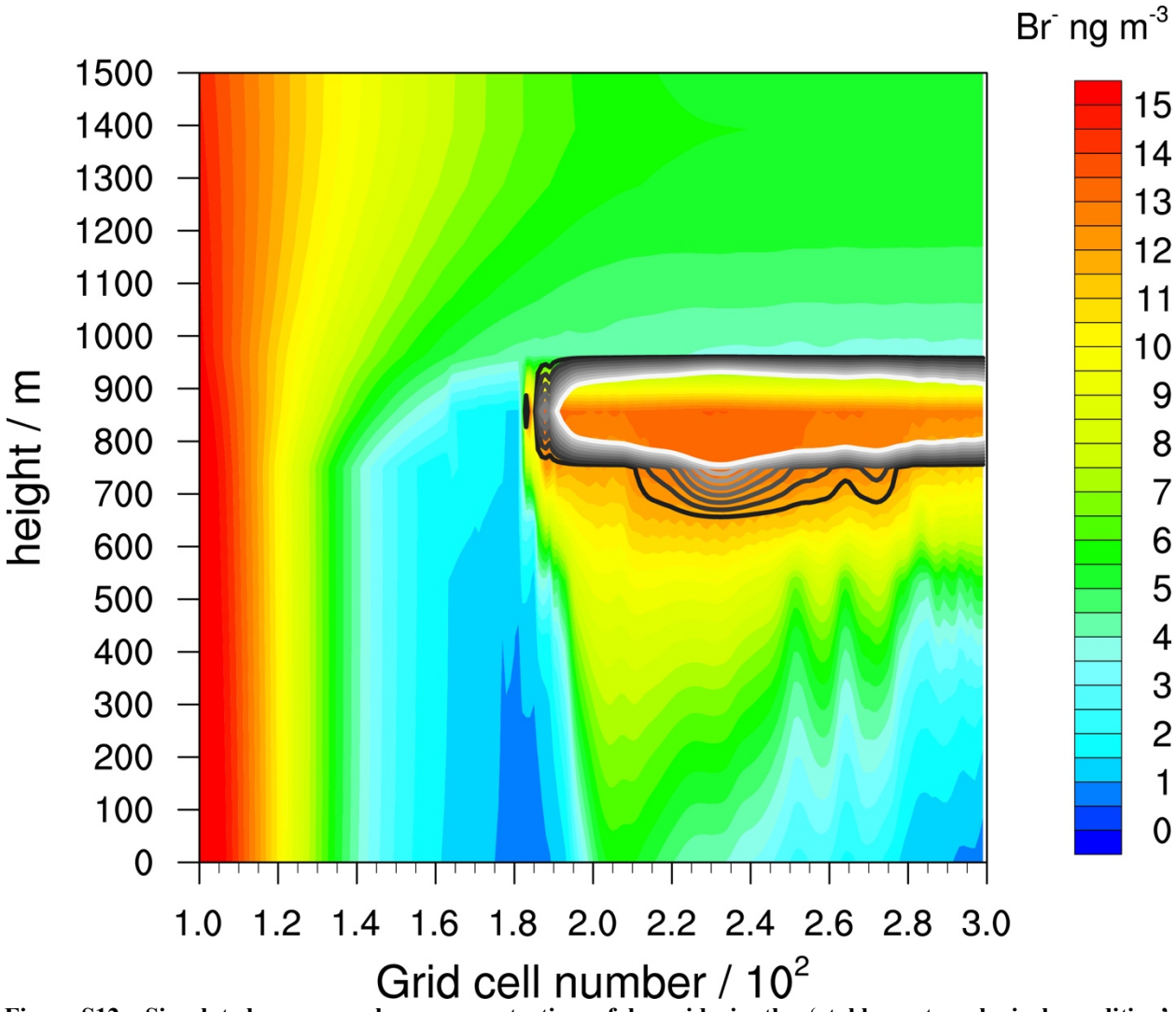

Figure S12 **Simulated aqueous-phase concentration of bromide in the 'stable meteorological condition' simulation with stratiform clouds after 12 hours of modelling time. The x-axis represents the innermost horizontal grid cells divided by 100. The black contour lines represent the simulated clouds. The black line corresponds to a liquid water content of 0.01 g m^{-3} and the white line to 0.1 g m^{-3}. The area framed by the white line includes LWC above 0.1 g m^{-3}. The initial background concentration is at about 16 ng m^{-3}.**

Table S1 **Implemented dry deposition, initial concentrations, and emission rates of chemical species for the open ocean simulation with COSMO-MUSCAT. Details on the dry deposition velocities are given in the previous CAPRAM studies Bräuer et al. (2013), Hoffmann et al. (2016) and Hoffmann et al. (2019a). Details on the initial concentrations and emission rates are given in Bräuer et al. (2013) and Hoffmann et al. (2016). In the term of I_2 and HOI, emission rates are derived from Prados-Roman et al. (2015). Aerosol initial concentrations are calculated from the SPACCIM simulations and were provided in the previous CAPRAM study Bräuer et al. (2013).**

Specie	Dry deposition / s^{-1}	Initial concentration / molecules cm^{-3}	Emission rates / mol m^{-2} s^{-1}	Aerosol initial concentration / mol m^{-3}
NH_3	$1.0 \cdot 10^{-2}$	$1.28 \cdot 10^{9}$	$7.589 \cdot 10^{-10}$	
NO	$2.0 \cdot 10^{-4}$	$2.50 \cdot 10^{8}$	$4.151 \cdot 10^{-12}$	
NO_2	$2.0 \cdot 10^{-4}$	$5.00 \cdot 10^{8}$		
NO_3	$1.0 \cdot 10^{-2}$			
N_2O_5	$1.0 \cdot 10^{-2}$			
HONO		$2.50 \cdot 10^{8}$		
HNO_3	$7.0 \cdot 10^{-3}$	$2.00 \cdot 10^{9}$		
HO_2NO_2	$5.0 \cdot 10^{-3}$			
O_3	$1.5 \cdot 10^{-3}$	$7.50 \cdot 10^{11}$		
CO	$1.0 \cdot 10^{-3}$	$4.25 \cdot 10^{12}$	$1.416 \cdot 10^{-9}$	
CO_2		$1.02 \cdot 10^{16}$		
SO_2	$8.7 \cdot 10^{-3}$	$2.55 \cdot 10^{9}$		
SULF	$1.0 \cdot 10^{-2}$			
H_2		$1.28 \cdot 10^{13}$		
H_2O_2	$5.0 \cdot 10^{-3}$	$1.50 \cdot 10^{10}$		
CH_4		$4.50 \cdot 10^{13}$	$2.923 \cdot 10^{-11}$	
C_2H_6		$1.28 \cdot 10^{10}$	$1.661 \cdot 10^{-13}$	
C_3H_8		$2.31 \cdot 10^{10}$	$3.321 \cdot 10^{-13}$	
C_2H_2		$2.42 \cdot 10^{9}$	$1.661 \cdot 10^{-13}$	
C_2H_4		$2.55 \cdot 10^{9}$	$3.985 \cdot 10^{-12}$	
C_3H_6			$1.661 \cdot 10^{-12}$	
BIGENE		$9.50 \cdot 10^{8}$		
HCHO	$5.0 \cdot 10^{-3}$	$5.00 \cdot 10^{9}$	$2.956 \cdot 10^{-14}$	
CH_3CHO		$1.40 \cdot 10^{8}$	$1.513 \cdot 10^{-10}$	
C_2H_5CHO		$5.13 \cdot 10^{9}$	$9.083 \cdot 10^{-11}$	
HYAC		$3.83 \cdot 10^{8}$	$4.151 \cdot 10^{-12}$	

Specie	Dry deposition / s^{-1}	Initial concentration / molecules cm^{-3}	Emission rates / mol m^{-2} s^{-1}	Aerosol initial concentration / mol m^{-3}
CH_3COCH_3		$1.10 \cdot 10^{10}$	$6.320 \cdot 10^{-12}$	
MEK		$6.89 \cdot 10^{8}$	$7.124 \cdot 10^{-16}$	
GLYOXAL		$2.55 \cdot 10^{8}$		
CH_3COCHO		$2.55 \cdot 10^{8}$		
CH_3OOH	$2.5 \cdot 10^{-3}$	$5.00 \cdot 10^{9}$		
CH_3CH_2OOH		$2.55 \cdot 10^{9}$		
CH_3COOOH		$2.55 \cdot 10^{7}$		
PAN	$1.0 \cdot 10^{-4}$	$2.50 \cdot 10^{8}$		
CH_3OH	$1.0 \cdot 10^{-2}$	$1.40 \cdot 10^{10}$	$9.797 \cdot 10^{-16}$	
CH_3CH_2OH	$5.0 \cdot 10^{-3}$	$2.00 \cdot 10^{9}$	$1.015 \cdot 10^{-11}$	
HCOOH	$1.0 \cdot 10^{-2}$	$6.25 \cdot 10^{9}$		
CH_3COOH		$5.00 \cdot 10^{9}$	$1.278 \cdot 10^{-12}$	
C_5H_8		$1.28 \cdot 10^{9}$	$2.341 \cdot 10^{-12}$	
APIN		$4.53 \cdot 10^{8}$	$2.541 \cdot 10^{-14}$	
BPIN		$3.02 \cdot 10^{8}$		
$CHBr_3$		$3.83 \cdot 10^{7}$	$2.225 \cdot 10^{-13}$	
C_3H_7I		$1.63 \cdot 10^{7}$	$8.170 \cdot 10^{-15}$	
CH_2I_2		$2.55 \cdot 10^{5}$	$1.876 \cdot 10^{-13}$	
CH_3I		$2.04 \cdot 10^{7}$	$2.458 \cdot 10^{-13}$	
CH_2ClI		$2.55 \cdot 10^{5}$	$1.524 \cdot 10^{-13}$	
CH_2BrI		$8.93 \cdot 10^{5}$	$8.751 \cdot 10^{-14}$	
HCl	$2.0 \cdot 10^{-2}$	$2.50 \cdot 10^{9}$		
HOCl	$2.0 \cdot 10^{-3}$			
$ClNO_2$	$1.0 \cdot 10^{-2}$			
$ClNO_3$	$1.0 \cdot 10^{-2}$			
HBr	$2.0 \cdot 10^{-2}$			
HOBr	$1.6 \cdot 10^{-3}$			
$BrNO_2$	$1.0 \cdot 10^{-2}$			
$BrNO_3$	$5.0 \cdot 10^{-3}$			
I_2			$1.744 \cdot 10^{-14}$	
HOI	$1.0 \cdot 10^{-2}$		$3.321 \cdot 10^{-13}$	

Specie	Dry deposition / s^{-1}	Initial concentration / molecules cm^{-3}	Emission rates / mol m^{-2} s^{-1}	Aerosol initial concentration / mol m^{-3}
INO_3	$1.0 \cdot 10^{-2}$			
I_2O_2	$1.0 \cdot 10^{-2}$			
I_2O_3	$1.0 \cdot 10^{-2}$			
I_2O_4	$1.0 \cdot 10^{-2}$			
DMS		$1.53 \cdot 10^{9}$	$1.026 \cdot 10^{-10}$	
DMSO	$5.0 \cdot 10^{-3}$			
$DMSO_2$	$5.0 \cdot 10^{-3}$			
MSA	$5.0 \cdot 10^{-3}$			
SO_4^{2-}				$1.05 \cdot 10^{-8}$
NO_3^-				$2.05 \cdot 10^{-9}$
Cl^-				$9.76 \cdot 10^{-8}$
Br^-				$2.14 \cdot 10^{-10}$
NH_4^+				$5.72 \cdot 10^{-9}$
Mn^{3+}				$3.93 \cdot 10^{-15}$
Fe^{3+}				$4.80 \cdot 10^{-15}$
Cu^{2+}				$1.72 \cdot 10^{-13}$
$HC_2O_4^-$				$3.94 \cdot 10^{-11}$
MSA				$3.26 \cdot 10^{-10}$
H^+				$1.00 \cdot 10^{-11}$

Table S2 Implemented gas-phase reactions in the CAPRAM-DM1.0red.

Nr.	Reaction	Rate constant[(a)]	Reference
D1	DMS + OH → $CH_3SCH_2O_2$ - O_2	k = $1.12 \cdot 10^{-11}$ exp(-250/T)	IUPAC, Atkinson et al. (2004)
D2	DMS + OH → 0.9 DMSO + 0.9 HO_2 + 0.1 CH_3SOH + 0.1 CH_3O_2 – O_2	**(1)**	see description at the table end
D3	DMS + NO_3 → $CH_3SCH_2O_2$ - O_2	k = $1.90 \cdot 10^{-13}$ exp(520/T)	IUPAC, Atkinson et al. (2004)
D4	DMS + Cl → 0.82 $CH_3SCH_2O_2$ + 0.82 HCl + 0.18 DMSO + 0.18 ClO – O_2	k = $1.88 \cdot 10^{-10}$	IUPAC, Urbanski and Wine (1999)
D5	DMS + ClO → 0.73 Cl + 0.73 DMSO + 0.27 HOCl + 0.27 $CH_3SCH_2O_2$ – 0.27 O_2	k = $1.70 \cdot 10^{-15}$ exp(340/T)	IUPAC
D6	DMS + BrO → DMSO + Br	k = $1.50 \cdot 10^{-14}$ exp(1000/T)	IUPAC
D7	DMS + Cl_2 → CH_3SCH_2Cl + HCl	k = $3.40 \cdot 10^{-14}$	Dyke et al. (2005)
D8	DMS + IO → DMSO + I	k = $3.30 \cdot 10^{-13}$ exp(-925/T)	IUPAC
D9	$CH_3SCH_2O_2$ + HO_2 → CH_3SCH_2OOH + O_2	k = $1.13 \cdot 10^{-13}$ exp(1300/T)	MCMv3.2, Rickard et al. (21.10.2013)
D10	$CH_3SCH_2O_2$ + NO → CH_3S + HCHO + NO_2	k = $4.90 \cdot 10^{-12}$ exp(260/T)	MCMv3.2, Rickard et al. (21.10.2013)
D11	$CH_3SCH_2O_2$ + NO_3 → CH_3S + HCHO + NO_2 + O_2	k = $2.30 \cdot 10^{-12}$	MCMv3.2, Rickard et al. (21.10.2013)
D12	$CH_3SCH_2O_2$ + CH_3O_2 → 0.89 CH_3S + 0.89 HCHO + 0.11 CH_3SCHO + O_2	k = $5.00 \cdot 10^{-13}$ exp(400/T)	In accordance to MCMv3.2 RO2 reaction
D13	CH_3SCH_2Cl + OH → CH_3SOH + $ClCH_2O_2$ - O_2	k = $2.50 \cdot 10^{-12}$	Shallcross et al. (2006)
D14	CH_3SCH_2OOH + OH → CH_3SCHO + OH + H_2O	k = $7.03 \cdot 10^{-11}$	MCMv3.2, Rickard et al. (21.10.2013)
D15	CH_3SCHO + OH → CH_3S + CO + H_2O	k = $1.11 \cdot 10^{-11}$	MCMv3.2, Rickard et al. (21.10.2013)
D16	DMSO + OH → MSIA + CH_3O_2 - O_2	k = $6.10 \cdot 10^{-12}$ exp(800/T)	MCMv3.2, Rickard et al. (21.10.2013)
D17	DMSO + NO_3 → $DMSO_2$ + NO_2	k = $2.90 \cdot 10^{-13}$	Sander et al. (2006)
D18	DMSO + Cl → 0.43 $DMSO_2$ + 0.43 ClO + 0.57 CH_3SO + 0.57 HCHO + HCl - 0.43 O_2	k = $1.45 \cdot 10^{-11}$	Falbe-Hansen et al. (2000); Nicovich et al. (2006); Kleissas et al. (2007)
D19	DMSO + BrO → $CH_3SO_2CH_3$ + Br	k = $1.00 \cdot 10^{-14}$	Ballesteros et al. (2002)
D20	CH_3SOH + OH → CH_3SO + H_2O	k = $5.00 \cdot 10^{-11}$	Lucas and Prinn (2002a)
D21	CH_3S + O_3 → CH_3SO + O_2	k = $1.15 \cdot 10^{-12}$ exp(430/T)	MCMv3.2, Rickard et al. (21.10.2013)
D22	CH_3S + O_2 → CH_3O_2 + SO_2 - O_2	**(2)**	see description at the table end
D23	CH_3S + O_2 → CH_3SO_2	**(3)**	see description at the table end
D24	MSIA + OH → CH_3O_2 + SO_2 + H_2O - O_2	k = $9.00 \cdot 10^{-11}$	MCMv3.2, Rickard et al. (21.10.2013)
D25	CH_3SO + O_3 → CH_3O_2 + SO_2	k = $4.00 \cdot 10^{-13}$	MCMv3.2, Rickard et al. (21.10.2013)
D26	CH_3SO_2 + O_3 → CH_3SO_3 + O_2	k = $3.00 \cdot 10^{-13}$	MCMv3.2, Rickard et al. (21.10.2013)

Nr.	Reaction	Rate constant[(a)]	Reference
D27	$CH_3SO_2 \rightarrow CH_3O_2 + SO_2 - O_2$	$k = 5.00 \cdot 10^{+13} \exp(-9673/T)$	MCMv3.2, Rickard et al. (21.10.2013)
D28	$CH_3SO_3 + HO_2 \rightarrow MSA + O_2$	$k = 5.00 \cdot 10^{-11}$	MCMv3.2, Rickard et al. (21.10.2013)
D29	$CH_3SO_3 \rightarrow CH_3O_2 + SULF - H_2O - O_2$	$k = 5.00 \cdot 10^{+13} \exp(-9946/T)$	MCMv3.2, Rickard et al. (21.10.2013)
Photolysis reactions			
D30	$CH_3SCH_2OOH \rightarrow CH_3S + HCHO + OH$	$J = 7.649 \cdot 10^{-06} \cos(\chi)^{0.682} \exp(-0.279/\cos(\chi))$	MCMv3.2, Rickard et al. (21.10.2013)
D31	$CH_3SCHO \rightarrow CH_3S + CO + HO_2 - O_2$	$J = 2.792 \cdot 10^{-05} \cos(\chi)^{0.805} \exp(-0.338/\cos(\chi))$	MCMv3.2, Rickard et al. (21.10.2013)
D32	$CH_3SCH_2Cl \rightarrow CH_3S + ClCH_2O_2 - O_2$	$J = 1.458 \cdot 10^{-04} \cos(\chi)^{0.314} \exp(-0.641/\cos(\chi))$	Hoffmann et al. (2016)

(a) k^{2nd} in cm^3 molecules^{-1} s^{-1}; k^{1st} in s^{-1}; J in s^{-1};

(1) $k = \frac{k1 \times k3}{k2+k3}$ with $k1 = \frac{9.5\times10^{-39}\times[O_2]\times e^{5270/T}}{1+7.5\times10^{-29}\times[O_2]\times e^{5610/T}}$; $k2 = \frac{2.05\times10^{-14}\times[O_2]\times e^{2674/T}}{\left(1+5.5\times10^{-31}\times[O_2]\times e^{7460/T}\right)\times T}$; rate calculated after Atkinson et al. (2004); Lucas and Prinn (2002b); Sander et al. (2006)

(2) $k = \frac{k1}{1+k2}$ with $k1 = 1.92\times10^{-10}\times e^{-5730/T}$; $k2 = 1.60\times10^{6}\times e^{-7310/T}$; rate calculated after MCMv3.2, Rickard et al. (21.10.2013)

(3) $k = \frac{k1}{1+k2}$ with $k1 = 3.43\times10^{-27}\times e^{-5140/T}$; $k2 = 2.86\times10^{-11}\times e^{-3560/T}$; rate calculated after Campolongo et al. (1999); Turnipseed et al. (1993); (Rickard et al., 21.10.2013)

Table S3 Implemented phase transfers in the CAPRAM-DM1.0red

② reactions that run in the cloud mode 'sub#1', ③ reactions that run in the aerosol mode 'sub#2'

Species	$K_{H\,(298\ K)}$[(a)]	$-\Delta H/R$[(b)]	Reference	α	Reference	$D_{g\,(298\ K)}$[(c)]	Reference
D33③ DMS	0.56	4480	Campolongo et al. (1999)	0.001	Zhu et al. (2006)	$1.08 \cdot 10^{-5}$	Fuller et al. (1966)
D34③ DMSO	$1.00 \cdot 10^{7}$	2580	Campolongo et al. (1999)	0.1	De Bruyn et al. (1994)	$1.01 \cdot 10^{-5}$	Fuller et al. (1966)
D35② $DMSO_2$	$1.00 \cdot 10^{7}$	5390	Campolongo et al. (1999)	0.1	De Bruyn et al. (1994)	$9.55 \cdot 10^{-6}$	Fuller et al. (1966)
D36② MSIA	$1.00 \cdot 10^{8}$	1760	between $DMSO_2$ and MSA	0.1	as for MSAa	$1.11 \cdot 10^{-5}$	Fuller et al. (1966)
D37② MSA	$5.09 \cdot 10^{13}$	1760	Campolongo et al. (1999)	0.1	De Bruyn et al. (1994)	$1.04 \cdot 10^{-5}$	Fuller et al. (1966)

(a) in M atm^{-1}; (b) in K; (c) in m^2 s^{-1}

Table S4 Implemented aqueous-phase reactions in the CAPRAM-DM1.0red

② reactions that run in the cloud mode 'sub#1', ③ reactions that run in the aerosol mode 'sub#2'

Nr.	Reaction	Rate constant[(a)]	Reference
D38	$DMS + O_3 \rightarrow DMSO + O_2$	$k = 8.61 \cdot 10^{+08} \exp(-2600/T)$	Gershenzon et al. (2001)
D39	$DMSO + OH \rightarrow MSIA + CH_3$	$k = 6.65 \cdot 10^{+09} \exp(-1270/T)$	Zhu et al. (2003a)
D40③	$DMSO + SO_4^- \rightarrow MSIA + CH_3 + H^+ + SO_4^{2-}$	$k = 2.97 \cdot 10^{+09} \exp(-1440/T)$	Zhu et al. (2003b)
D41③	$DMSO + Cl_2^- \rightarrow MSIA + HCl + CH_3 + Cl^- - H_2O$	$k = 1.60 \cdot 10^{+07}$	Zhu (2004)
D42②	$MSIA + O_3 \rightarrow MSA + O_2$	$k = 3.50 \cdot 10^{+07}$	Herrmann and Zellner (1997)
D43	$MSI^- + OH \rightarrow CH_3 + 0.135\ SO_2 + 0.765\ MS^- + 0.765\ SO_3 - 0.765\ MSI^- + 0.9\ OH^- + 0.1\ HSO_3^-$	$k = 1.20 \cdot 10^{+10}$	Bardouki et al. (2002)
D44③	$MSI^- + Cl_2^- \rightarrow CH_3 + 0.15\ SO_2 + 0.85\ MS^- + 0.85\ SO_3 - 0.85\ MSI^- + 2\ Cl^-$	$k = 8.00 \cdot 10^{+08}$	Zhu et al. (2005)
D45②	$MSI^- + O_3 \rightarrow CH_3SO_3^- + O_2$	$k = 2.00 \cdot 10^{+06}$	Flyunt et al. (2001)
D46	$MS^- + OH \rightarrow HCHO + SO_3^- + H_2O - 0.5\ O_2$	$k = 1.29 \cdot 10^{+07} \exp(-2630/T)$	Zhu et al. (2003a)
D47②	$MS^- + Cl_2^- \rightarrow CH_3 + SO_3 + 2\ Cl^-$	$k = 3.89 \cdot 10^{+03}$	Zhu (2004)

(a) k^{2nd} in $l^3\ mol^{-1}\ s^{-1}$

Table S5 Implemented aqueous-phase equilibria in the CAPRAM-DM1.0red

② reactions that run in the cloud mode 'sub#1', ③ reactions that run in the aerosol mode 'sub#2'

	Equilibrium	K[(a)]	$k_{f,\,298}$[(b)]	E_A/R[(c)]	$k_{b,\,298}$[(b)]	E_A/R[(c)]	Reference
D48②	$MSIA \rightleftharpoons MSI^- + H^+$	$5.0 \cdot 10^{-03}$	$2.50 \cdot 10^{08}$		$5.00 \cdot 10^{10}$		Wudl et al. (1967)
D49②	$MSA \rightleftharpoons MS^- + H^+$	73	$3.65 \cdot 10^{12}$		$5.00 \cdot 10^{10}$		Clarke and Woodward (1966)

(a) in M^{m-n}, n order of reaction of forward reaction, m order of reaction of backward reaction; (b) k_{298}^{2nd} in $l^1\ mol^{-1}\ s^{-1}$, k_{298}^{1st} in s^{-1}; (c) in K

Table S6 Implemented gas-phase reactions in the CAPRAM-HM3.0red

Nr.	Reaction	Rate constant[(a)]	Comment
H1	$Cl + O_3 \rightarrow ClO$	$k = 2.80 \cdot 10^{-11} \exp(-250/T)$	Atkinson et al. (2007)
H2	$ClO + HO_2 \rightarrow HOCl$	$k = 2.20 \cdot 10^{-12} \exp(340/T)$	Atkinson et al. (2007)
H3	$HCl + OH \rightarrow Cl$	$k = 1.70 \cdot 10^{-12} \exp(-230/T)$	Atkinson et al. (2007)
H4	$ClO + NO \rightarrow Cl + NO_2$	$k = 6.20 \cdot 10^{-12} \exp(295/T)$	Atkinson et al. (2007)
H5	$Cl + NO_2 \rightarrow ClNO_2$	TROE	Sander et al. (2006)
H6	$ClO + NO_2 \rightarrow ClNO_3$	TROE	Atkinson et al. (2007)
H7	$ClNO_3 \rightarrow ClO + NO_2$	$k = [M]*2.75 \cdot 10^{-6} \exp(11438/T)$	Anderson and Fahey (1990)
H8	$Cl + CH_4 \rightarrow CH_3O_2 + HCl$	$k = 6.60 \cdot 10^{-12} \exp(-1240/T)$	IUPAC, Atkinson et al. (2006)
H9	$Cl + C_2H_6 \rightarrow C_2H_5O_2 + HCl$	$k = 8.30 \cdot 10^{-11} \exp(-100/T)$	MCMv3.2, Rickard et al. (21.10.2013)
H10	$Cl + C_3H_8 \rightarrow C_3H_7O_2 + HCl$	$k = 1.40 \cdot 10^{-10}$	IUPAC, Atkinson et al. (2006)
H11	$Cl + BIGALKANE \rightarrow ALKO2 + HCl$	$k = 2.05 \cdot 10^{-10}$	IUPAC, Atkinson et al. (2006)
H12	$Cl + CH_3OH \rightarrow HCHO + HO_2 + HCl$	$k = 7.10 \cdot 10^{-11} \exp(-75/T)$	IUPAC, Atkinson et al. (2006)
H13	$Cl + C_2H_5OH \rightarrow 0.92\ CH_3CHO + 0.92\ HO_2 + 0.08\ EO2 + HCl$	$k = 6.05 \cdot 10^{-11} \exp(155/T)$	IUPAC, Atkinson et al. (2006)
H14	$Cl + ALKOH \rightarrow 1.25\ MEK + HO_2 + HCl$	$k = 2.70 \cdot 10^{-11} \exp(525/T)$	IUPAC, Atkinson et al. (2006)
H15	$Cl + CH_3OOH \rightarrow HCl + 0.6\ CH_3O_2 + 0.4\ HCHO + 0.4\ OH$	$k = 5.90 \cdot 10^{-11}$	IUPAC, Atkinson et al. (2006)
H16	$Cl + C_2H_5OOH \rightarrow HCl + CH_3CHO + OH$	$k = 1.07 \cdot 10^{-10}$	Wallington et al. (1989)
H17	$ClO + CH_3O_2 \rightarrow Cl + O_2 + HCHO + HO_2$	$k = 1.80 \cdot 10^{-11} \exp(-600/T)$	Burkholder et al. (2015)
H18	$Cl + HCHO \rightarrow HCl + CO + HO_2$	$k = 8.10 \cdot 10^{-11} \exp(-34/T)$	IUPAC, Atkinson et al. (2006)
H19	$Cl + CH_3CHO \rightarrow HCl + CH_3CO_3$	$k = 8.00 \cdot 10^{-11}$	IUPAC, Atkinson et al. (2006)
H20	$Cl + C_2H_5CHO \rightarrow HCl + 1.5\ CH_3CO_3$	$k = 1.30 \cdot 10^{-10}$	IUPAC, Atkinson et al. (2006)
H21	$Cl + HYAC \rightarrow HCl + MGLY + HO_2$	$k = 5.70 \cdot 10^{-11}$	Orlando et al. (1999)
H22	$Cl + CH_3COCHO \rightarrow HCl + CH_3CO_3 + CO$	$k = 4.80 \cdot 10^{-11}$	Green et al. (1990)
H23	$Cl + GLYOXAL \rightarrow HCl + 2.0\ CO + HO_2$	$k = 3.80 \cdot 10^{-11}$	Niki et al. (1985)
H24	$Cl + MEK \rightarrow HCl + MEKO2$	$k = 3.05 \cdot 10^{-11} \exp(80/T)$	IUPAC, Atkinson et al. (2006)
H25	$Cl + MACR \rightarrow 0.2\ MACRO2 + 0.8\ CC(O[O])(CCl)C{=}O + 0.2\ HCl$	$k = 2.55 \cdot 10^{-10}$	Rate constant average Canosa-Mas et al. (2001), Wang et al. (2002), Orlando et al. (2003) & Kaiser et al. (2010),
H26	$CC(O[O])(CCl)C{=}O + HO_2 \rightarrow CH_3COCH_2Cl + CO + HO_2 + OH$	$k = 1.00 \cdot 10^{-11}$	Hasson et al. (2012)
H27	$CC(O[O])(CCl)C{=}O + NO \rightarrow CH_3COCH_2Cl + CO + HO_2 + NO_2$	$k = 1.17 \cdot 10^{-11}$	Hsin and Elrod (2007)

Nr.	Reaction	Rate constant[(a)]	Comment
H28	CC(O[O])(CCl)C=O + CH_3O_2 → CH_3COCH_2Cl + CO + HO_2 + HCHO	k = $1.00 \cdot 10^{-12}$	Hasson et al. (2012)
H29	CC(O[O])(CCl)C=O + CH_3CO_3 → CH_3COCH_2Cl + CO + HO_2 + CH_3O_2	k = $1.00 \cdot 10^{-11}$	estimated
H30	OH + CC(OO)(CCl)C=O → CH_3COCH_2Cl + CO + OH	k = $3.77 \cdot 10^{-11}$	estimated
H31	Cl + MVK → CC(=O)C(O[O])CCl	k = $2.10 \cdot 10^{-10}$	Canosa-Mas et al. (2001)
H32	CC(=O)C(O[O])CCl + HO_2 → CC(=O)C(OO)CCl	k = $1.82 \cdot 10^{-13}$exp(1300/T)	MCMv3.2, Rickard et al. (21.10.2013)
H33	CC(=O)C(O[O])CCl + NO → $ClCH_2CHO$ + NO_2 + CH_3CO_3	k = $2.70 \cdot 10^{-12}$exp(360/T)	MCMv3.2, Rickard et al. (21.10.2013)
H34	CC(=O)C(O[O])CCl+ NO_3 → $ClCH_2CHO$ + NO_2 + CH_3CO_3	k = $2.30 \cdot 10^{-12}$	MCMv3.2, Rickard et al. (21.10.2013)
H35	CC(=O)C(O[O])CCl + CH_3O_2 → $ClCH_2CHO$ + CH_3CO_3 + HCHO	k = $1.00 \cdot 10^{-12}$	estimated
H36	CC(=O)C(O[O])CCl + CH_3CO_3 → $ClCH_2CHO$ + CH_3CO_3 + CH_3O_2	k = $1.00 \cdot 10^{-11}$	estimated
H37	OH + CC(=O)C(OO)CCl → $ClCH_2CHO$ + CH_3CO_3 + OH	k = $3.95 \cdot 10^{-11}$	after MVKOOH in MCMv3.2, Rickard et al. (21.10.2013)
H38	Cl + BIGALD1 → MALO2 + HO_2 + HCl	k = $1.35 \cdot 10^{-10}$	Martín et al. (2013)
H39	Cl + TOL → HCl + TOLO2	k = $6.20 \cdot 10^{-11}$	Wang et al. (2005)
H40	Cl + XYL → HCl + XYLNO2	k = $1.40 \cdot 10^{-10}$	Wang et al. (2005)
H41	Cl + BZALD → HCl + ACBZO2	k = $1.00 \cdot 10^{-10}$	Thiault et al. (2002)
H42	Cl + GLYALD → HCl + $HOCH_2CO_3$	k = $7.00 \cdot 10^{-11}$	Niki et al. (1987)
H43	Cl + CH_3COCH_3 → HCl + $CH_3COCH_2O_2$	k = $3.20 \cdot 10^{-11}$exp(-815/T)	Atkinson et al. (2006)
H44	Cl + C_2H_2 → 0.26 ClCHO + 0.21 Cl + 0.53 HCl + 0.21 GLYOXAL + 1.32 CO + 0.79 HO_2	TROE	Atkinson et al. (2006)
H45	Cl + C_2H_4 → $ClCH_2CH_2O_2$	TROE	Atkinson et al. (2006)
H46	$ClCH_2CH_2O_2$ + HO_2 → $ClCH_2CH_2OOH$	k = $3.30 \cdot 10^{-13}$exp(820/T)	MCMv3.2, Rickard et al. (21.10.2013)
H47	$ClCH_2CH_2O_2$ + NO → $ClCH_2CHO$ + HO_2 + NO_2	k = $3.24 \cdot 10^{-12}$exp(360/T)	Atkinson et al. (2008)
H48	$ClCH_2CH_2O_2$ + NO_3 → $ClCH_2CHO$ + HO_2 + NO_2	k = $2.30 \cdot 10^{-12}$	MCMv3.2, Rickard et al. (21.10.2013)
H49	$ClCH_2CH_2O_2$ + CH_3O_2 → $ClCH_2CHO$ + 0.8 HCHO + 0.2 CH_3OH + 1.4 HO_2	k = $2.00 \cdot 10^{-12}$	estimated
H50	$ClCH_2CHO$ + NO_3 → $ClCH_2CO_3$ + HNO_3	k = $1.40 \cdot 10^{-12}$exp(-1860/T)	MCMv3.2, Rickard et al. (21.10.2013)
H51	$ClCH_2CHO$ + OH → $ClCH_2CO_3$ + H_2O	k = $2.09 \cdot 10^{-11}$	Atkinson et al. (2008)
H52	$ClCH_2CO_3$ + HO_2 → 0.44 $ClCH_2O_2$ + 0.44 OH + 0.15 $ClCH_2COOH$ + 0.15 O_3 + 0.41 $ClCH_2C(O)OOH$	k = $5.20 \cdot 10^{-13}$exp(980/T)	MCMv3.2, Rickard et al. (21.10.2013)
H53	$ClCH_2CO_3$ + NO → $ClCH_2O_2$ + NO_2	k = $7.50 \cdot 10^{-12}$exp(290/T)	MCMv3.2, Rickard et al. (21.10.2013)
H54	$ClCH_2CO_3$ + NO_2 → ClPAN	TROE	MCMv3.2, Rickard et al. (21.10.2013)
H55	$ClCH_2CO_3$ + NO_3 → $ClCH_2O_2$ + NO_2	k = $4.00 \cdot 10^{-12}$	MCMv3.2, Rickard et al. (21.10.2013)

Nr.	Reaction	Rate constant[(a)]	Comment
H56	$ClCH_2CO_3 + CH_3O_2 \rightarrow 0.7\ ClCH_2O_2 + 0.3\ ClCH_2COOH + 0.7\ HO_2 + HCHO$	$k = 1.00 \cdot 10^{-11}$	estimated
H57	$ClCH_2COOH + OH \rightarrow ClCH_2O_2$	$k = 1.90 \cdot 10^{-12} exp(190/T)$	MCMv3.2, Rickard et al. (21.10.2013)
H58	$ClCH_2C(O)OOH + OH \rightarrow ClCH_2O_2$	$k = 4.29 \cdot 10^{-12}$	MCMv3.2, Rickard et al. (21.10.2013)
H59	$ClPAN + OH \rightarrow ClCHO + CO + NO_2$	$k = 6.26 \cdot 10^{-13}$	MCMv3.2, Rickard et al. (21.10.2013)
H60	$ClPAN \rightarrow ClCH_2CO_3 + NO_2$	TROE	MCMv3.2, Rickard et al. (21.10.2013)
H61	$ClCH_2O_2 + HO_2 \rightarrow 0.3\ ClCH_2OOH + 0.7\ ClCHO$	$k = 3.20 \cdot 10^{-13} exp(820/T)$	MCMv3.2, Rickard et al. (21.10.2013)
H62	$ClCH_2O_2 + NO \rightarrow ClCHO + HO_2 + NO_2$	$k = 4.05 \cdot 10^{-12} exp(360/T)$	MCMv3.2, Rickard et al. (21.10.2013)
H63	$ClCH_2O_2 + NO_3 \rightarrow ClCHO + HO_2 + NO_2$	$k = 2.30 \cdot 10^{-12}$	MCMv3.2, Rickard et al. (21.10.2013)
H64	$ClCH_2O_2 + CH_3O_2 \rightarrow 1.4\ HO_2 + ClCHO + 0.8\ HCHO + 0.2\ CH_3OH$	$k = 2.50 \cdot 10^{-12}$	estimated
H65	$Cl + C_3H_6 \rightarrow 0.4\ CH_3CH(O_2)CH_2Cl + 0.5\ CH_3CH(Cl)CH_2O_2 + 0.1\ HYAC$	$k = 1.43 \cdot 10^{-14} exp(2886/T)$	Atkinson et al. (2006)
H66	$CH_3CH(O_2)CH_2Cl + NO \rightarrow CH_3COCH_2Cl + HO_2 + NO_2$	$k = 2.70 \cdot 10^{-12} exp(360/T)$	Atkinson et al. (2008)
H67	$CH_3CH(Cl)CH_2O_2 + NO \rightarrow CH_3CH(Cl)CHO + NO_2 + HO_2$	$k = 2.70 \cdot 10^{-12} exp(360/T)$	MCMv3.2, Rickard et al. (21.10.2013)
H68	$CH_3CH(O_2)CH_2Cl + CH_3O_2 \rightarrow CH_3COCH_2Cl + 0.8\ HCHO + 0.2\ CH_3OH + 1.4\ HO_2$	$k = 4.00 \cdot 10^{-14}$	estimated
H69	$CH_3CH(Cl)CH_2O_2 + CH_3O_2 \rightarrow CH_3CH(Cl)CHO + 0.8\ HCHO + 0.2\ CH_3OH + 1.4\ HO_2$	$k = 6.48 \cdot 10^{-13}$	estimated
H70	$CH_3COCH_2Cl + OH \rightarrow CH_3COCHClO_2$	$k = 3.68 \cdot 10^{-13}$	Atkinson et al. (2008)
H71	$CH_3COCHClO_2 + HO_2 \rightarrow CH_3COCHClOOH$	$k = 3.30 \cdot 10^{-13} exp(820/T)$	MCMv3.2, Rickard et al. (21.10.2013)
H72	$CH_3COCHClO_2 + NO \rightarrow ClCHO + CH_3CO_3 + NO_2$	$k = 2.70 \cdot 10^{-12} exp(360/T)$	Atkinson et al. (2008)
H73	$CH_3COCHClO_2 + NO_3 \rightarrow ClCHO + CH_3CO_3 + NO_2$	$k = 2.30 \cdot 10^{-12}$	MCMv3.2, Rickard et al. (21.10.2013)
H74	$CH_3COCHClO_2 + CH_3O_2 \rightarrow ClCHO + CH_3CO_3 + 0.8\ HCHO + 0.2\ CH_3OH + HO_2$	$k = 2.00 \cdot 10^{-12}$	estimated
H75	$CH_3COCHClOOH + OH \rightarrow CH_3COCHClO_2$	$k = 8.34 \cdot 10^{-12}$	MCMv3.2, Rickard et al. (21.10.2013)
H76	$ClCHO + NO_3 \rightarrow CO + Cl + HNO_3$	$k = 1.40 \cdot 10^{-12} exp(-1860/T)$	Atkinson et al. (2008)
H77	$ClCHO + OH \rightarrow CO + Cl + H_2O$	$k = 6.12 \cdot 10^{-12}$	Atkinson et al. (2008)
H78	$CH_3CH(Cl)CHO + OH \rightarrow CH_3CH(Cl)C(O)O_2$	$k = 4.90 \cdot 10^{-12} exp(405/T)$	MCMv3.2, Rickard et al. (21.10.2013)
H79	$CH_3CH(Cl)CHO + NO_3 \rightarrow CH_3CH(Cl)C(O)O_2 + HNO_3$	$k = 3.24 \cdot 10^{-12} exp(-1860/T)$	MCMv3.2, Rickard et al. (21.10.2013)
H80	$CH_3CH(Cl)C(O)O_2 + HO_2 \rightarrow 0.15\ CH_3CH(Cl)COOH + 0.15\ O_3 + 0.41\ CH_3CH(Cl)C(O)OOH + 0.44\ CH_3CH(Cl)O_2 + 0.44\ OH$	$k = 5.20 \cdot 10^{-13} exp(980/T)$	MCMv3.2, Rickard et al. (21.10.2013)
H81	$CH_3CH(Cl)C(O)O_2 + NO \rightarrow CH_3CH(Cl)O_2 + NO_2$	$k = 7.50 \cdot 10^{-12} exp(290/T)$	MCMv3.2, Rickard et al. (21.10.2013)
H82	$CH_3CH(Cl)CO_3 + NO_2 \rightarrow CH_3ClPAN$	TROE	MCMv3.2, Rickard et al. (21.10.2013)

Nr.	Reaction	Rate constant[(a)]	Comment
H83	$CH_3ClPAN \rightarrow CH_3CH(Cl)CO_3 + NO_2$	TROE	MCMv3.2, Rickard et al. (21.10.2013)
H84	$CH_3CH(Cl)C(O)O_2 + NO_3 \rightarrow CH_3CH(Cl)O_2 + NO_2$	$k = 4.00 \cdot 10^{-12}$	MCMv3.2, Rickard et al. (21.10.2013)
H85	$CH_3CH(Cl)C(O)O_2 + CH_3O_2 \rightarrow 0.3\ CH_3CH(Cl)COOH + 0.7\ CH_3CH(Cl)O_2 + HCHO + HO_2$	$k = 1.00 \cdot 10^{-11}$	estimated
H86	$CC(Cl)C(=O)OO + OH \rightarrow CC(Cl)C(=O)O[O]$	$k = 4.42 \cdot 10^{-12}$	MCMv3.2, Rickard et al. (21.10.2013)
H87	$CH_3CH(Cl)COOH + OH \rightarrow CH_3CH(Cl)O_2$	$k = 1.20 \cdot 10^{-12}$	MCMv3.2, Rickard et al. (21.10.2013)
H88	$CH_3CH(Cl)O_2 + HO_2 \rightarrow CH_3CH(Cl)OOH$	$k = 3.30 \cdot 10^{-13} \exp(820/T)$	MCMv3.2, Rickard et al. (21.10.2013)
H89	$CH_3CH(Cl)O_2 + NO \rightarrow CH_3CHO + Cl + NO_2$	$k = 4.05 \cdot 10^{-12} \exp(360/T)$	MCMv3.2, Rickard et al. (21.10.2013)
H90	$CH_3CH(Cl)O_2 + NO_3 \rightarrow CH_3CHO + Cl + NO_2$	$k = 2.30 \cdot 10^{-12}$	MCMv3.2, Rickard et al. (21.10.2013)
H91	$CH_3CH(Cl)O_2 + CH_3O_2 \rightarrow 0.6\ CH_3CHO + 0.6\ Cl + 0.4\ CH_3C(O)Cl + 0.8\ HCHO + 0.2\ CH_3OH + 0.8\ HO_2$	$k = 2.65 \cdot 10^{-12}$	estimated
H92	$CH_3CH(Cl)OOH + OH \rightarrow CH_3CH(Cl)O_2 + H_2O$	$k = 1.90 \cdot 10^{-12} \exp(190/T)$	MCMv3.2, Rickard et al. (21.10.2013)
H93	$CH_3CH(Cl)OOH + OH \rightarrow CH_3C(O)Cl + OH + H_2O$	$k = 9.95 \cdot 10^{-12}$	MCMv3.2, Rickard et al. (21.10.2013)
H94	$CH_3C(O)Cl + OH \rightarrow ClCOCH_2O_2 + H_2O$	$k = 3.88 \cdot 10^{-14}$	MCMv3.2, Rickard et al. (21.10.2013)
H95	$ClCOCH_2O_2 + HO_2 \rightarrow ClCOCH_2OOH$	$k = 3.30 \cdot 10^{-13} \exp(820/T)$	MCMv3.2, Rickard et al. (21.10.2013)
H96	$ClCOCH_2O_2 + NO \rightarrow HCHO + Cl + CO + NO_2$	$k = 3.24 \cdot 10^{-12} \exp(360/T)$	MCMv3.2, Rickard et al. (21.10.2013)
H97	$ClCOCH_2O_2 + NO_3 \rightarrow HCHO + Cl + CO + NO_2$	$k = 2.30 \cdot 10^{-12}$	MCMv3.2, Rickard et al. (21.10.2013)
H98	$ClCOCH_2O_2 + CH_3O_2 \rightarrow 2\ HCHO + Cl + CO + HO_2$	$k = 2.00 \cdot 10^{-12}$	MCMv3.2, Rickard et al. (21.10.2013)
H99	$Br + O_3 \rightarrow BrO$	$k = 1.70 \cdot 10^{-11} \exp(-800/T)$	Atkinson et al. (2007)
H100	$BrO + HO_2 \rightarrow HOBr$	$k = 4.50 \cdot 10^{-12} \exp(-500/T)$	Atkinson et al. (2007)
H101	$BrO + BrO \rightarrow 1.7\ Br + 0.15\ Br_2$	$k = 1.60 \cdot 10^{-12} \exp(-210/T)$	Atkinson et al. (2007)
H102	$Br + NO_2 \rightarrow BrNO_2$	TROE	Atkinson et al. (2007)
H103	$BrO + NO \rightarrow Br + NO_2$	$k = 8.70 \cdot 10^{-12} \exp(-260/T)$	Atkinson et al. (2007)
H104	$BrO + NO_2 \rightarrow BrNO_3$	TROE	Atkinson et al. (2007)
H105	$BrNO_3 \rightarrow BrO + NO_2$	$k = 2.79 \cdot 10^{13} \exp(-12360/T)$	Orlando and Tyndall (1996)
H106	$Br + BrNO_3 \rightarrow Br_2 + NO_3$	$k = 4.90 \cdot 10^{-11}$	Orlando and Tyndall (1996)
H107	$BrO + ClO \rightarrow 0.95\ Br + 0.5\ OClO + 0.45\ Cl + 0.05\ BrCl$	$k = 7.32 \cdot 10^{-12} \exp(-200/T)$	Summation A-Factor Burkholder et al. (2015)
H108	$BrO + CH_3O_2 \rightarrow 0.25\ Br + 0.25\ HCHO + 0.25\ HO_2 + 0.75\ HOBr + 0.75\ HCOOH$	$k = 4.10 \cdot 10^{-13} \exp(-800/T)$	Bräuer et al. (2013)
H109	$Br + C_2H_2 \rightarrow 0.17\ BrCHO + 0.09\ Br + 0.74\ HBr + 0.09\ GLYOXAL + 1.65\ CO + 0.91\ HO_2$	$k = 6.35 \cdot 10^{-15} \exp(-440/T)$	Atkinson et al. (2006)

Nr.	Reaction	Rate constant[(a)]	Comment
H110	$Br + HCHO \rightarrow HBr + CO + HO_2$	$k = 1.70 \cdot 10^{-11} exp(-800/T)$	Sander et al. (2006)
H111	$BrO + HCHO \rightarrow HOBr + CO + HO_2$	$k = 1.50 \cdot 10^{-14}$	Hansen et al. (1999)
H112	$Br + CH_3CHO \rightarrow HBr + CH_3CO_3$	$k = 1.80 \cdot 10^{-11} exp(-460/T)$	Atkinson et al. (2006)
H113	$Br + C_2H_5CHO \rightarrow HBr + 1.5\ CH_3CO_3$	$k = 5.75 \cdot 10^{-11} exp(-610/T)$	Ramacher et al. (2000)
H114	$Br + C_2H_4 \rightarrow BrCH_2CH_2O_2$	$k = 2.25 \cdot 10^{-13} exp(-277/T)$	Atkinson et al. (2006)
H115	$BrCH_2CH_2O_2 + NO \rightarrow BrCH_2CHO + HO_2 + NO_2$	$k = 9.70 \cdot 10^{-12}$	Atkinson et al. (2008)
H116	$BrCH_2CH_2O_2 + CH_3O_2 \rightarrow BrCH_2CHO + 0.8\ HCHO + 0.2\ CH_3OH + 1.4\ HO_2$	$k = 2.00 \cdot 10^{-12}$	Bräuer et al. (2013)
H117	$BrCH_2CHO + OH \rightarrow BrCH_2CO_3 + H_2O$	$k = 2.05 \cdot 10^{-12}$	Atkinson et al. (2008)
H118	$BrCH_2CO_3 + HO_2 \rightarrow$ $0.15\ BrCH_2COOH + 0.15\ O_3 + 0.41\ BrCH_2C(O)OOH + 0.44\ BrCH_2O_2 + 0.44\ OH$	$k = 5.20 \cdot 10^{-13} exp(980/T)$	MCMv3.2, Rickard et al. (21.10.2013)
H119	$BrCH_2CO_3 + NO \rightarrow BrCH_2O_2 + NO_2$	$k = 7.50 \cdot 10^{-12} exp(290/T)$	MCMv3.2, Rickard et al. (21.10.2013)
H120	$BrCH_2CO_3 + CH_3O_2 \rightarrow 0.7\ BrCH_2O_2 + 0.3\ BrCH_2COOH + 0.7\ HO_2 + HCHO$	$k = 1.00 \cdot 10^{-11}$	Bräuer et al. (2013)
H121	$BrCH_2COOH + OH \rightarrow BrCH_2O_2 + H_2O$	$k = 1.90 \cdot 10^{-12} exp(190/T)$	MCMv3.2, Rickard et al. (21.10.2013)
H122	$BrCH_2C(O)OOH + OH \rightarrow BrCH_2CO_3 + H_2O$	$k = 3.79 \cdot 10^{-12}$	MCMv3.2, Rickard et al. (21.10.2013)
H123	$BrCH_2O_2 + HO_2 \rightarrow BrCH_2OOH$	$k = 4.28 \cdot 10^{-13} exp(820/T)$	MCMv3.2, Rickard et al. (21.10.2013)
H124	$BrCH_2O_2 + NO \rightarrow BrCHO + HO_2 + NO_2$	$k = 4.05 \cdot 10^{-12} exp(360/T)$	MCMv3.2, Rickard et al. (21.10.2013)
H125	$BrCH_2O_2 + NO_3 \rightarrow BrCHO + HO_2 + NO_2$	$k = 2.30 \cdot 10^{-12}$	MCMv3.2, Rickard et al. (21.10.2013)
H126	$BrCH_2O_2 + CH_3O_2 \rightarrow 1.4\ HO_2 + BrCHO + 0.8\ HCHO + 0.2\ CH_3OH$	$k = 2.00 \cdot 10^{-12}$	Bräuer et al. (2013)
H127	$BrCH_2OOH + OH \rightarrow BrCH_2O_2 + H_2O$	$k = 1.90 \cdot 10^{-12} exp(190/T)$	MCMv3.2, Rickard et al. (21.10.2013)
H128	$BrCH_2OOH + OH \rightarrow BrCHO + OH + H_2O$	$k = 5.79 \cdot 10^{-12}$	MCMv3.2, Rickard et al. (21.10.2013)
H129	$BrCHO + NO_3 \rightarrow CO + Br + HNO_3$	$k = 1.40 \cdot 10^{-12} exp(-1860/T)$	Atkinson et al. (2008)
H130	$BrCHO + OH \rightarrow CO + Br + H_2O$	$k = 1.16 \cdot 10^{-12}$	Atkinson et al. (2008)
H131	$Br + C_3H_6 \rightarrow CH_3CH(O_2)CH_2Br$	$k = 3.60 \cdot 10^{-12}$	Atkinson et al. (2006)
H132	$CH_3CH(O_2)CH_2Br + NO \rightarrow CH_3COCH_2Br + HO_2 + NO_2$	$k = 2.70 \cdot 10^{-12} exp(360/T)$	Atkinson et al. (2008)
H133	$CH_3CH(O_2)CH_2Br + CH_3O_2 \rightarrow CH_3COCH_2Br + 0.8\ HCHO + 0.2\ CH_3OH + 1.4\ HO_2$	$k = 4.00 \cdot 10^{-14}$	Bräuer et al. (2013)
H134	$CH_3COCH_2Br + OH \rightarrow CH_3COCHBrO_2$	$k = 8.80 \cdot 10^{-12} exp(-1320/T)$	Atkinson et al. (2008)
H135	$CH_3COCHBrO_2 + NO \rightarrow CH_3CO_3 + BrCHO + NO_2$	$k = 8.00 \cdot 10^{-12}$	Atkinson et al. (2008)
H136	$CH_3COCHBrO_2 + CH_3O_2 \rightarrow 0.4\ CH_3COC(O)Br + 0.6\ CH_3CO_3 + 0.6\ BrCHO + 0.8\ HO_2 + 0.8\ HCHO + 0.2\ CH_3OH$	$k = 2.00 \cdot 10^{-12}$	Bräuer et al. (2013)

Nr.	Reaction	Rate constant[(a)]	Comment
H137	$I + O_3 \rightarrow IO$	$k = 2.10 \cdot 10^{-11} \exp(-830/T)$	Atkinson et al. (2007)
H138	$I_2 + OH \rightarrow I + HOI$	$k = 2.10 \cdot 10^{-10}$	Atkinson et al. (2007)
H139	$IO + HO_2 \rightarrow HOI$	$k = 1.40 \cdot 10^{-11} \exp(540/T)$	Atkinson et al. (2007)
H140	$IO + IO \rightarrow 0.38\ OIO + 0.46\ I_2O_2 + 0.6\ I + 0.05\ I_2$	$k = 5.40 \cdot 10^{-11} \exp(180/T)$	Sander et al. (2006)
H141	$OIO + OH \rightarrow HIO_3$	$k = 2.20 \cdot 10^{-10} \exp(243/T)$	von Glasow et al. (2002)
H142	$IO + O_3 \rightarrow 0.83\ I + 0.17\ OIO$	$k = 1.20 \cdot 10^{-15}$	(Larin et al., 1999)
H143	$IO + OIO \rightarrow I_2O_3$	$k = 1.00 \cdot 10^{-10}$	(Gómez Martín et al., 2007)
H144	$I_2O_3 \rightarrow IO + OIO$	$k = 2.78 \cdot 10^{-11}$	(Kaltsoyannis and Plane, 2008)
H145	$OIO + OIO \rightarrow I_2O_4$	$k = 1.00 \cdot 10^{-10}$	(Saunders and Plane, 2005)
H146	$I_2O_4 \rightarrow OIO + OIO$	$k = 1.67 \cdot 10^{+00}$	(Kaltsoyannis and Plane, 2008)
H147	$I_2 + O_3 \rightarrow IO + I$	$k = 4.02 \cdot 10^{-15} \exp(-2050/T)$	(Vikis and Macfarlane, 1985)
H148	$I_2O_2 \rightarrow 0.995\ OIO + 0.995\ I + 0.01\ IO$	$k = 1.00 \cdot 10^{+01}$	(Kaltsoyannis and Plane, 2008)
H149	$I_2 + NO_3 \rightarrow I + INO_3$	$k = 1.50 \cdot 10^{-12}$	Atkinson et al. (2007)
H150	$IO + NO \rightarrow I + NO_2$	$k = 7.15 \cdot 10^{-12} \exp(300/T)$	Atkinson et al. (2007)
H151	$IO + NO_2 \rightarrow INO_3$	TROE	Atkinson et al. (2007)
H152	$INO_3 \rightarrow IO + NO_2$	$k = [M] * 4.40 \cdot 10^{-05} \exp(12060/T)$	Atkinson et al. (2007)
H153	$IO + CH_3O_2 \rightarrow I + HO_2 + HCHO$	$k = 2.00 \cdot 10^{-12}$	(Dillon et al., 2006)
H154	$IO + ClO \rightarrow 0.8\ I + 0.55\ OClO + 0.25\ Cl + 0.2\ ICl$	$k = 4.70 \cdot 10^{-12} \exp(280/T)$	Atkinson et al. (2007)
H155	$IO + BrO \rightarrow 0.8\ OIO + Br + 0.2\ I$	$k = 1.50 \cdot 10^{-11} \exp(510/T)$	Atkinson et al. (2007)
Photolysis reactions			
H156	$Cl_2 \rightarrow Cl + Cl$	$J = 3.827 \cdot 10^{-03} \cos(\chi)^{0.543} \exp(-0.244/\cos(\chi))$	Bräuer et al. (2013)
H157	$ClO \rightarrow Cl + O(^3P)$	$J = 4.755 \cdot 10^{-04} \cos(\chi)^{1.258} \exp(-0.588/\cos(\chi))$	Bräuer et al. (2013)
H158	$OClO \rightarrow ClO + O(^3P)$	$J = 1.332 \cdot 10^{-01} \cos(\chi)^{0.416} \exp(-0.244/\cos(\chi))$	Bräuer et al. (2013)
H159	$HOCl \rightarrow Cl + OH$	$J = 4.615 \cdot 10^{-04} \cos(\chi)^{0.656} \exp(-0.240/\cos(\chi))$	Bräuer et al. (2013)
H160	$ClNO_2 \rightarrow Cl + NO_2$	$J = 6.219 \cdot 10^{-04} \cos(\chi)^{0.774} \exp(-0.255/\cos(\chi))$	Bräuer et al. (2013)
H161	$ClNO_3 \rightarrow Cl + NO_3$	$J = 6.420 \cdot 10^{-05} \cos(\chi)^{0.648} \exp(-0.217/\cos(\chi))$	Bräuer et al. (2013)
H162	$ClNO_3 \rightarrow ClO + NO_2$	$J = 1.393 \cdot 10^{-05} \cos(\chi)^{1.052} \exp(-0.243/\cos(\chi))$	Bräuer et al. (2013)
H163	$CC(=O)C(OO)CCl \rightarrow ClCH_2CHO + CH_3CO_3 + OH$	$J = 7.649 \cdot 10^{-05} \cos(\chi)^{0.682} \exp(-0.279/\cos(\chi))$	Bräuer et al. (2013)
H164	$ClCH_2CH_2OOH \rightarrow ClCH_2CHO + HO_2 + OH$	$J = 7.649 \cdot 10^{-06} \cos(\chi)^{0.682} \exp(-0.279/\cos(\chi))$	Bräuer et al. (2013)
H165	$ClCH_2CHO \rightarrow ClCH_2O_2 + HO_2 + CO$	$J = 4.642 \cdot 10^{-05} \cos(\chi)^{0.762} \exp(-0.353/\cos(\chi))$	Bräuer et al. (2013)

Nr.	Reaction	Rate constant[(a)]	Comment
H166	$ClCH_2C(O)OOH \rightarrow ClCH_2O_2 + OH$	$J = 7.649 \cdot 10^{-06} \cos(\chi)^{0.682} \exp(-0.279/\cos(\chi))$	Bräuer et al. (2013)
H167	$ClCH_2OOH \rightarrow ClCHO + HO_2 + OH$	$J = 7.649 \cdot 10^{-06} \cos(\chi)^{0.682} \exp(-0.279/\cos(\chi))$	Bräuer et al. (2013)
H168	$CH_3CH(O)CH_2Cl \rightarrow CH_3O_2 + ClCH_2CO_3$	$J = 5.804 \cdot 10^{-06} \cos(\chi)^{1.092} \exp(-0.377/\cos(\chi))$	Bräuer et al. (2013)
H169	$CH_3CH(O)CHClOOH \rightarrow ClCHO + CH_3CO_3 + OH$	$J = 7.649 \cdot 10^{-06} \cos(\chi)^{0.682} \exp(-0.279/\cos(\chi))$	Bräuer et al. (2013)
H170	$ClCHO \rightarrow HO_2 + CO + Cl$	$J = 4.642 \cdot 10^{-05} \cos(\chi)^{0.762} \exp(-0.353/\cos(\chi))$	Bräuer et al. (2013)
H171	$CH_3CH(Cl)CHO \rightarrow CH_3CH(Cl)O_2 + HO_2 + CO$	$J = 2.879 \cdot 10^{-05} \cos(\chi)^{1.067} \exp(-0.358/\cos(\chi))$	Bräuer et al. (2013)
H172	$CH_3CH(Cl)OOH \rightarrow CH_3CHO + Cl + OH$	$J = 7.649 \cdot 10^{-06} \cos(\chi)^{0.682} \exp(-0.279/\cos(\chi))$	Bräuer et al. (2013)
H173	$CH_3C(O)Cl \rightarrow CH_3CO_3 + Cl$	$J = 5.804 \cdot 10^{-06} \cos(\chi)^{1.092} \exp(-0.377/\cos(\chi))$	Bräuer et al. (2013)
H174	$ClCOCH_2OOH \rightarrow ClCOCH_2O_2 + OH$	$J = 7.649 \cdot 10^{-06} \cos(\chi)^{0.682} \exp(-0.279/\cos(\chi))$	Bräuer et al. (2013)
H175	$Br_2 \rightarrow Br + Br$	$J = 4.773 \cdot 10^{-02} \cos(\chi)^{0.193} \exp(-0.213/\cos(\chi))$	Bräuer et al. (2013)
H176	$BrO \rightarrow Br + O(^3P)$	$J = 6.368 \cdot 10^{-02} \cos(\chi)^{0.605} \exp(-0.269/\cos(\chi))$	Bräuer et al. (2013)
H177	$HOBr \rightarrow Br + OH$	$J = 3.464 \cdot 10^{-03} \cos(\chi)^{0.441} \exp(-0.214/\cos(\chi))$	Bräuer et al. (2013)
H178	$BrNO_2 \rightarrow Br + NO_2$	$J = 7.443 \cdot 10^{-03} \cos(\chi)^{0.355} \exp(-0.236/\cos(\chi))$	Bräuer et al. (2013)
H179	$BrNO_3 \rightarrow 0.29\ Br + 0.29\ NO_3 + 0.71\ BrO + 0.71\ NO_2$	$J = 2.194 \cdot 10^{-04} \cos(\chi)^{0.492} \exp(-0.215/\cos(\chi))$	Bräuer et al. (2013)
H180	$BrCl \rightarrow Br + Cl$	$J = 1.650 \cdot 10^{-02} \cos(\chi)^{0.297} \exp(-0.224/\cos(\chi))$	Bräuer et al. (2013)
H181	$BrCH_2CHO \rightarrow BrCH_2O_2 + HO_2 + CO$	$J = 4.642 \cdot 10^{-05} \cos(\chi)^{0.762} \exp(-0.353/\cos(\chi))$	Bräuer et al. (2013)
H182	$BrCH_2C(O)OOH \rightarrow BrCH_2O_2 + OH$	$J = 7.649 \cdot 10^{-06} \cos(\chi)^{0.682} \exp(-0.279/\cos(\chi))$	Bräuer et al. (2013)
H183	$BrCH_2OOH \rightarrow BrCHO + OH + HO_2$	$J = 7.649 \cdot 10^{-06} \cos(\chi)^{0.682} \exp(-0.279/\cos(\chi))$	Bräuer et al. (2013)
H184	$BrCHO \rightarrow HO_2 + CO + Br$	$J = 4.642 \cdot 10^{-05} \cos(\chi)^{0.762} \exp(-0.353/\cos(\chi))$	Bräuer et al. (2013)
H185	$CH_3COCH_2Br \rightarrow 0.7\ CO + 0.7\ Br + 0.7\ CH_3CO_3 + 0.3\ BrCH_2CO_3 + 0.3\ CH_3O_2$	$J = 3.523 \cdot 10^{-04} \cos(\chi)^{0.885} \exp(-0.283/\cos(\chi))$	Bräuer et al. (2013)
H186	$CH_3COC(O)Br \rightarrow CO + Br + CH_3CO_3$	$J = 1.853 \cdot 10^{-04} \cos(\chi)^{0.583} \exp(-0.225/\cos(\chi))$	Bräuer et al. (2013)
H187	$CHBr_3 \rightarrow 3\ Br + CO + HO_2$	$J = 2.228 \cdot 10^{-06} \cos(\chi)^{1.471} \exp(-0.230/\cos(\chi))$	Bräuer et al. (2013)
H188	$I_2 \rightarrow I + I$	$J = 2.165 \cdot 10^{-01} \cos(\chi)^{0.125} \exp(-0.185/\cos(\chi))$	Bräuer et al. (2013)
H189	$IO \rightarrow I + O(^3P)$	$J = 2.640 \cdot 10^{-03} \cos(\chi)^{0.240} \exp(-0.240/\cos(\chi))$	Bräuer et al. (2013)
H190	$OIO \rightarrow 0.96\ I + 0.04\ IO + 0.04\ O(^3P)$	$J = 4.054 \cdot 10^{-02} \cos(\chi)^{0.119} \exp(-0.185/\cos(\chi))$	Bräuer et al. (2013)
H191	$HOI \rightarrow I + OH$	$J = 1.469 \cdot 10^{-02} \cos(\chi)^{0.342} \exp(-0.236/\cos(\chi))$	Bräuer et al. (2013)
H192	$INO_3 \rightarrow 0.85\ I + 0.85\ NO_3 + 0.15\ IO + 0.15\ NO_2$	$J = 6.599 \cdot 10^{-02} \cos(\chi)^{0.530} \exp(-0.243/\cos(\chi))$	Bräuer et al. (2013)
H193	$ICl \rightarrow I + Cl$	$J = 3.403 \cdot 10^{-02} \cos(\chi)^{0.179} \exp(-0.207/\cos(\chi))$	Bräuer et al. (2013)
H194	$IBr \rightarrow I + Br$	$J = 1.000 \cdot 10^{-01} \cos(\chi)^{0.149} \exp(-0.197/\cos(\chi))$	Bräuer et al. (2013)
H195	$C_3H_7I \rightarrow I + C_3H_7O_2$	$J = 3.731 \cdot 10^{-05} \cos(\chi)^{1.292} \exp(-0.217/\cos(\chi))$	Bräuer et al. (2013)
H196	$CH_2I_2 \rightarrow 2\ I + 2\ HO_2$	$J = 1.496 \cdot 10^{-02} \cos(\chi)^{0.801} \exp(-0.265/\cos(\chi))$	Bräuer et al. (2013)

Nr.	Reaction	Rate constant[(a)]	Comment
H197	$CH_3I \rightarrow I + CH_3O_2$	$J = 1.206 \cdot 10^{-05} \cos(\chi)^{1.254} \exp(-0.231/\cos(\chi))$	Bräuer et al. (2013)
H198	$ClCH_2I \rightarrow I + ClCH_2O_2$	$J = 6.910 \cdot 10^{-04} \cos(\chi)^{1.057} \exp(-0.238/\cos(\chi))$	Bräuer et al. (2013)
H199	$BrCH_2I \rightarrow I + BrCH_2O_2$	$J = 4.261 \cdot 10^{-04} \cos(\chi)^{0.976} \exp(-0.250/\cos(\chi))$	Bräuer et al. (2013)

(a) k^{2nd} in cm^3 $molecules^{-1}$ s^{-1}; k^{1st} in s^{-1}; J in s^{-1}

Table S7 Parameters for pressure dependent reactions.

	Reaction	TYPE	k_0[(a)]	k_∞[(a)]	F_C
H5	$Cl + NO_2 \rightarrow ClNO_2$	TROE	$1.80 \cdot 10^{-31} * (T/298)^{-2.0}$	$1.00 \cdot 10^{-10} * (T/298)^{-1.0}$	0.6
H6	$ClO + NO_2 \rightarrow ClNO_3$	TROE	$1.60 \cdot 10^{-31} * (T/298)^{-3.4}$	$7.00 \cdot 10^{-11}$	0.4
H44	$Cl + C_2H_2 \rightarrow 0.26\ ClCHO + 0.21\ Cl + 0.53\ HCl + 0.21\ GLYOXAL + 1.32\ CO + 0.79\ HO_2$	TROE	$6.10 \cdot 10^{-30} * (T/298)^{-3.0}$	$2.00 \cdot 10^{-10}$	0.6
H45	$Cl + C_2H_4 \rightarrow ClCH_2CH_2O_2$	TROE	$1.85 \cdot 10^{-29} * (T/298)^{-3.3}$	$6.00 \cdot 10^{-10}$	0.4
H54	$ClCH_2CO_3 + NO_2 \rightarrow ClPAN$	TROE	$2.70 \cdot 10^{-28} * (T/298)^{7.1}$	$1.20 \cdot 10^{-11} * (T/298)^{0.9}$	0.3
H60	$ClPAN \rightarrow ClCH_2CO_3 + NO_2$	TROE	$4.90 \cdot 10^{-03} \exp(-12100/T)$	$5.40 \cdot 10^{+16} \exp(-13830/T)$	0.3
H82	$CH_3CH(Cl)CO_3 + NO_2 \rightarrow CH_3ClPAN$	TROE	$2.70 \cdot 10^{-28} * (T/298)^{7.1}$	$1.20 \cdot 10^{-11} * (T/298)^{0.9}$	0.3
H83	$CH_3ClPAN \rightarrow CH_3CH(Cl)CO_3 + NO_2$	TROE	$4.90 \cdot 10^{-03} \exp(-12100/T)$	$5.40 \cdot 10^{+16} \exp(-13830/T)$	0.3
H102	$Br + NO_2 \rightarrow BrNO_2$	TROE	$4.20 \cdot 10^{-31} * (T/298)^{-2.4}$	$2.70 \cdot 10^{-11}$	0.55
H104	$BrO + NO_2 \rightarrow BrNO_3$	TROE	$4.70 \cdot 10^{-31} * (T/298)^{-3.1}$	$1.80 \cdot 10^{-11}$	0.4
H151	$IO + NO_2 \rightarrow INO_3$	TROE	$7.70 \cdot 10^{-31} (T/300)^{-5.0}$	$1.60 \cdot 10^{-11}$	0.6

(a) k^{2nd} in cm^3 $molecules^{-1}$ s^{-1}; k^{1st} in s^{-1}

Rate constants calculated with TROE formula: $k(T) = \frac{k_0(T)[M]}{1+\frac{k_0(T)[M]}{k_\infty(T)}} \times F_C^{\left\{1+log_{10}\left(\frac{k_0(T)[M]}{k_\infty(T)}\right)^2\right\}^{-1}}$

Table S8 Implemented phase transfers in the CAPRAM-HM3.0red

② reactions that run in the cloud mode 'sub#1', ③ reactions that run in the aerosol mode 'sub#2', ● already included in CAPRAM3.0red						
	Species	**$K_{H\ (298\ K)}$[(a)]**	**$-\Delta H/R$[(b)]**	**α**	**$D_{g\ (298\ K)}$[(c)]**	**Comment**
H200③●	Cl_2	$9.15 \cdot 10^{-2}$	2490	0.08	1.28	Bräuer et al. (2013)
H201	Cl	$2.00 \cdot 10^{-1}$		0.05	1.82	Bräuer et al. (2013)
H202②●	HCl	$1.10 \cdot 10^{0}$	2020	0.1026	1.89	Bräuer et al. (2013)
H203③	HOCl	$6.60 \cdot 10^{2}$	5862	0.5	1.51	Bräuer et al. (2013)
H204③●	$ClNO_2$	$2.40 \cdot 10^{-2}$		0.01	1.27	Bräuer et al. (2013)
H205③	$ClNO_3$	$2.10 \cdot 10^{5}$	8700	0.1	1.18	Bräuer et al. (2013)
H206	ClCHO	$3.00 \cdot 10^{3}$	7216	0.02	1.23	Bräuer et al. (2013)
H207③●	Br_2	$7.60 \cdot 10^{-1}$	4100	0.08	1.00	Bräuer et al. (2013)
H208	Br	$1.20 \cdot 10^{0}$		0.05	1.29	Bräuer et al. (2013)
H209③	HBr	$1.30 \cdot 10^{0}$	10239	0.0481	1.26	Bräuer et al. (2013)
H210③	HOBr	$9.30 \cdot 10^{1}$	5862	0.5	1.16	Bräuer et al. (2013)
H211③	$BrNO_3$	$2.10 \cdot 10^{5}$	8700	0.8	1.01	Bräuer et al. (2013)
H212③	BrCl	$9.40 \cdot 10^{-1}$	-5600	0.33	1.05	Bräuer et al. (2013)
H213	$BrCH_2CO_3$	$6.69 \cdot 10^{2}$	5893	0.019	0.84	Bräuer et al. (2013)
H214②	$BrCH_2COOH$	$1.52 \cdot 10^{5}$	9300	0.0322	0.84	Bräuer et al. (2013); Sander (2015)
H215	BrCHO	$7.40 \cdot 10^{1}$		0.02	1.02	Bräuer et al. (2013)
H216	I_2	$3.00 \cdot 10^{0}$	4431	0.0126	0.86	Bräuer et al. (2013)
H217③	HOI	$4.50 \cdot 10^{2}$	5862	0.5	1.08	Bräuer et al. (2013)
H218	HIO_3	$2.10 \cdot 10^{5}$	8700	0.0126	0.98	Bräuer et al. (2013)
H219③	INO_3	$2.10 \cdot 10^{5}$	8700	0.123	0.96	Bräuer et al. (2013)
H220③	I_2O_2	$1.00 \cdot 10^{4}$		0.123	0.80	Bräuer et al. (2013); Sander (2015)
H221③	ICl	$1.10 \cdot 10^{2}$	5600	0.0126	0.98	Bräuer et al. (2013)
H222③	IBr	$2.40 \cdot 10^{1}$	5600	0.0126	0.88	Bräuer et al. (2013)
(a) in M atm^{-1}; (b) in K; (c) in $m^2\ s^{-1}$						

Table S9 Implemented aqueous-phase reactions in the CAPRAM-HM3.0red

② reactions that run in the cloud mode 'sub#1', ③ reactions that run in the aerosol mode 'sub#2', ● already included in CAPRAM3.0red				
	Reaction	**k_{298}[(a)]**	**E_A/R[(b)]**	**Comment**
H223●	$Cl_2^- + H_2O_2 \rightarrow 2\ Cl^- + H^+ + HO_2$	$6.20 \cdot 10^5$	3340	Jacobi et al. (1999)
H224②●	$Cl_2^- + H_2O \rightarrow H^+ + Cl^- + ClOH^-$	$2.34 \cdot 10^1$		Buxton et al. (1998)
H225②	$HOCl + HO_2 \rightarrow Cl + H_2O + O_2$	$7.50 \cdot 10^6$		Bräuer et al. (2013)
H226	$HOCl + OH \rightarrow ClO + H_2O$	$2.00 \cdot 10^9$		Bräuer et al. (2013)
H227●	$Cl_2^- + HSO_3^- \rightarrow 2\ Cl^- + H^+ + SO_3^-$	$1.70 \cdot 10^8$	400	Jacobi (1996)
H228③	$HOCl + HSO_3^- \rightarrow Cl^- + H^+ + HSO_4^{2-}$	$7.60 \cdot 10^8$		Herrmann (2003)
H229	$Cl^- + HSO_5^- \rightarrow HOCl + SO_4^{2-}$	$1.80 \cdot 10^{-3}$	7352	Fortnum et al. (1960)
H230●	$Cl_2^- + Fe_2^+ \rightarrow 2\ Cl^- + Fe_3^+$	$1.00 \cdot 10^7$	3030	Thornton and Laurence (1973)
H231②●	$Cl^- + FeO_2^+ \rightarrow Fe_3^+ + ClOH^- + OH\text{-} - H_2O$	$1.00 \cdot 10^2$		Jacobsen et al. (1998)
H232●	$Cl_2^- + Mn_2^+ \rightarrow MnCl_2^+$	$2.00 \cdot 10^7$	4090	Laurence and Thornton (1973)
H233●	$MnCl_2^+ \rightarrow 0.588\ Cl_2^- + 0.588\ Mn^{2+} + 0.824\ Cl^- + 0.412\ Mn^{3+}$	$5.10 \cdot 10^5$		Deguillaume et al. (2010); Laurence and Thornton (1973)
H234	$2\ ClO \rightarrow Cl^- + ClO_3^- + 2\ H^+$	$2.50 \cdot 10^9$		Klaning and Wolff (1985)
H235	$OH + ClO_3^- \rightarrow ClO + O_2 + OH^-$	$1.00 \cdot 10^6$		Buxton and Subhani (1972)
H236	$Cl_2 + H_2O_2 \rightarrow 2\ H^+ + 2\ Cl^- + O_2$	$1.83 \cdot 10^2$	5387	Connick (1947)
H237③	$ClNO_3 \rightarrow HOCl + HNO_3$	$1.62 \cdot 10^6$	2800	Shi et al. (2001)
H238②	$Cl_2^- + HC_2O_4^- \rightarrow 2\ Cl^- + H^+ + C_2O_4^-$	$1.30 \cdot 10^6$		Bräuer et al. (2013)
H239②	$Cl_2^- + C_2O_4^{2-} \rightarrow 2\ Cl^- + C_2O_4^-$	$4.00 \cdot 10^6$		Bräuer et al. (2013)
H240②	$ClCHO \rightarrow CO + H^+ + Cl^-$	$1.00 \cdot 10^4$		Prager et al. (2001)
H241	$Br + H_2O_2 \rightarrow H^+ + Br^- + HO_2$	$4.00 \cdot 10^9$		Sutton et al. (1965)
H242②	$Br_2^- + HO_2 \rightarrow Br^- + 0.5\ Br_2 + 0.5\ H_2O_2 + 0.5\ O_2$	$8.80 \cdot 10^9$		Sutton and Downes (1972)
H243	$BrO + BrO \rightarrow BrO_2^- + HOBr + H^+$	$2.80 \cdot 10^9$		Klaning and Wolff (1985)
H244	$HOBr + OH \rightarrow BrO + H_2O$	$2.00 \cdot 10^9$		Klaning and Wolff (1985)
H245②	$HOBr + HO_2 \rightarrow Br + H_2O + O_2$	$1.00 \cdot 10^9$		Bräuer et al. (2013)
H246②	$HOBr + H_2O_2 \rightarrow H^+ + Br^- + H_2O + O_2$	$3.50 \cdot 10^6$		Young (1950)
H247③	$HOBr + HSO_3^- \rightarrow H+ + Br^- + HSO_4^-$	$5.00 \cdot 10^9$		Bräuer et al. (2013)
H248	$Br^- + HSO_5^- \rightarrow HOBr + SO_4^{2-}$	$1.00 \cdot 10^0$	5338	Fortnum et al. (1960)

② reactions that run in the cloud mode 'sub#1', ③ reactions that run in the aerosol mode 'sub#2', ● already included in CAPRAM3.0red

	Reaction	k_{298}[(a)]	E_A/R[(b)]	Comment
H249	$Br^- + NO_3 \rightarrow Br + NO_3^-$	$3.80 \cdot 10^9$		Zellner et al. (1996)
H250	$Br_2^- + Fe^{2+} \rightarrow 2\ Br^- + Fe^{3+}$	$3.60 \cdot 10^6$	3330	Thornton and Laurence (1973)
H251●	$Br_2^- + Mn^{2+} \rightarrow MnBr_2^+$	$6.30 \cdot 10^6$	4330	Thornton and Laurence (1973)
H252●	$MnBr_2^+ \rightarrow 0.577\ Br_2^- + 0.577\ Mn^{2+} + 0.846\ Br^- + 0.423\ Mn^{3+}$	$5.20 \cdot 10^5$		Thornton and Laurence (1973); Deguillaume et al. (2010)
H253	$BrO_3^- + SO_4^- \rightarrow BrO + O_2 + SO_4^{2-}$	$1.40 \cdot 10^6$		Zuo and Katsumura (1998)
H254	$Br + O_3 \rightarrow BrO + O_2$	$1.50 \cdot 10^8$		Von Gunten and Oliveras (1998)
H255	$BrO_3^- + HSO_3^- \rightarrow BrO_2^- + SO_4^{2-} + H^+$	$2.70 \cdot 10^{-2}$		Szirovicza and Boga (1998)
H256	$BrO_3^- + OH \rightarrow BrO + O_2 + OH^-$	$5.00 \cdot 10^6$		Amichai et al. (1969)
H257③	$BrNO_3 \rightarrow HOBr + HNO_3$	$1.00 \cdot 10^9$		Hanson et al. (1996)
H258	$BrO_3^- + HC_2O_4^- \rightarrow BrO_2^- + 2\ CO_2 + H_2O$	$7.47 \cdot 10^{-4}$		Pelle et al. (2004)
H259②	$BrCHO \rightarrow CO + H^+ + Br^-$	$1.00 \cdot 10^4$		Bräuer et al. (2013)
H260②	$CH_2BrCO_3 + H_2O \rightarrow CH_2BrCOOH + HO_2$	$3.55 \cdot 10^5$		Bräuer et al. (2013)
H261	$Br_2^- + HCOO^- \rightarrow 2\ Br^- + COOH$	$4.90 \cdot 10^3$		Jacobi et al. (1996)
H262③	$Br^- + HOCl \rightarrow BrCl + H_2O - H^+$	$1.30 \cdot 10^6$		Kumar and Margerum (1987)
H263②	$BrO_2^- + HOCl \rightarrow 0.85\ ClO_3^- + 0.93\ HOBr + 0.08\ ClO_2^- + 0.07\ BrO_3^- + 0.92\ Cl^- + 0.92\ H^+ - 0.85\ HOCl$	$1.60 \cdot 10^2$		Nicoson et al. (2003)
H264	$I^- + O_3 \rightarrow HOI + O_2$	$2.17 \cdot 10^9$	8790	Magi et al. (1997)
H265②	$IO + IO \rightarrow HOI + HIO_3 + H^+ - H_2O - H_2O_2$	$1.50 \cdot 10^9$		Buxton et al. (1986)
H266③	$HOI + HSO_3^- \rightarrow H^+ + I^- + HSO_4^-$	$5.00 \cdot 10^9$		Pechtl and von Glasow (2007)
H267	$HOI + OH \rightarrow IO + H_2O$	$7.00 \cdot 10^9$		Buxton and Mulazzani (2007)
H268③	$INO_3 \rightarrow HOI + HNO_3$	$1.62 \cdot 10^6$	2800	Hoffmann et al. (2019b)
H269	$I_2O_2 + H^+ \rightarrow HIO_3 + HOI + H^+$	$3.20 \cdot 10^4$		Valkai and Horvath (2016)
H270	$IO_3^- + OH \rightarrow IO + O_2 + OH^-$	$1.08 \cdot 10^5$		Mezyk (1996)

(a) k_{298}^{2nd} in $l^1\ mol^{-1}\ s^{-1}$; k_{298}^{1st} in s^{-1}; (b) in K

Table S10 Implemented aqueous-phase equilibrium reactions in the CAPRAM-HM3.0red

② reactions that run in the cloud mode 'sub#1', ③ reactions that run in the aerosol mode 'sub#2', ● already included in CAPRAM3.0red

	Reaction	K[(a)]	$k_{f,298}$[(b)]	E_A/R[(c)]	$k_{b,298}$[(b)]	E_A/R[(c)]	References
H271②●	$Cl + Cl^- \rightleftharpoons Cl_2^-$	$1.4 \cdot 10^5$	$8.50 \cdot 10^9$		$6.00 \cdot 10^4$		Buxton et al. (1998)
H272③●	$Cl_2 + H_2O \rightleftharpoons H^+ + Cl^- + HOCl$	$1.90 \cdot 10^{-5} e^{-4500/T}$	$4.00 \cdot 10^{-1}$	8000	$2.10 \cdot 10^4$	3500	Wang and Margerum (1994)
H273③●	$HCl \rightleftharpoons H^+ + Cl^-$	$1.72 \cdot 10^6\ e^{6890/T}$	$5.00 \cdot 10^{11}$	-6890	$2.90 \cdot 10^5$		Marsh and McElroy (1985); Graedel and Weschler (1981)
H274②●	$Cl^- + OH \rightleftharpoons ClOH^-$	$7.00 \cdot 10^{-1}$	$4.30 \cdot 10^9$		$6.10 \cdot 10^9$		Jayson et al. (1973)
H275②	$Cl + OH^- \rightleftharpoons ClOH^-$	$7.83 \cdot 10^8$	$1.80 \cdot 10^{10}$		$2.30 \cdot 10^1$		Klaning and Wolff (1985)
H276②●	$ClOH^- + H^+ \rightleftharpoons Cl + H_2O$	$5.10 \cdot 10^6$	$2.1 \cdot 10^{10}$		$4.10 \cdot 10^3$		Jayson et al. (1973)
H277②●	$ClOH^- + Cl^- \rightleftharpoons Cl_2^- + OH^-$	$2.20 \cdot 10^{-4}$	$1.00 \cdot 10^4$		$4.50 \cdot 10^7$		Grigor'ev et al. (1987)
H278②●	$Cl^- + SO_4^- \rightleftharpoons Cl + SO_4^{2-}$	$1.20 \cdot 10^0$	$2.52 \cdot 10^8$		$2.10 \cdot 10^8$		Buxton et al. (1999b)
H279②●	$Cl^- + NO_3 \rightleftharpoons Cl + NO_3^-$	$3.40 \cdot 10^0\ e^{-4300/T}$	$3.40 \cdot 10^8$	4300	$1.00 \cdot 10^8$		Buxton et al. (1999a)
H280	$HOCl + NO_2^- \rightleftharpoons ClNO_2 + OH^-$	$3.97 \cdot 10^{-4}$	$1.99 \cdot 10^7$		$5.00 \cdot 10^{10}$		Lahoutifard et al. (2002)
H281③	$Cl_2 + SO_4^{2-} \rightleftharpoons Cl^- + HOCl + HSO_4^-$	$1.14 \cdot 10^{-3}$	$3.20 \cdot 10^1$		$2.80 \cdot 10^3$		Wang and Margerum (1994)
H282③●	$Cl^- + NO_2^+ \rightleftharpoons ClNO_2$	$1.44 \cdot 10^8$	$3.90 \cdot 10^{10}$		$2.70 \cdot 10^2$		Behnke et al. (1997)
H283②●	$Br + Br^- \rightleftharpoons Br_2^-$	$6.32 \cdot 10^5$	$1.20 \cdot 10^{10}$		$1.90 \cdot 10^4$		Merenyi and Lind (1994)
H284③	$Br_2 + H_2O \rightleftharpoons H^+ + Br^- + HOBr$	$1.06 \cdot 10^{-10} e^{-7500/T}$	$1.70 \cdot 10^0$	7500	$1.60 \cdot 10^{10}$		Beckwith et al. (1996)
H285③	$HBr \rightleftharpoons H^+ + Br^-$	$1.00 \cdot 10^9$	$5.00 \cdot 10^{11}$		$5.00 \cdot 10^2$		Lax (1969)
H286②●	$Br^- + OH \rightleftharpoons BrOH^-$	$3.33 \cdot 10^2$	$1.10 \cdot 10^{10}$		$3.30 \cdot 10^7$		Zehavi and Rabani (1972)
H287②	$Br + OH^- \rightleftharpoons BrOH^-$	$3.10 \cdot 10^3$	$1.30 \cdot 10^{10}$		$4.20 \cdot 10^6$		Zehavi and Rabani (1972); Klaning and Wolff (1985)
H288②●	$BrOH^- + H^+ \rightleftharpoons Br + H_2O$	$1.80 \cdot 10^{12}$	$4.40 \cdot 10^{10}$		$2.45 \cdot 10^{-2}$		Zehavi and Rabani (1972); Klaning and Wolff (1985)
H289②●	$BrOH^- + Br^- \rightleftharpoons Br_2^- + OH^-$	$7.00 \cdot 10^1$	$1.90 \cdot 10^8$		$2.70 \cdot 10^6$		Zehavi and Rabani (1972); de Violet (1981)
H290	$HOBr + HOBr \rightleftharpoons H^+ + Br^- + BrO_2^-$	$6.70 \cdot 10^{-12}$	$2.00 \cdot 10^{-5}$		$3.00 \cdot 10^6$		Field and Foersterling (1986)
H291	$HOBr + BrO_2^- \rightleftharpoons H^+ + Br^- + BrO_3^-$	$1.70 \cdot 10^0$	$3.20 \cdot 10^0$		$2.00 \cdot 10^0$		Field and Foersterling (1986)
H292②	$CH_2BrCOOH \rightleftharpoons CH_2BrCOO^- + H^+$	$1.75 \cdot 10^{-5}\ e^{46/T}$	$8.75 \cdot 10^5$	-46	$5.00 \cdot 10^{10}$		Bräuer et al. (2013)
H293③	$Br_2 + SO_4^{2-} + H_2O \rightleftharpoons HOBr + Br^- + HSO_4^-$	$6.15 \cdot 10^{-6}$	$2.28 \cdot 10^4$		$3.70 \cdot 10^9$		Beckwith et al. (1996)
H294③	$BrCl \rightleftharpoons HOBr + H^+ + Cl^- - H_2O$	$1.80 \cdot 10^{-5}$	$1.00 \cdot 10^5$		$5.60 \cdot 10^9$		Wang et al. (1994)
H295③	$BrCl^- \rightleftharpoons Br^- + Cl$	$1.60 \cdot 10^{-7}$	$1.90 \cdot 10^3$		$1.20 \cdot 10^{10}$		Donati (2002)

② reactions that run in the cloud mode 'sub#1', ③ reactions that run in the aerosol mode 'sub#2', ● already included in CAPRAM3.0red							
	Reaction	**K[(a)]**	**$k_{f,298}$[(b)]**	**E_A/R[(c)]**	**$k_{b,298}$[(b)]**	**E_A/R[(c)]**	**References**
H296③	$BrCl^- \rightleftharpoons Br + Cl^-$	$6.10 \cdot 10^{-4}$	$6.10 \cdot 10^{4}$		$1.00 \cdot 10^{8}$		Donati (2002)
H297③	$BrCl^- + Br^- \rightleftharpoons Br_2^- + Cl^-$	$1.86 \cdot 10^{3}$	$8.00 \cdot 10^{9}$		$4.30 \cdot 10^{6}$		Ershov (2004)
H298③	$BrCl^- + Cl^- \rightleftharpoons Br^- + Cl_2^-$	$2.75 \cdot 10^{-8}$	$1.10 \cdot 10^{2}$		$4.00 \cdot 10^{9}$		Ershov (2004)
H299③	$Br_2Cl^- \rightleftharpoons BrCl + Br^-$	$5.60 \cdot 10^{-5}$	$4.30 \cdot 10^{5}$		$7.70 \cdot 10^{9}$		Wang et al. (1994)
H300③	$Br_2Cl^- \rightleftharpoons Br_2 + Cl^-$	$7.60 \cdot 10^{-1}$	$3.80 \cdot 10^{4}$		$5.00 \cdot 10^{4}$		Wang et al. (1994); Matthew and Anastasio (2006)
H301③	$BrCl_2^- \rightleftharpoons BrCl + Cl^-$	$1.70 \cdot 10^{-1}$	$1.70 \cdot 10^{5}$		$1.00 \cdot 10^{6}$		Ershov (2004)
H302③	$BrCl_2^- \rightleftharpoons Br^- + Cl_2$	$1.50 \cdot 10^{-6}$	$9.00 \cdot 10^{3}$		$6.00 \cdot 10^{9}$		Ershov (2004)
H303	$I_2 + OH^- \rightleftharpoons I_2OH^-$	$5.00 \cdot 10^{0}$	$1.00 \cdot 10^{10}$		$2.00 \cdot 10^{9}$		Buxton and Mulazzani (2007)
H304	$I_2OH^- \rightleftharpoons HOI + I^-$	$8.30 \cdot 10^{0}$	$2.49 \cdot 10^{9}$		$3.00 \cdot 10^{8}$		Buxton and Mulazzani (2007)
H305	$HOI + H^+ + I^- \rightleftharpoons I_2 + H_2O$	$1.47 \cdot 10^{12}$	$4.40 \cdot 10^{12}$		$3.00 \cdot 10^{0}$		Eigen and Kustin (1962)
H306②	$HIO_3 \rightleftharpoons H^+ + IO_3^-$	$1.70 \cdot 10^{-1}$	$8.50 \cdot 10^{9}$		$5.00 \cdot 10^{10}$		Lide et al. (1995)
H307③	$HOI + H^+ + Cl^- \rightleftharpoons ICl$	$1.20 \cdot 10^{4}$	$2.90 \cdot 10^{10}$		$2.40 \cdot 10^{6}$		Wang et al. (1989)
H308③	$HOI + H^+ + Br^- \rightleftharpoons IBr$	$5.10 \cdot 10^{6}$	$4.10 \cdot 10^{12}$		$8.00 \cdot 10^{5}$		De Barros Faria et al. (1993)
H309③	$ICl + Br^- \rightleftharpoons IBr + Cl^-$	$3.30 \cdot 10^{3}$	$1.65 \cdot 10^{14}$		$5.00 \cdot 10^{10}$		Wagman et al. (1982)
(a) in M^{m-n}, n order of reaction of forward reaction, m order of reaction of backward reaction; (b) k_{298}^{2nd} in l^1 mol^{-1} s^{-1}, k_{298}^{1st} in s^{-1}; (c) in K							

Table S11 Measured values of HCl and BrO in marine environments.

HCl	BrO*	Location	Comment	Reference
daily average: 133 – 675 ppt		Bermuda		Keene and Savoie (1999)
range: 30-250 ppt		Hawaii		Pszenny et al. (2004)
median: 351 ppt		Appledore Island		Keene et al. (2007)
daily median: 82-682 ppt		North to South Atlantic		Keene et al. (2009)
median: 206 ppt		Cape Verde	range: 26 – 613 ppt	Sander et al. (2013)
	max. 1-3.6 ppt	Canary Island	in remote ocean below detection limit	Leser et al. (2003)
	average 2.3 ppt	Mace Head	Coastal region	Saiz-Lopez et al. (2004)
	average max. 2.5 ± 1.1 ppt	Cape Verde		Read et al. (2008)
	< 0.5 ppt	Eastern tropical Pacific	MBL: below detection limit	Volkamer et al. (2015)
	0.03 ± 0.26 ppt	Western tropical Pacific	clean MBL outflow	Chen et al. (2016)
	0.17-1.64 ppt	Western Pacific	between 0.5 – 7 km height	Le Breton et al. (2017)

DL – Detection Limit; * for a more detailed overview on measurements before 2003 see Sander et al. (2003)

References

Amichai, O., Czapski, G., and Treinin, A.: Flash Photolysis of Oxybromine Anions, Israel J. Chem., 7, 351-359, https://doi.org/10.1002/ijch.196900046, 1969.

Anderson, L. C., and Fahey, D. W.: Studies with nitryl hypochlorite: thermal dissociation rate and catalytic conversion to nitric oxide using an NO/O3 chemiluminescence detector, J. Phys. Chem., 94, 644-652, https://doi.org/10.1021/j100365a027, 1990.

Atkinson, R., Baulch, D. L., Cox, R. A., Crowley, J. N., Hampson, R. F., Hynes, R. G., Jenkin, M. E., Rossi, M. J., and Troe, J.: Evaluated kinetic and photochemical data for atmospheric chemistry: Volume I – gas phase reactions of O_x, HO_x, NO_x and SO_x species, Atmos. Chem. Phys., 4, 1461-1738, https://doi.org/10.5194/acp-4-1461-2004, 2004.

Atkinson, R., Baulch, D. L., Cox, R. A., Crowley, J. N., Hampson, R. F., Hynes, R. G., Jenkin, M. E., Rossi, M. J., Troe, J., and Subcommittee, I.: Evaluated kinetic and photochemical data for atmospheric chemistry: Volume II – gas phase reactions of organic species, Atmos. Chem. Phys., 6, 3625-4055, https://doi.org/10.5194/acp-6-3625-2006, 2006.

Atkinson, R., Baulch, D. L., Cox, R. A., Crowley, J. N., Hampson, R. F., Hynes, R. G., Jenkin, M. E., Rossi, M. J., and Troe, J.: Evaluated kinetic and photochemical data for atmospheric chemistry: Volume III – gas phase reactions of inorganic halogens, Atmos. Chem. Phys., 7, 981-1191, https://doi.org/10.5194/acp-7-981-2007, 2007.

Atkinson, R., Baulch, D. L., Cox, R. A., Crowley, J. N., Hampson, R. F., Hynes, R. G., Jenkin, M. E., Rossi, M. J., Troe, J., and Wallington, T. J.: Evaluated kinetic and photochemical data for atmospheric chemistry: Volume IV – gas phase reactions of organic halogen species, Atmos. Chem. Phys., 8, 4141-4496, https://doi.org/10.5194/acp-8-4141-2008, 2008.

Ballesteros, B., Jensen, N. R., and Hjorth, J.: FT-IR study of the kinetics and products of the reactions of dimethylsulphide, dimethylsulphoxide and dimethylsulphone with Br and BrO, J. Atmos. Chem., 43, 135-150, https://doi.org/10.1023/A:1019922224137, 2002.

Bardouki, H., da Rosa, M. B., Mihalopoulos, N., Palm, W. U., and Zetzsch, C.: Kinetics and mechanism of the oxidation of dimethylsulfoxide (DMSO) and methanesulfinate (MSI^-) by OH radicals in aqueous medium, Atmos. Environ., 36, 4627-4634, https://doi.org/10.1016/S1352-2310(02)00460-0, 2002.

Beckwith, R. C., Wang, T. X., and Margerum, D. W.: Equilibrium and kinetics of bromine hydrolysis, Inorg. Chem., 35, 995-1000, https://doi.org/10.1021/ic950909w, 1996.

Behnke, W., George, C., Scheer, V., and Zetzsch, C.: Production and decay of $ClNO_2$ from the reaction of gaseous N_2O_5 with NaCl solution: Bulk and aerosol experiments, J. Geophys. Res.-Atmos., 102, 3795-3804, https://doi.org/10.1029/96jd03057, 1997.

Bräuer, P., Tilgner, A., Wolke, R., and Herrmann, H.: Mechanism development and modelling of tropospheric multiphase halogen chemistry: The CAPRAM Halogen Module 2.0 (HM2), J. Atmos. Chem., 70, 19-52, https://doi.org/10.1007/s10874-013-9249-6, 2013.

Burkholder, J. B., Sander, S. P., Abbatt, J., Barker, J. R., Huie, R. E., Kolb, C. E., Kurylo, M. J., Orkin, V. L., Wilmouth, D. M., and Wine, P. H.: Chemical Kinetics and Photochemical Data for Use in Atmospheric Studies, Evaluation No. 18, Jet Propulsion Laboratory, Pasadena, 2015.
Buxton, G., V., Arthur Salmon, G., and Wang, J.: The equilibrium $NO_3^\bullet + Cl^- \rightleftharpoons NO_3^- + Cl^\bullet$: A laser flash photolysis and pulse radiolysis study of the reactivity of $NO_3^\bullet$ with chloride ion in aqueous solution, Phys. Chem. Chem. Phys., 1, 3589-3593, https://doi.org/10.1039/A903286J, 1999a.
Buxton, G., V., Bydder, M., and Arthur Salmon, G.: The reactivity of chlorine atoms in aqueous solution Part II. The equilibrium $SO_4^{-\bullet} + Cl^- \rightleftharpoons Cl^\bullet + SO_4^{2-}$, Phys. Chem. Chem. Phys., 1, 269-273, https://doi.org/10.1039/A807808D, 1999b.
Buxton, G. V., and Subhani, M. S.: Radiation-Chemistry and Photochemistry of Oxychlorine Ions .1. Radiolysis of Aqueous-Solutions of Hypochlorite and Chlorite Ions, J. Chem. Soc. Farad. Trans. 1, 68, 947-957, https://doi.org/10.1039/f19726800947, 1972.
Buxton, G. V., Kilner, C., and Sellers, R. M.: Pulse radiolysis of HOI and IO^- in aqueous solution, formation and characterization of I^{II}, 6th Symposium on Radiation Chemistry, 1986, 155-159,
Buxton, G. V., Bydder, M., and Arthur Salmon, G.: Reactivity of chlorine atoms in aqueous solution Part I. The equilibrium $Cl^\bullet + Cl^- \rightleftharpoons Cl_2^{-\bullet}$, 94, 653-657, https://doi.org/10.1039/A707377A, 1998.
Buxton, G. V., and Mulazzani, Q. G.: On the hydrolysis of iodine in alkaline solution: A radiation chemical study, Rad. Phys. Chem., 76, 932-940, https://doi.org/10.1016/j.radphyschem.2006.06.009, 2007.
Campolongo, F., Saltelli, A., Jensen, N. R., Wilson, J., and Hjorth, J.: The role of multiphase chemistry in the oxidation of dimethylsulphide (DMS). A latitude dependent analysis, J. Atmos. Chem., 32, 327-356, https://doi.org/10.1023/A:1006154618511, 1999.
Canosa-Mas, C. E., Cotter, E. S. N., Duffy, J., Thompson, K. C., and Wayne, R. P.: The reactions of atomic chlorine with acrolein, methacrolein and methyl vinyl ketone, Phys. Chem. Chem. Phys., 3, 3075-3084, https://doi.org/10.1039/b101434j, 2001.
Chen, D., Huey, L. G., Tanner, D. J., Salawitch, R. J., Anderson, D. C., Wales, P. A., Pan, L. L., Atlas, E. L., Hornbrook, R. S., Apel, E. C., Blake, N. J., Campos, T. L., Donets, V., Flocke, F. M., Hall, S. R., Hanisco, T. F., Hills, A. J., Honomichl, S. B., Jensen, J. B., Kaser, L., Montzka, D. D., Nicely, J. M., Reeves, J. M., Riemer, D. D., Schauffler, S. M., Ullmann, K., Weinheimer, A. J., and Wolfe, G. M.: Airborne measurements of BrO and the sum of HOBr and Br_2 over the Tropical West Pacific from 1 to 15 km during the CONvective TRansport of Active Species in the Tropics (CONTRAST) experiment, J. Geophys. Res.-Atmos., 121, 12560-12578, https://doi.org/10.1002/2016JD025561, 2016.
Clarke, J. H. R., and Woodward, L. A.: Raman spectrophotometric determination of degrees of dissociation of methanesulphonic acid in aqueous solution at 25°C, Trans. Faraday Soc., 62, 2226-2233, https://doi.org/10.1039/Tf9666202226, 1966.
Connick, R. E.: The Interaction of Hydrogen Peroxide and Hypochlorous Acid in Acidic Solutions Containing Chloride Ion, J. Am. Chem. Soc., 69, 1509-1514, https://doi.org/10.1021/ja01198a074, 1947.
De Barros Faria, R., Lengyel, I., Epstein, I. R., and Kustin, K.: Systematic design of chemical oscillators. 86. Combined mechanism explaining nonlinear dynamics in bromine(III) and bromine(V) oxidations of iodide ion, J. Phys. Chem., 97, 1164-1171, https://doi.org/10.1021/j100108a011, 1993.

De Bruyn, W. J., Shorter, J. A., Davidovits, P., Worsnop, D. R., Zahniser, M. S., and Kolb, C. E.: Uptake of gas-phase sulfur species methanesulfonic-acid, dimethylsulfoxide, and dimethyl sulfone by aqueous surfaces, J. Geophys. Res.-Atmos., 99, 16927-16932, https://doi.org/10.1029/94jd00684, 1994.
de Violet, P. F.: Polyhalide radical anions as intermediates in chemistry, Rev. Chem. Interm., 4, 121-169, https://doi.org/10.1007/BF03052414, 1981.
Deguillaume, L., Tilgner, A., Schrödner, R., Wolke, R., Chaumerliac, N., and Herrmann, H.: Towards an operational aqueous phase chemistry mechanism for regional chemistry-transport models: CAPRAM-RED and its application to the COSMO-MUSCAT model, J. Atmos. Chem., 64, 1-35, https://doi.org/10.1007/s10874-010-9168-8, 2010.
Dillon, T. J., Tucceri, M. E., and Crowley, J. N.: Laser induced fluorescence studies of iodine oxide chemistry Part II. The reactions of IO with CH_3O_2, CF_3O_2 and O_3, Phys. Chem. Chem. Phys., 8, 5185-5198, https://doi.org/10.1039/B611116E, 2006.
Donati, A.: Spectroscopic and kinetic investigations of halogen-containing radicals in the tropospheric

aqueous phase, University of Leipzig, Leipzig, Germany, 2002.
Dyke, J. M., Ghosh, M. V., Kinnison, D. J., Levita, G., Morris, A., and Shallcross, D. E.: A kinetics and mechanistic study of the atmospherically relevant reaction between molecular chlorine and dimethyl sulfide (DMS), Phys. Chem. Chem. Phys., 7, 866, https://doi.org/10.1039/b415566a, 2005.
Eigen, M., and Kustin, K.: The Kinetics of Halogen Hydrolysis, J. Am. Chem. Soc., 84, 1355-1361, https://doi.org/10.1021/ja00867a005, 1962.
Ershov, B. G.: Kinetics, mechanism and intermediates of some radiation-induced reactions in aqueous solutions, Rus. Chem. Rev., 73, 101-113, https://doi.org/10.1070/rc2004v073n01abeh000865, 2004.
Falbe-Hansen, H., Sorensen, S., Jensen, N. R., Pedersen, T., and Hjorth, J.: Atmospheric gas-phase reactions of dimethylsulphoxide and dimethylsulphone with OH and NO_3 radicals, Cl atoms and ozone, Atmos. Environ., 34, 1543-1551, https://doi.org/10.1016/S1352-2310(99)00407-0, 2000.
Field, R. J., and Foersterling, H. D.: On the oxybromine chemistry rate constants with cerium ions in the Field-Koeroes-Noyes mechanism of the Belousov-Zhabotinskii reaction: the equilibrium $HBrO_2 + BrO_3^- + H^+ \rightleftharpoons 2\ BrO_2\text{-} + H_2O$, J. Phys. Chem., 90, 5400-5407, https://doi.org/10.1021/j100412a101, 1986.
Flyunt, R., Makogon, O., Schuchmann, M. N., Asmus, K.-D., and von Sonntag, C.: OH-Radical-induced oxidation of methanesulfinic acid. The reactions of the methanesulfonyl radical in the absence and presence of dioxygen, J. Chem. Soc. Perkin. Trans. 2, 787-792, https://doi.org/10.1039/b009631h, 2001.
Fortnum, D. H., Battaglia, C. J., Cohen, S. R., and Edwards, J. O.: The Kinetics of the Oxidation of Halide Ions by Monosubstituted Peroxides, J. Am. Chem. Soc., 82, 778-782, https://doi.org/10.1021/ja01489a004, 1960.
Fuller, E. N., Schettle.Pd, and Giddings, J. C.: A new method for prediction of binary gas-phase diffusion coeffecients, Ind. Eng. Chem., 58, 19-27, https://doi.org/10.1021/ie50677a007, 1966.

Gershenzon, M., Davidovits, P., Jayne, J. T., Kolb, C. E., and Worsnop, D. R.: Simultaneous uptake of DMS and ozone on water, J. Phys. Chem. A, 105, 7031-7036, https://doi.org/10.1021/Jp010696y, 2001.
Gómez Martín, J. C., Spietz, P., and Burrows, J. P.: Kinetic and mechanistic studies of the I_2/O_3 photochemistry, J. Phys. Chem. A, 111, 306-320, https://doi.org/10.1021/jp061186c, 2007.
Graedel, T. E., and Weschler, C. J.: Chemistry within aqueous atmospheric aerosols and raindrops, Rev. Geophys., 19, 505-539, https://doi.org/10.1029/RG019i004p00505, 1981.
Green, M., Yarwood, G., and Niki, H.: FTIR study of the Cl-atom initiated oxidation of methylglyoxal, Int. J. Chem. Kin., 22, 689-699, https://doi.org/10.1002/kin.550220705, 1990.
Grigor'ev, A. E., Makarov, I. E., and Pikaev, A. K.: Formation of Cl_2^- in the bulk of solution during radiolysis of concentrated aqueous solutions of chlorides, High Energy Chem., 21, 123-126, 1987.
Hansen, J. C., Li, Y., Francisco, J. S., and Li, Z.: On the Mechanism of the BrO + CH_2O Reaction, J. Phys. Chem. A, 103, 8543-8546, https://doi.org/10.1021/jp991757j, 1999.
Hanson, D. R., Ravishankara, A. R., and Lovejoy, E. R.: Reaction of $BrONO_2$ with H_2O on submicron sulfuric acid aerosol and the implications for the lower stratosphere, J. Geophys. Res.-Atmos., 101, 9063-9069, https://doi.org/10.1029/96jd00347, 1996.
Hasson, A. S., Tyndall, G. S., Orlando, J. J., Singh, S., Hernandez, S. Q., Campbell, S., and Ibarra, Y.: Branching Ratios for the Reaction of Selected Carbonyl-Containing Peroxy Radicals with Hydroperoxy Radicals, J. Phys. Chem. A, 116, 6264-6281, https://doi.org/10.1021/jp211799c, 2012.
Herrmann, H., and Zellner, R.: Removal and interconversions of oxidants in the atmospheric aqueous phase, Part 2 (RINOXA 2), Universität Essen, Essen, Deutschland, 1997.
Herrmann, H.: Kinetics of aqueous phase reactions relevant for atmospheric chemistry, Chem. Rev., 103, 4691-4716, https://doi.org/10.1021/cr020658q, 2003.
Hoffmann, E. H., Tilgner, A., Schrodner, R., Brauer, P., Wolke, R., and Herrmann, H.: An advanced modeling study on the impacts and atmospheric implications of multiphase dimethyl sulfide chemistry, Proc. Natl. Acad. Sci. USA, 113, 11776-11781, https://doi.org/10.1073/pnas.1606320113, 2016.
Hoffmann, E. H., Tilgner, A., Vogelsberg, U., Wolke, R., and Herrmann, H.: Near-explicit multiphase modeling of halogen chemistry in a mixed urban and maritime coastal area, ACS Earth Space Chem., 3, 2452-2471, https://doi.org/10.1021/acsearthspacechem.9b00184, 2019a.
Hoffmann, E. H., Tilgner, A., Wolke, R., and Herrmann, H.: Enhanced chlorine and bromine atom activation by hydrolysis of halogen nitrates from marine aerosols at polluted coastal areas, Environ. Sci. Technol., 53, 771-778, https://doi.org/10.1021/acs.est.8b05165, 2019b.
Hsin, H. Y., and Elrod, M. J.: Overall rate constant measurements of the reaction of hydroxy- and chloroalkylperoxy radicals derived from methacrolein and methyl vinyl ketone with nitric oxide, J. Phys. Chem. A, 111, 613-619, https://doi.org/10.1021/jp0665574, 2007.

Jacobi, H.-W., Herrmann, H., and Zellner, R.: Kinetic investigation of the Cl_2^- radical in the aqueous phase, in: Air Pollution Research Report, 57(Homogenous and heterogenous chemical Processes in the Troposphere), edited by: Mirabel, P., Office for official Publications of the European Communities, Luxembourg, 172-176, 1996.
Jacobi, H. W.: Kinetische Untersuchungen und Modellrechnungen zur troposphärischen Chemie von Radikalanionen und Ozon in wäßriger Phase, Universität-GH-Essen, Essen, Germany, 1996.
Jacobi, H. W., Wicktor, F., Herrmann, H., and Zellner, R.: A laser flash photolysis kinetic study of reactions of the Cl_2^- radical anion with oxygenated hydrocarbons in aqueous solution, Int. J. Chem. Kinet., 31, 169-181, https://doi.org/10.1002/(Sici)1097-4601(1999)31:3<169::Aid-Kin2>3.0.Co;2-K, 1999.
Jacobsen, F., Holcman, J., and Sehested, K.: Reactions of the ferryl ion with some compounds found in cloud water, Int. J. Chem. Kin., 30, 215-221, https://doi.org/10.1002/(SICI)1097-4601(1998)30:3<215::AID-KIN7>3.0.CO;2-V, 1998.
Jayson, G. G., Parsons, B. J., and Swallow, A. J.: Some simple, highly reactive, inorganic chlorine derivatives in aqueous solution. Their formation using pulses of radiation and their role in the mechanism of the Fricke dosimeter, J. Chem. Soc., Faraday Trans., 69, 1597-1607, https://doi.org/10.1039/F19736901597, 1973.
Kaiser, E. W., Wallington, T. J., and Hurley, M. D.: Products and Mechanism of the Reaction of Chlorine Atoms with 3-Pentanone in 700-950 Torr of N_2/O_2 Diluent at 297-515 K, J. Phys. Chem. A, 114, 343-354, https://doi.org/10.1021/jp9083663, 2010.
Kaltsoyannis, N., and Plane, J. M. C.: Quantum chemical calculations on a selection of iodine-containing species (IO, OIO, INO_3, $(IO)_2$, I_2O_3, I_2O_4 and I_2O_5) of importance in the atmosphere, Phys. Chem. Chem. Phys., 10, 1723-1733, https://doi.org/10.1039/b715687c, 2008.
Keene, W. C., and Savoie, D. L.: Correction to "The pH of deliquesced sea-salt aerosol in polluted marine air", Geophys. Res. Lett., 26, 1315-1316, https://doi.org/10.1029/1999gl900221, 1999.
Keene, W. C., Stutz, J., Pszenny, A. A. P., Maben, J. R., Fischer, E. V., Smith, A. M., von Glasow, R., Pechtl, S., Sive, B. C., and Varner, R. K.: Inorganic chlorine and bromine in coastal New England air during summer, J. Geophys. Res.-Atmos., 112, https://doi.org/10.1029/2006jd007689, 2007.
Keene, W. C., Long, M. S., Pszenny, A. A. P., Sander, R., Maben, J. R., Wall, A. J., O'Halloran, T. L., Kerkweg, A., Fischer, E. V., and Schrems, O.: Latitudinal variation in the multiphase chemical processing of inorganic halogens and related species over the eastern North and South Atlantic Oceans, Atmos. Chem. Phys., 9, 7361-7385, https://doi.org/10.5194/acp-9-7361-2009, 2009.
Klaning, U. K., and Wolff, T.: Laser Flash-Photolysis of HClO, ClO^-, HBrO, and BrO^- in Aqueous-Solution - Reactions of Cl-Atoms and Br-Atoms, Ber. Bunsen Phys. Chem., 89, 243-245, https://doi.org/10.1002/bbpc.19850890309, 1985.
Kleissas, K. M., Nicovich, J. M., and Wine, P. H.: Spectroscopy and kinetics of the gas phase addition complex of atomic chlorine with dimethyl sulfoxide, J. Photoch. Photobio. A, 187, 1-9, https://doi.org/10.1016/j.jphotochem.2006.08.020, 2007.

Kumar, K., and Margerum, D. W.: Kinetics and Mechanism of General-Acid-Assisted Oxidation of Bromide by Hypochlorite and Hypochlorous Acid, Inorg. Chem., 26, 2706-2711, https://doi.org/10.1021/ic00263a030, 1987.
Lahoutifard, N., Lagrange, P., Lagrange, J., and Scott, S. L.: Kinetics and mechanism of nitrite oxidation by HOBr/BrO^- in atmospheric water and comparison with oxidation by HOCl/ClO^-, J. Phys. Chem. A, 106, 11891-11896, https://doi.org/10.1021/jp021185u, 2002.
Larin, I. K., Nevozhai, D. V., Spasskii, A. I., Trofimova, E. M., and Turkin, L. E.: Measurement of rate constants for the reaction of iodine monoxide with ozone, Kinet. Catal., 40, 435-442, 1999.
Laurence, G. S., and Thornton, A. T.: Kinetics of oxidation of transition-metal ions by halogen radical anions. Part III. The oxidation of manganese(II) by dibromide and dichloride ions generated by flash photolysis, J. Chem. Soc., Dalton Trans., 1637-1644, https://doi.org/10.1039/DT9730001637, 1973.
Lax, E.: Taschenbuch für Chemiker und Physiker, Springer Verlag, Berlin, Germany, 1969.
Le Breton, M., Bannan, T. J., Shallcross, D. E., Khan, M. A., Evans, M. J., Lee, J., Lidster, R., Andrews, S., Carpenter, L. J., Schmidt, J., Jacob, D., Harris, N. R. P., Bauguitte, S., Gallagher, M., Bacak, A., Leather, K. E., and Percival, C. J.: Enhanced ozone loss by active inorganic bromine chemistry in the tropical troposphere, Atmos. Environ., 155, 21-28, https://doi.org/10.1016/j.atmosenv.2017.02.003, 2017.
Leser, H., Hönninger, G., and Platt, U.: MAX-DOAS measurements of BrO and NO_2 in the marine boundary layer, Geophys. Res. Lett., 30, 1537, https://doi.org/10.1029/2002gl015811, 2003.
Lide, D. R., Frederickse, H. P. R., Bass, M., Brewer, L., DiSalvo, F. J., Donnelly, R. J., Karger, B. L., Lineberger, W. C., Palmer, D. A., Seyferth, D., and Westbrook, J. H.: CRC Handbook of Chemistry and Physics, CRC Press, 1995.
Lucas, D. D., and Prinn, R. G.: Mechanistic studies of dimethylsulfide oxidation products using an observationally constrained model, J. Geophys. Res.-Atmos., 107, https://doi.org/10.1029/2001jd000843, 2002a.
Lucas, D. D., and Prinn, R. G.: Mechanistic studies of dimethylsulfide oxidation products using an observationally constrained model, J. Geophys. Res.-Atmos., 107, ACH 12-11-ACH 12-26, https://doi.org/10.1029/2001JD000843, 2002b.
Magi, L., Schweitzer, F., Pallares, C., Cherif, S., Mirabel, P., and George, C.: Investigation of the Uptake Rate of Ozone and Methyl Hydroperoxide by Water Surfaces, J. Phys. Chem. A, 101, 4943-4949, https://doi.org/10.1021/jp970646m, 1997.
Marsh, A. R. W., and McElroy, W. J.: The dissociation constant and Henry's law constant of HCl in aqueous solution, Atmos. Environ., 19, 1075-1080, https://doi.org/10.1016/0004-6981(85)90192-1, 1985.
Martín, P., Cabañas, B., Colmenar, I., Salgado, M. S., Villanueva, F., and Tapia, A.: Reactivity of e-butenedial with the major atmospheric oxidants, Atmos. Environ., 70, 351-360, https://doi.org/10.1016/j.atmosenv.2013.01.041, 2013.
Matthew, B. M., and Anastasio, C.: A chemical probe technique for the determination of reactive halogen species in aqueous solution: Part 1 - bromide solutions, Atmos. Chem. Phys., 6, 2423-2437, https://doi.org/10.5194/acp-6-2423-2006, 2006.

Merenyi, G., and Lind, J.: Reaction Mechanism of Hydrogen Abstraction by the Bromine Atom in Water, J. Am. Chem. Soc., 116, 7872-7876, https://doi.org/10.1021/ja00096a050, 1994.
Mezyk, S. P.: Arrhenius parameter determination for the reaction of the oxide radical, hydrated electron and hydroxyl radical with iodate in aqueous solution, J. Chem. Soc. Faraday Trans., 92, 2251-2254, https://doi.org/10.1039/ft9969202251, 1996.
Nicoson, J. S., Perrone, T. F., Hartz, K. E. H., Wang, L., and Margerum, D. W.: Kinetics and mechanisms of the reactions of hypochlorous acid, chlorine, and chlorine monoxide with bromite ion, Inorg. Chem., 42, 5818-5824, https://doi.org/10.1021/ic0301223, 2003.
Nicovich, J. M., Parthasarathy, S., Pope, F. D., Pegus, A. T., McKee, M. L., and Wine, P. H.: Kinetics, mechanism, and thermochemistry of the gas phase reaction of atomic chlorine with dimethyl sulfoxide, J .Phys. Chem. A, 110, 6874-6885, https://doi.org/10.1021/Jp0567467, 2006.
Niki, H., Maker, P. D., Savage, C. M., and Breitenbach, L. P.: An FTIR study of the Cl-atom-initiated reaction of glyoxal, Int. J. Chem. Kin., 17, 547-558, https://doi.org/10.1002/kin.550170507, 1985.
Niki, H., Maker, P. D., Savage, C. M., and Hurley, M. D.: Fourier transform infrared study of the kinetics and mechanisms for the chlorine-atom- and hydroxyl-radical-initiated oxidation of glycolaldehyde, J. Phys. Chem., 91, 2174-2178, https://doi.org/10.1021/j100292a038, 1987.
Orlando, J. J., and Tyndall, G. S.: Rate Coefficients for the Thermal Decomposition of $BrONO_2$ and the Heat of Formation of $BrONO_2$, J. Phys. Chem., 100, 19398-19405, https://doi.org/10.1021/jp9620274, 1996.
Orlando, J. J., Tyndall, G. S., Fracheboud, J.-M., Estupiñan, E. G., Haberkorn, S., and Zimmer, A.: The rate and mechanism of the gas-phase oxidation of hydroxyacetone, Atmos. Environ., 33, 1621-1629, https://doi.org/10.1016/S1352-2310(98)00386-0, 1999.
Orlando, J. J., Tyndall, G. S., Apel, E. C., Riemer, D. D., and Paulson, S. E.: Rate coefficients and mechanisms of the reaction of Cl-atoms with a series of unsaturated hydrocarbons under atmospheric conditions, Int. J. Chem. Kinet., 35, 334-353, https://doi.org/10.1002/kin.10135, 2003.
Pechtl, S., and von Glasow, R.: Reactive chlorine in the marine boundary layer in the outflow of polluted continental air: A model study, Geophys. Res. Lett., 34, https://doi.org/10.1029/2007gl029761, 2007.
Pelle, K., Wittmann, M., Lovrics, K., Noszticzius, Z., Liveri, M. L. T., and Lombardo, R.: Mechanistic investigations of the BZ reaction with oxalic acid substrate. I. The oscillatory parameter region and rate constants measured for the reactions of HOBr, $HBrO_2$, and acidic BrO_3^- with oxalic acid, J. Phys. Chem. A, 108, 5377-5385, https://doi.org/10.1021/jp048817s, 2004.
Prados-Roman, C., Cuevas, C. A., Fernandez, R. P., Kinnison, D. E., Lamarque, J. F., and Saiz-Lopez, A.: A negative feedback between anthropogenic ozone pollution and enhanced ocean emissions of iodine, Atmos. Chem. Phys., 15, 2215-2224, https://doi.org/10.5194/acp-15-2215-2015, 2015.
Prager, L., Dowideit, P., Langguth, H., Schuchmann, H.-P., and von Sonntag, C.: Hydrolytic removal of the chlorinated products from the oxidative free-radical-induced degradation of chloroethylenes: acid chlorides and chlorinated acetic acids, J. Chem. Soc., Perkin Trans. 2, 1641-1647, https://doi.org/10.1039/B101687N, 2001.

Pszenny, A. A. P., Moldanov , J., Keene, W. C., Sander, R., Maben, J. R., Martinez, M., Crutzen, P. J., Perner, D., and Prinn, R. G.: Halogen cycling and aerosol pH in the Hawaiian marine boundary layer, Atmos. Chem. Phys., 4, 147-168, https://doi.org/10.5194/acp-4-147-2004, 2004.
Ramacher, B., Orlando, J. J., and Tyndall, G. S.: Temperature-dependent rate coefficient measurements for the reaction of bromine atoms with a series of aldehydes, Int. J. Chem. Kinet., 32, 460-465, https://doi.org/10.1002/1097-4601(2000)32:8<460::Aid-Kin2>3.0.Co;2-P, 2000.
Read, K. A., Mahajan, A. S., Carpenter, L. J., Evans, M. J., Faria, B. V., Heard, D. E., Hopkins, J. R., Lee, J. D., Moller, S. J., Lewis, A. C., Mendes, L., McQuaid, J. B., Oetjen, H., Saiz-Lopez, A., Pilling, M. J., and Plane, J. M.: Extensive halogen-mediated ozone destruction over the tropical Atlantic Ocean, Nature, 453, 1232-1235, https://doi.org/10.1038/nature07035, 2008.
The chemical mechanistic information was taken from the Master Chemical Mechanism, MCM v3.2 (reference), URL: http://mcm.leeds.ac.uk/MCM, 21.10.2013.
Saiz-Lopez, A., Plane, J. M. C., and Shillito, J. A.: Bromine oxide in the mid-latitude marine boundary layer, Geophys. Res. Lett., 31, https://doi.org/10.1029/2003GL018956, 2004.
Sander, R., Keene, W. C., Pszenny, A. A. P., Arimoto, R., Ayers, G. P., Baboukas, E., Cainey, J. M., Crutzen, P. J., Duce, R. A., Hönninger, G., Huebert, B. J., Maenhaut, W., Mihalopoulos, N., Turekian, V. C., and Van Dingenen, R.: Inorganic bromine in the marine boundary layer: a critical review, Atmos. Chem. Phys., 3, 1301-1336, https://doi.org/10.5194/acp-3-1301-2003, 2003.
Sander, R., Pszenny, A. A. P., Keene, W. C., Crete, E., Deegan, B., Long, M. S., Maben, J. R., and Young, A. H.: Gas phase acid, ammonia and aerosol ionic and trace element concentrations at Cape Verde during the Reactive Halogens in the Marine Boundary Layer (RHaMBLe) 2007 intensive sampling period, Earth Syst. Sci. Data, 5, 385-392, https://doi.org/10.5194/essd-5-385-2013, 2013.
Sander, R.: Compilation of Henry's law constants (version 4.0) for water as solvent, Atmos. Chem. Phys., 15, 4399-4981, https://doi.org/10.5194/acp-15-4399-2015, 2015.
Sander, S. P., Friedl, R. R., Golden, D. M., Kurylo, M. J., Moortgat, G. K., Wine, P. H., Ravishankara, A. R., Kolb, C. E., Molina, M. J., Finlayson-Pitts, B. J., Huie, R. E., and Orkin, V. L.: Chemical Kinetics and Photochemical Data for Use in Atmospheric Studies, Evaluation No. 15, Jet Propulsion Laboratory, Pasadena, 2006.
Saunders, R. W., and Plane, J. M. C.: Formation Pathways and Composition of Iodine Oxide Ultra-Fine Particles, Environ. Chem., 2, 299-303, https://doi.org/10.1071/en05079, 2005.
Shallcross, D. E., Vaughan, S., Trease, D. R., Canosa-Mas, C. E., Ghosh, M. V., Dyke, J. M., and Wayne, R. P.: Kinetics of the reaction between OH radicals and monochlorodimethylsulphide (CH_3SCH_2Cl), Atmos. Environ., 40, 6899-6904, https://doi.org/10.1016/j.atmosenv.2006.06.037, 2006.
Shi, Q., Jayne, J. T., Kolb, C. E., Worsnop, D. R., and Davidovits, P.: Kinetic model for reaction of $ClONO_2$ with H_2O and HCl and HOCl with HCl in sulfuric acid solutions, J. Geophys. Res.-Atmos., 106, 24259-24274, https://doi.org/10.1029/2000jd000181, 2001.

Sutton, H. C., and Downes, M. T.: Reactions of the HO_2 radical in aqueous solution with bromine and related compounds, J. Chem. Soc., Faraday Trans. 1, 68, 1498-1507, https://doi.org/10.1039/F19726801498, 1972.
Sutton, H. E., Adams, G. E., Boag, J. W., and Michael, B. D.: Radical yields and kinetics in the pulse radiolysis of potassium bromide solutions, in: International Symposium on Pulse Radiolysis, edited by: Ebert, M., Keene, J. P., and Swallow, A. J., Academic Press, Manchester, England, 61-81, 1965.
Szirovicza, L., and Boga, E.: The kinetics of the bromate-sulfite reaction system, Int. J. Chem. Kinet., 30, 869-874, https://doi.org/10.1002/(Sici)1097-4601(1998)30:12<869::Aid-Kin1>3.0.Co;2-0, 1998.
Thiault, G., Mellouki, A., and Le Bras, G.: Kinetics of gas phase reactions of OH and Cl with aromatic aldehydes, Phys. Chem. Chem. Phys., 4, 2194-2199, https://doi.org/10.1039/b200609j, 2002.
Thornton, A. T., and Laurence, G. S.: Kinetics of oxidation of transition-metal ions by halogen radical anions. Part I. The oxidation of iron(II) by dibromide and dichloride ions generated by flash photolysis, J. Chem. Soc, Dalto Trans., 804-813, https://doi.org/10.1039/DT9730000804, 1973.
Turnipseed, A. A., Barone, S. B., and Ravishankara, A. R.: Reactions of CH_3S and CH_3SOO with O_3, NO_2, and NO, J. Phys. Chem., 97, 5926-5934, https://doi.org/10.1021/j100124a025, 1993.
Urbanski, S. P., and Wine, P. H.: Spectroscopic and kinetic study of the Cl-S$(CH_3)_2$ adduct, J. Phys. Chem. A, 103, 10935-10944, https://doi.org/10.1021/Jp992682m, 1999.
Valkai, L., and Horvath, A. K.: Compatible Mechanism for a Simultaneous Description of the Roebuck, Dushman, and Iodate-Arsenous Acid Reactions in an Acidic Medium, Inorg. Chem., 55, 1595-1603, https://doi.org/10.1021/acs.inorgchem.5b02513, 2016.
Vikis, A. C., and Macfarlane, R.: Reaction of Iodine with Ozone in the Gas-Phase, J. Phys. Chem., 89, 812-815, https://doi.org/10.1021/j100251a019, 1985.
Volkamer, R., Baidar, S., Campos, T. L., Coburn, S., DiGangi, J. P., Dix, B., Eloranta, E. W., Koenig, T. K., Morley, B., Ortega, I., Pierce, B. R., Reeves, M., Sinreich, R., Wang, S., Zondlo, M. A., and Romashkin, P. A.: Aircraft measurements of BrO, IO, glyoxal, NO_2, H_2O, O_2–O_2 and aerosol extinction profiles in the tropics: comparison with aircraft-/ship-based in situ and lidar measurements, Atmos. Meas. Tech., 8, 2121-2148, https://doi.org/10.5194/amt-8-2121-2015, 2015.
von Glasow, R., Sander, R., Bott, A., and Crutzen, P.: Modeling halogen chemistry in the marine boundary layer - 1. Cloud-free MBL, J. Geophys. Res.-Atmos., 107, https://doi.org/10.1029/2001JD000942, 2002.
Von Gunten, U., and Oliveras, Y.: Advanced oxidation of bromide-containing waters: Bromate formation mechanisms, Environ. Sci. Technol., 32, 63-70, https://doi.org/10.1021/es970477j, 1998.
Wagman, D. D., Evans, W. H., Parker, V. B., Schumm, R. H., Halow, I., Bailey, S. M., Churney, K. L., and Nuttall, R. L.: The NBS tables of chemical thermodynamic properties; Selected values for inorganic and C_1 and C_2 organic substances in SI units, J. Phys. Chem. Ref. Data, 11, 1982.

Wallington, T. J., Gierczak, C. A., Ball, J. C., and Japar, S. M.: Fourier-Transform Infrared Study of the Self Reaction of $C_2H_5O_2$ Radicals in Air at 295 K, Int. J. Chem. Kinet., 21, 1077-1089, https://doi.org/10.1002/kin.550211109, 1989.
Wang, L., Arey, J., and Atkinson, R.: Reactions of chlorine atoms with a series of aromatic hydrocarbons, Environ. Sci. Technol., 39, 5302-5310, https://doi.org/10.1021/es0479437, 2005.
Wang, T. X., Kelley, M. D., Cooper, J. N., Beckwith, R. C., and Margerum, D. W.: Equilibrium, Kinetic, and UV-Spectral Characteristics of Aqueous Bromine Chloride, Bromine, and Chlorine Species, Inorg. Chem., 33, 5872-5878, https://doi.org/10.1021/ic00103a040, 1994.
Wang, T. X., and Margerum, D. W.: Kinetics of Reversible Chlorine Hydrolysis - Temperature-Dependence and General Acid Base-Assisted Mechanisms, Inorg. Chem., 33, 1050-1055, https://doi.org/10.1021/ic00084a014, 1994.
Wang, W., Ezell, M. J., Ezell, A. A., Soskin, G., and Finlayson-Pitts, B. J.: Rate constants for the reactions of chlorine atoms with a series of unsaturated aldehydes and ketones at 298 K: structure and reactivity, Phys. Chem. Chem. Phys., 4, 1824-1831, https://doi.org/10.1039/b111557j, 2002.
Wang, Y. L., Nagy, J. C., and Margerum, D. W.: Kinetics of Hydrolysis of Iodine Monochloride Measured by the Pulsed-Accelerated-Flow Method, J. Am. Chem. Soc., 111, 7838-7844, https://doi.org/10.1021/ja00202a026, 1989.
Wudl, F., Lightner, D. A., and Cram, D. J.: Methanesulfinic acid and Its properties, J. Am. Chem. Soc., 89, 4099-4101, https://doi.org/10.1021/Ja00992a026, 1967.
Young, H. A.: The Reduction of Bromic Acid by Hydrobromic Acid in the Presence of Hydrogen Peroxide, J. Am. Chem. Soc., 72, 3310-3312, https://doi.org/10.1021/ja01163a542, 1950.
Zehavi, D., and Rabani, J.: Oxidation of aqueous bromide ions by hydroxyl radicals. Pulse radiolytic investigation, J. Phys. Chem., 76, 312-319, https://doi.org/10.1021/j100647a006, 1972.
Zellner, R., Herrmann, H., Exner, M., Jacobi, H.-W., Raabe, G., and Reese, A.: Formation and Reactions of Oxidants in the Aqueous Phase, in: Heterogeneous and Liquid Phase Processes, edited by: Warneck, P., Springer Verlag, Berlin, Germany, 146-152, 1996.
Zhu, L., Nicovich, J. M., and Wine, P. H.: Temperature-dependent kinetics studies of aqueous phase reactions of hydroxyl radicals with dimethylsulfoxide, dimethylsulfone, and methanesulfonate, Aquat. Sci., 65, 425-435, https://doi.org/10.1007/s00027-003-0673-6, 2003a.
Zhu, L., Nicovich, J. M., and Wine, P. H.: Temperature-dependent kinetics studies of aqueous phase reactions of SO_4^- radicals with dimethylsulfoxide, dimethylsulfone, and methanesulfonate, J. Photochem. Photobiol. A: Chem., 157, 311-319, https://doi.org/10.1016/s1010-6030(03)00064-9, 2003b.
Zhu, L.: Aqueous phase reaction kinetics of organic sulfur compounds of atmospheric interest, Dissertation, Georgia Institute of Technology, 2004.
Zhu, L., Nicovich, J. M., and Wine, P. H.: Kinetics studies of aqueous phase reactions of Cl atoms and Cl_2^- radicals with organic sulfur compounds of atmospheric interest, J. Phys. Chem. A, 109, 3903-3911, https://doi.org/10.1021/Jp044306u, 2005.

Zhu, L., Nenes, A., Wine, P. H., and Nicovich, J. M.: Effects of aqueous organosulfur chemistry on particulate methanesulfonate to non–sea salt sulfate ratios in the marine atmosphere, J. Geophys. Res., 111, https://doi.org/10.1029/2005jd006326, 2006.
Zuo, Z. H., and Katsumura, Y.: Formation of hydrated electron and BrO_3 radical from laser photolysis of BrO_3^- aqueous solution, J. Chem. Soc. Faraday Trans., 94, 3577-3580, https://doi.org/10.1039/a806861e, 1998.